UNIVERSITY OF BEIRA INTERIOR
Engineering

High Performance Computing for 3D Image Segmentation: Application to Medical Imaging

Przemyslaw Lenkiewicz

Thesis for obtaining the degree of Doctor of Philosophy in
Computer Science and Engineering
(3rd Cycle Studies)

Supervisor: Maria Manuela Areias da Costa Pereira de Sousa
Co-supervisor: José Joaquim Gomes Fernandes

Covilhã, October 2013

HPC for 3D Image Segmentation: Application to Medical Imaging

This thesis has been prepared at Microsoft Portugal at the Developer Platform Evangelism group, and at Instituto de Telecomunicações, within Multimedia Signal Processing - Covilhã Group, and submitted to University of Beira Interior for defence in a public examination session.

This work has been partially supported by Portuguese Fundação para a Ciência e a Tecnologia through the grant contract SFRH/BD/61265/2009, by MSFT-Microsoft Portugal through HIPER-CAMBIO project: High Performance Computing Applied to Medical Data and Bioinformatics, by Instituto de Telecomunicações and by University of Beira Interior.

Thanks and Acknowledgments

The journey that I needed to take in order for this thesis to be concluded was a long and a very interesting one. It would never be successful if it wasn't for many wonderful people that I have met along the way. It is hard to measure and compare the importance that they represent to me, so I cannot think of a better order to thank them than chronologically.

I have to start with my parents, who have made me the person that I am right now and who have guided me through my education. So whenever I could say that I am successful at anything, they have contributed to that in large amount. Kochani rodzice, dziekuje Wam za wszystko! The same goes for the rest of my family, my brother Dawid and sister Monika and everyone that I have been growing up with.

Four years of high-school at "I l.o." started some of the best friendships, so thanks everyone from my class! Further three years of my bachelor of science at the Technical University of Bialystok brought some more great memories, friends and of course first steps in professional Information Technology.

After that it was time to say goodbye to Bialystok, my home town, and move to Portugal. In Siemens I have met some wonderful people, who have helped me to initiate my adventure with research. Big thanks to Nuno Garcia, who has been my mentor and until this day is a very close friend. Nuno, you have also helped a lot to conclude the work on this thesis, so thanks a lot! Thanks to Marek Hajduczenia, Pedro Inácio, prof. Paulo Monteiro and the rest of Siemens Research & Development team. Guys, it was you who showed me that I am in the right place and that I want to find out what the research world has to offer. You have also contributed a lot to my first steps, helped me to run my first experiments and to write my first papers - all this cannot be overvalued.

Soon afterwards I have met the most amazing person in the world, with whom I still share every moment of my life. Ania, you have been with me every step along the way and supported me at all the difficulties of this PhD and of our life together. I can never express my gratitude and I can never say how happy I am to have you! You and our daughters, Kinga and Sara, are my motivation for everything that I do.

The beginning of my collaboration with University of Beira Interior opens a very interesting and challenging chapter that is ongoing to this present day. I would like to thank prof. Manuela Pereira and prof. Mario Freire for inviting me into their team and helping me in my first steps, for teaching me what to be a researcher means. Countless hours of discussions, countless advice and guidance has resulted in everything that I have achieved in the academic world, including this thesis. Also I would like to thank the staff of Department of Information Technology, who have taught the classes which I attended or who have otherwise contributed to my education and my research efforts. Prof. Simão de Sousa, prof. Abel Gomes, prof. Gael Dias, prof. Paula Prata, prof. Paulo Moura, thank you.

On February 2007 I have officially started the work which results in the thesis you can see in front of your eyes. The team of Microsoft Portugal has welcomed me as one of their own and

made me feel at home for more than 3 years. Also there I have learned a lot about the world, which would soon become my playground, my future career - the world of Information Technology as a job. Vitor Santos, thank you for starting this whole project and for being there for me. José Fernandes, thank you for everyday guidance with my PhD and introduction to the business world. My office mates, who have been my family during these years - you guys are the best! Joana Monteiro, Ana Ferreira, Sara Fernades, Sara Fonseca, João Abréu, Miguel Vicente, Ricardo Escovinha, Gonçalo Cháves, Cesar Mendes, Nuno Martins, Nuno Silva, João Antao - this time wouldn't be the same without you! The DPE team - Pedro Rosa, Nuno Costa, Cristina Carvalho, thanks for being there!

When I decided it was time to say goodbye to Portugal I have found my new home at the Max Planck Institute for Psycholinguistics in Nijmegen, Netherlands. I was welcomed by Peter Wittenburg in his team and have learned a lot from himself and from the group of smart people, who are my colleagues to this day, when I conclude this PhD. Thanks to the entire team of The Language Archive!

Preface

This thesis has been written in an environment of a close collaboration between the University of Beira Interior, Instituto de Telecomunicaçoẽs and Microsoft Portugal. Each of the partners has contributed a lot to this joint work and the outcome would not be possible without any of them.

The concept of this research topic has sparked as an idea of prof. Mario Freire and dr. Vitor Santos, who have discussed the possibility of investigating how High Performance Computing solutions (HPC) could be used in order to improve the detection rate of breast cancer. The idea included developing an innovative model capable of segmenting areas of 3D (volumetric) medical images, originating at modern high-resolution medical acquisition devices, which would be executed on a computer cluster. This idea was the beginning of a project called HIPERCAMBIO, which stands for High Performance Computing Applied to Medicine and Bioinformatics.

The initial funding came from Microsoft Portugal and was arranged by Vitor Santos from several departments of Microsoft. The funding included an initial PhD grant for the author of this thesis and the resources to buy a powerful computer cluster.

The PhD position was officially started on February 2007. At that time the area of parallel processing did not yet resemble what we witness nowadays, when this thesis is concluded. The multi-core processors have already begun their way towards home desktop computers, but their capabilities were not yet properly used by nearly any popular software. It was then when the main software vendors understood that the increase of performance for their applications will not anymore come from the increasing bus speeds of modern computers, but from parallelizm and multi-core processing.

Also at that time Microsoft has started sales of their new solution - Windows HPC Server 2005. It has aimed at delivering a friendly user experience with all the tasks connected with HPC solutions - starting with a deployment of a computer cluster, managing such a solution and developing software that can take advantage of such an advanced and powerful tool. The first version of the HPC Server has included a simple set of tools for platform deployment and management. Also the programming tools have not yet included the desired functionality - although initial bindings for a Message Passing Interface implementation (MPI) have been included, they have existed only for a not-managed language, C++, and tools for debugging were rather primitive.

During the development of this research work the situation has matured significantly. The multi-core processors have arrived in the vast majority of computers sold nowadays. Most of the popular software available at this time is also fully capable of using multi-core platforms for computationally intensive tasks, like media encoding, image processing, computer graphics, and so forth. Also the HPC Server from Microsoft has seen several releases of new versions, each offering a significant improvement in functionality and user experience of the HPC solution management. The programming tools have been adapted to C# language and programming environment, including debugging tools, have matured to resemble the way of programming known from traditional single-core solutions.

A competitive solution for massive parallel processing has been introduced and developed intensively also in the time when this PhD thesis has started. This refers to the Graphical Processing Units (GPUs) of modern video cards, compatible with solutions like the OpenCL or nVidia CUDA. These GPUs have offered the possibility of very efficient processing on a multi-core approach reaching the level of hundreds of processing units within a single computer equipped with

just one or several video cards. However, their usability remains to this day limited. The programming model and bindings to popular programming languages remain complicated and not straightforward to learn and use. The application of such GPU-based computing remains restricted to specialized labs and enterprise environments.
In the scope of the above-described changes the work described in this thesis remains competitive and well motivated. The Whole Mesh Deformation (WMD) model has been designed and developed as a solution that could be easily adopted and used by any medical practitioner in any lab or hospital, without the need for specialized computer hardware or medical equipment. The application of a user-friendly operating system with user experience, optimized towards efficient usability rather than high configurability and control over every aspect, has lowered the amount of expertise required for adaptation and later use of this solution. At any medical lab, where a multi-core or multi-processor computer is available, the WMD model can be easily executed and will deliver an efficient and accurate segmentation of medical images, like Computed Tomography, Magnetic Resonance Imaging, etc. In case that two or more computers are available, it will be possible to connect them and form a computer cluster using a solution like Windows HPC server, and even more performance gain will be reached.

Abstract

Digital image processing is a very popular and still very promising field of science, which has been successfully applied to numerous areas and problems, reaching fields like forensic analysis, security systems, multimedia processing, aerospace, automotive, and many more.
A very important part of the image processing area is image segmentation. This refers to the task of partitioning a given image into multiple regions and is typically used to locate and mark objects and boundaries in input scenes. After segmentation the image represents a set of data far more suitable for further algorithmic processing and decision making. Image segmentation algorithms are a very broad field and they have received significant amount of research interest
A good example of an area, in which image processing plays a constantly growing role, is the field of medical solutions. The expectations and demands that are presented in this branch of science are very high and difficult to meet for the applied technology. The problems are challenging and the potential benefits are significant and clearly visible. For over thirty years image processing has been applied to different problems and questions in medicine and the practitioners have exploited the rich possibilities that it offered. As a result, the field of medicine has seen significant improvements in the interpretation of examined medical data.
Clearly, the medical knowledge has also evolved significantly over these years, as well as the medical equipment that serves doctors and researchers. Also the common computer hardware, which is present at homes, offices and laboratories, is constantly evolving and changing. All of these factors have sculptured the shape of modern image processing techniques and established in which ways it is currently used and developed. Modern medical image processing is centered around 3D images with high spatial and temporal resolution, which can bring a tremendous amount of data for medical practitioners. Processing of such large sets of data is not an easy task, requiring high computational power. Furthermore, in present times the computational power is not as easily available as in recent years, as the growth of possibilities of a single processing unit is very limited - a trend towards multi-unit processing and parallelization of the workload is clearly visible. Therefore, in order to continue the development of more complex and more advanced image processing techniques, a new direction is necessary.
A very interesting family of image segmentation algorithms, which has been gaining a lot of focus in the last three decades, is called Deformable Models. They are based on the concept of placing a geometrical object in the scene of interest and deforming it until it assumes the shape of objects of interest. This process is usually guided by several forces, which originate in mathematical functions, features of the input images and other constraints of the deformation process, like object curvature or continuity. A range of very desired features of Deformable Models include their high capability for customization and specialization for different tasks and also extensibility with various approaches for prior knowledge incorporation. This set of characteristics makes Deformable Models a very efficient approach, which is capable of delivering results in competitive times and with very good quality of segmentation, robust to noisy and incomplete data.
However, despite the large amount of work carried out in this area, Deformable Models still suffer from a number of drawbacks. Those that have been gaining the most focus are e.g. sensitivity to the initial position and shape of the model, sensitivity to noise in the input images and to flawed input data, or the need for user supervision over the process.
The work described in this thesis aims at addressing the problems of modern image segmentation, which has raised from the combination of above-mentioned factors: the significant growth

of image volumes sizes, the growth of complexity of image processing algorithms, coupled with the change in processor development and turn towards multi-processing units instead of growing bus speeds and the number of operations per second of a single processing unit. We present our innovative model for 3D image segmentation, called the The Whole Mesh Deformation model, which holds a set of very desired features that successfully address the above-mentioned requirements. Our model has been designed specifically for execution on parallel architectures and with the purpose of working well with very large 3D images that are created by modern medical acquisition devices.
Our solution is based on Deformable Models and is characterized by a very effective and precise segmentation capability. The proposed Whole Mesh Deformation (WMD) model uses a 3D mesh instead of a contour or a surface to represent the segmented shapes of interest, which allows exploiting more information in the image and obtaining results in shorter times. The model offers a very good ability for topology changes and allows effective parallelization of workflow, which makes it a very good choice for large data-sets. In this thesis we present a precise model description, followed by experiments on artificial images and real medical data.

Keywords

Image segmentation, medical imaging, parallel processing, high performance computing, Deformable Models, topology changes.

Resumo Alargado em Português

Introdução

Nesta secção é apresentado o Resumo Alargado em Português da tese intitulada *Computação de Alto Desempenho para Segmentação de Imagens 3D: Aplicação em Imagiologia Médica* - "High Performance Computing for 3D Image Segmentation: Application to Medical Imaging". Este resumo alargado serve para introduzir o leitor aos assuntos descritos na tese e dar-lhe uma visão global adequada dos trabalhos de investigação realizados. Todos os aspetos dos trabalhos de investigação mencionados neste secção são descritos em maior pormenor no desenvolvimento desta tese.

O resumo alargado tem a seguinte organização: na primeira secção são apresentados o problema e a motivação para a realização dos trabalhos de investigação. Nesta secção é também apresentada uma revisão dos trabalhos mais relevantes realizados sobre métodos de segmentação de imagem. Esta secção termina com a definição do problema, dos objetivos e das contribuições desta tese. Na secção *Descrição do Modelo Deformação da Malha Completa* é introduzido o modelo de segmentação de imagem proposto nesta tese (WMD). Na secção *Modelo de Alteração de Topologia Dinâmica*, a capacidade do modelo WMD de realizar alterações na topologia é descrita. Na secção *Implementação paralela* discute-se a capacidade do modelo WMD de ser executado em arquitecturas paralelas, uma característica muito importante, que será mencionada ao longo desta tese. Na secção *Modelo Estendido da Deformação da Malha Completa* é introduzida uma extenção do modelo WMD, que permite um verdadeiro processamento 3D dos dados de entrada; finalmente, na última secção apresentam-se as conclusões e o trabalho futuro.

Enquadramento e Motivação

O procedimento de segmentação de imagens é um dos passos mais importantes do processo de análise de imagens. Refere-se à tarefa de divisão de uma imagem em múltiplas regiões e é normalmente utilizado para localizar e marcar objetos e limites em cenários de entrada. Depois da segmentação, a imagem representa um conjunto de dados muito mais apropriado para os algoritmos de processamento e tomada de decisão. Os métodos de segmentação de imagem são um tópico muito amplo e têm recebido grande interesse na comunidade científica.

Uma família de modelos de segmentação de imagem muito interessante, e que tem vindo a ganhar muito foco nas últimas três décadas, é denominada Modelos Deformáveis. Estes são baseados no conceito de colocação de um objeto geométrico no cenário de interesse e deformação do mesmo até que este assuma a forma dos objetos de interesse. Este processo é geralmente guiado por várias forças, com origem em funções matemáticas, características das imagens de entrada e outras restrições do processo de deformação, tais como a curvatura ou continuidade do objeto. A gama de características desejáveis dos Modelos Deformáveis inclui a sua grande capacidade de personalização e especialização para diferentes tarefas e também a extensibilidade com várias abordagens para a incorporação de conhecimento prévio. Este conjunto de características fazem dos Modelos Deformáveis uma abordagem muito eficiente, a qual é capaz de fornecer resultados em tempos competitivos, com muito boa qualidade de segmentação, e é robusto ao ruído e a dados incompletos.

Revisão de Trabalho Prévio

Vários exemplos da utilização dos Modelos Deformáveis podem ser encontrados, começando com os primeiros anos de processamento de imagem até aos últimos esforços de investigação. O primeiro trabalho neste tópico foi apresentado por Kass et al. [KWT88a]. Estes autores descreveram um método chamado Snakes, que propunha colocar um único contorno no cenário de interesse e em seguida submetê-lo a deformações até que este assumisse a forma dos objetos presentes nesse cenário. As deformações são forçadas pelas energias externa e interna, que descrevem as características do cenário e do próprio contorno, respectivamente. Esta ideia despertou um grande interesse no campo de segmentação de imagem em geral e particularmente em relação Ã imagem medica. Muitos autores começaram a propor melhorias e alterações à formulação original, incluindo modelos de contornos geométricos activos [Cas95] (aplicados a imagens de Ressonância Magnética do cérebro) ou contornos activos para segmentação de objetos sem contornos rigorosamente definidos [CV01a] (testado apenas para imagens e fotografias artificiais), entre os mais notáveis.

As soluções derivadas do método original formulado por Kass in [KWT88a] utilizam geralmente uma equação diferencial de Euler para determinar a solução. Uma abordagem diferente foi apresentada pot Amini e Tehrani na sua publicação inicial [ATW88b], onde os autores propuseram uma solução baseada em programação dinâmica. O método permitia a introdução de um novo tipo de restrições descrevendo regras que não podiam ser violadas. Este também garantiu a estabilidade numérica da solução, endereçando assim uma grande desvantagem do método Kass, onde as iterações que formavam os passos intermédios de execução mostraram um grande grau de instabilidade e para a solução final tinham de ser considerados sem significado. A desvantagem da solução de Amini foi uma grande sobrecarga em termos dos requisitos de memória e tempos de execução.

A capacidade de alterar a topologia da forma tem sido uma componente muito significativa dos Modelos Deformáveis, e vários trabalhos foram apresentados com o objetivo de classificar e descrever os diferentes aspetos de alteração de topologia [DM00, MT96a]. Em [MT95] e [MT99a] McInemey e Terzopoulos consideraram a incapacidade dos modelos deformáveis paramétricos de fazerem transformações topológicas sem mecanismos adicionais. Eles introduziram um modelo chamado T-snake, capaz de adaptar dinamicamente a sua topologia à do objeto alvo, fluir em torno dos objetos incorporados dentro do objeto alvo, e/ou automaticamente juntar-se com outros modelos introduzidos interativamente pelo utilizador.

Uma solução muito importante foi proposta por Casselles [Cas95], que apresentou um modelo baseado numa abordagem de evolução da curva em vez de uma de minimização de energia. Esta permite alterações automáticas na topologia quando implementada utilizando o algoritmo numérico baseado em conjunto de níveis [OS88] e, naturalmente, previne também auto-intersecção, que é um procedimento dispendioso em modelos deformáveis paramétricos. A sua solução serviu de base para inúmeros trabalhos [FS06a, LEGF00, MSV95a]. Contudo, a capacidade de alterar a topologia não é sempre desejável. Especialmente no campo de imagiologia médica, existem muitas situações em que a topologia do objecto de interesse é sabida do conhecimento anatómico e pode ser definida na execução do algoritmo. De forma a proporcionar tal funcionalidade, uma formulação que preserva a topologia foi proposta em [XXP03]. Foi no entanto atingido o objetivo impondo uma limitação severa sobre o número de componentes ligados, que tem de ser conhecido antes e não pode ser modificado durante a segmentação. Por se tornar muito restritivo para algumas aplicações, foi proposto um método mais súbtil em [SPF05]. Os autores formularam a sua solução de uma forma que permita aos componentes da

forma segmentada fundir-se, dividir-se ou desaparecer sem alterar o género do Modelo Deformável inicial.

Definição do Problema

Devido às suas características atrativas, uma das áreas em que os Modelos Deformáveis têm um bom desempenho, e na qual são uma escolha muito popular, é a área da análise de imagem médica. O processamento de imagem digital tem sido aplicado com sucesso nesta área por mais de três décadas. As inúmeras vantagens que oferecem incluem, nomeadamente, a melhoria na interpretação dos dados analisados, automação completa ou quase completa das tarefas normalmente desempenhadas por um médico, melhor precisão e exatidão dos resultados obtidos e também a possibilidade de explorar novas modalidades de imagem, levando a uma nova perceção anatómica e funcional.
Contudo, apesar da grande quantidade de trabalhos realizados nesta área, os Modelos Deformáveis continuam a ter algumas desvantagens. Aquelas que têm ganho mais foco são:

- sensibilidade à posição e forma inicial do modelo - sem uma inicialização adequada, o modelo pode ficar preso em mínimos locais e portanto não atingir os objetos de interesse ou não detetar corretamente algumas das suas características;

- sensibilidade ao ruído nas imagens de entrada e a dados de entrada defeituosos;

- mudanças de topologia problemáticas - quando o cenário de interesse inclui mais de um objeto ou quando os objetos presentes no cenário contêm descontinuidades, os Modelos Deformáveis necessitam de alterar a topologia da sua forma. Isto não é linear na formulação paramétrica do método e requer passos específicos nos algoritmos;

- a necessidade de supervisão do utilizador no processo.

Algumas destas desvantagens foram abordadas com sucesso num trabalho interessante de Barreira e Penedo em [BP05] e ainda descrito em [BPAR08]. Eles formularam um modelo chamado Volumes Topológicos Ativos (VTA) que foi introduzido como um modelo geral para segmentação automática de cenários 3D. Este difere dos métodos iniciais baseados nos Modelos Deformáveis, na medida em que a forma deformada foi representada com uma malha volumétrica, com alguns nós sendo responsáveis por descrever os limites dos objetos e outros por modelar a sua estrutura interior. Ainda assim, o modelo VTA não só não atendeu todos os problemas persistentes como também introduziu os seus próprios, como por exemplo o alto custo computacional de execução.
A imagiologia médica moderna está centrada em imagens de alta resolução, que são capazes de fornecer cada vez mais informação aos médicos, que por sua vez leva a uma melhoria nas taxas de deteção e aumento na precisão de cirurgias e planeamento assistidos por computador. No entanto, o processamento de grandes conjuntos de dados apresenta novos desafios, que são em parte resultado dos atuais desenvolvimentos no campo dos microprocessadores. Já não estamos na presença de um crescimento significativo das possibilidades de uma única unidade de processamento, mas sim de uma tendência para o processamento multi-unidade. Inúmeras tentativas foram tomadas para paralelizar o fluxo de trabalho de processamento de imagem médica usando clusters de computadores [NK95, TMT+01, NJ02].

Objetivos e Contribuições

Nesta tese abordamos os problemas da segmentação de imagem que provÃªm da combinação de diferentes fatores, nomeadamente: o crescimento significativo do tamanho das imagens; o aumento da complexidade dos modelos de processamento de imagem; juntamente com as alterações no desenvolvimento dos processadores e alteração para unidades de multi-processamento, em vez de crescimento de velocidades de barramento e do número de operações por segundo de uma única unidade de processamento. Propomos nesta tese um novo modelo de segmentação de imagem 3D denominado "Whole Mesh Deformation model" (WMD), o qual apresenta um conjunto de características bastante desejÃ¡veis que resolvem com sucesso os requerimentos acima mencionados. O modelo proposto foi desenhado de forma a permitir uma execução ótima em arquiteturas paralelas e com o propósito de ser eficiente mesmo quando se pretende trabalhar com imagens 3D de muito grande dimensão, como é o caso das imagens que são criadas pelos modernos dispositivos de aquisição de imagem médica.
A solução apresentada é baseada no conceito dos Modelos Deformáveis e é caraterizada por uma capacidade de segmentação muito efetiva e precisa. O modelo Deformação da Malha Completa proposto [LPFF13], [LPFF09a] utiliza uma malha 3D em vez de um contorno ou uma superfície para representar as formas de interesse segmentadas, o que permite explorar mais informação na imagem e obter resultados num intervalo de tempo menor. O modelo oferece uma capacidade muito boa para alterações de topologia e permite paralelização efetiva do fluxo de trabalho [LPFF08], [LPFF09e] , o que faz dele uma boa escolha para grandes conjuntos de dados. é também proposta uma extensão do modelo inicial a qual permite uma verdadeira segmentação 3D mantendo as boas características do modelo inicial [LPFF09d], [LPFF11a]. Nesta tese, é apresentada uma descrição precisa do modelo, seguida da aplicação em imagens artificiais e dados médicos reais.

Descrição do Modelo Deformação da Malha Completa

Descrição Geral do Modelo

Como mencionado anteriormente, o modelo WMD foi concebido usando como fundamento as ideias dos Modelos Deformáveis. O processo de segmentação é realizado através da construção de uma estrutura em malha tridimensional que cubra todos os dados da imagem de entrada. De seguida, a malha é deformada movendo os seus nós de modo a detetar os objetos presentes no cenário de interesse. Todos os nós são tratados da mesma forma e o seu comportamento depende apenas das características da imagem na sua vizinhança mais próxima. Durante o processo de segmentação cada nó irá descobrir por si só qual o comportamento que deve seguir e proceder da forma desejada para o resto do pro + cesso. Como consequência da diferença descrita acima, o processo de segmentação é realizado da seguinte forma: os nós, que foram instanciados perto dos contornos do objeto, começam a avançar na sua direção, enquanto que os restantes nós mudam a sua posição apenas o suficiente para manterem uma estrutura estável e regular da malha. No fim do processo, os nós irrelevantes são descartados. A maioria das fases deste processo são totalmente ou quase totalmente automatizadas e toda a parametrização e opções necessárias são realizadas por algoritmos apropriados, que operam com base nas características do cenário de interesse. Isto será descrito em maior detalhe no desenvolvimento

da tese.

Formulação da Função Energia

A função energia do modelo, que guia o processo de segmentação, é definido para assumir os seus valores mínimos quando os nós da malha se posicionam na forma de interesse. A função é descrita da seguinte forma:

$$E(\nu) = E_{int}(\nu) + E_{ext}(\nu). \tag{1}$$

onde ν representa o estado atual do modelo. Como se verifica, consiste em dois grupos de forças: internas e externas, que são responsáveis por preservar a estrutura dos objetos e por aplicar as características das imagens de entrada, respetivamente. Estes componentes serão descritos em maior detalhe nas duas secções seguintes.

De modo a calcular a energia para um dado estado do modelo, o domínio [0, 1]x[0, 1]x[0, 1] é discretizado como uma malha regular definida pelo espaçamento entre os nós Gx, Gy, Gz, e cada uma das forças contributivas, descritas nas secções seguintes, é calculada usando um algoritmo apropriado.

Formulação da Energia Interna

A energia interna é composta por duas forças, nomeadamente de continuidade e curvatura [KWT88a], e é definida da seguinte forma:

$$E_{int}(\nu) = \alpha \sum_{n=1}^{k} |m_n - \overline{m}| + \beta \sum_{n=1}^{k} \left| \arctan \mu_n - \frac{\pi}{2} \right| \tag{2}$$

O parâmetro k é o número total de nós na malha. O parâmetro $\overline{m}$ representa a distância média entre os nós vizinhos (comprimento médio da aresta). Os parâmetros m_n e μ_n são respetivamente a distância média e o ângulo entre as arestas incidentes no nó n e são calculados dividindo a soma dos comprimentos (ou ângulos) das ligações na vizinhança do nó pelo seu número. Apenas as ligações que não são maiores do que o que o parâmetro de flexibilidade permite são consideradas neste passo. O parâmetro de flexibilidade das ligações é uma característica utilizada na tarefa das alterações topológicas do modelo "Whole Mesh Deformation" e será descrito em maior detalhe no secção 'Proposta do Modelo de Alteração da Topologia Dinâmica'. Os símbolos α e β nas expressões de soma representam o seu peso e servem para equilibrar o seu impacto na totalidade da função e serão descritos no secção 'Proposta da Parametrização Numérica da Função de Energia'. Como se pode ver na equação (2), a força de continuidade atrai os nós da malha para manter distâncias iguais entre si, da mesma forma que o termo curvatura atrai os nós para manterem um ângulo de 90 graus. Isto serve para preservar a estrutura inicial da malha, baseado em elementos regulares e cúbicos.

Formulação da Energia Externa

A energia externa é composta por três forças e é definida por:

$$E_{ext}(\nu) = \gamma \sum_{n=1}^{k} (1 - I(\nu_n)) + \delta \sum_{n=1}^{k} (1 - G(\nu_n)) + \\ + \varepsilon \sum_{n=1}^{k} Edg(\nu_n). \quad (3)$$

O símbolo $I(v)$ representa os valores de intensidade tirados diretamente das imagens de entrada. O símbolo $G(v)$ é o Vector Gradiente de Fluxo [XP98], que é determinado usando o algoritmo VGF nas imagens de entrada. Similarmente, o símbolo $Edg(v)$ representa os valores do detetor de arestas, que são definidos utilizando o algoritmo Canny Edge Detector [Can86] nas imagens de entrada. Identicamente à equação (2), os símbolos γ, δ e ε representam os pesos de determinados componentes e serão descritos no secção 'Proposta da Parametrização Numérica da Função de Energia'.

Proposta da Optimização da Forma da Malha

O processo de segmentação é realizado através da resolução de uma tarefa de optimização utilizando o Algoritmo Greedy [WS92a]. A função de energia é usada como função optimizada e a forma atual da malha é a sua entrada. Durante o procedimento, para cada nó N da malha é feito o seguinte: se as coordenadas (x_n, y_n, z_n) descrevem a posição do nó N no momento t, então para o momento $t + 1$ as coordenadas de N serão descritas por (x_{n+k}, y_{n+l}, z_n) onde $k, l \in \{-1, 0, 1\}$ e corresponde ao menor valor possível de:

$$E(N_{x+k,y+l,z}) = E_{int}(N) + E_{ext}(N). \quad (4)$$

que é a energia do nó N calculado com as equações (2) e (3) nas coordenadas dadas. Como pode ser visto, o nó é movido na sua vizinhança mais próxima nos planos X e Y e a posição com a energia mais baixa é escolhida como a nova posição do nó. Estes passos são repetidos para cada nó da malha até que a seguinte regra seja satisfeita:

$$\sum N : (N_{(x,y,z,t)} \neq N_{(x+k,y+l,z)}) < \mu \quad (5)$$

onde μ é um valor próximo de zero.
A equação (5) verifica o número de nós que alteraram a sua posição na última iteração do algoritmo. Sempre que este número é decai para zero (ou muito próximo de zero) a malha é assumida na sua posição estável e a segmentação é terminada.

Complexidade do Modelo WMD

O modelo WMD proposto segue um padrão de optimização do algoritmo Greedy para todos os nós da malha. Os passos realizados nesse padrão incluem: a) determinação da energia (eq. (2) e (3)) em todos os locais vizinhos de um dado nó; b) definição do local com a energia mais baixa como a nova localização do dado nó; c) repetição dos passos a) e b) para todos os nós da

malha, até que a energia global continue a diminuir. Destes passos podemos ver que o tempo de execução da tarefa de segmentação depende linearmente do número de nós na malha e do número necessário de repetições do algoritmo (determinação da nova posição para cada nó da malha). Além disso, o número de iterações necessário depende estritamente da distância na qual os nós precisam de viajar durante o passo de optimização. No modelo WMD o foco é na maior diminuição possível desse valor. Como resultado, a complexidade geral dos modelos WMD e VTA é semelhante, mas o tempo de execução do modelo WMD é severamente menor que o tempo de execução do algoritmo baseado no VTA.

Proposta da Parametrização Numérica da Função de Energia

Os símbolos $\alpha, \beta, \gamma, \delta$ e ε das expressões de soma nas equações (2) e (3) representam o seu peso e servem para ponderar o seu impacto na equação total. A fim de obter o comportamento desejado da malha, como mostrado na Fig. 1, é necessário escolher esses valores corretamente. Os testes experimentais realizados permitiram estabelecer uma relação, que é correta para cada cenário de execução testado e, portanto, reduz muito o risco de uma escolha incorreta dos valores desses parâmetros. A relação é a seguinte:

$$\beta < \alpha < \delta < \gamma < \varepsilon \tag{6}$$

Os símbolos representam, da esquerda para a direira, os pesos de: curvatura, continuidade, Vector Gradiente de Fluxo, intensidade da imagem e detetor de arestas. A justificação da hipótese acima é a seguinte:

- Os termos continuidade e curvatura precisam de ser ponderados com valores suficientemente elevados para manter uma alta regularidade da malha. Isto não diminuirá a qualidade da segmentação, uma vez que a maioria dos nós tem de viajar apenas distâncias pequenas durante todo o processo.
- Os nós que são inicializados na proximidade dos objetos de interesse precisam de ser atraídos para os seus contornos e devem ser os únicos a ser atraídos - os nós que são inicializados mais longe devem manter as suas posições e regularidade da malha. é por isso que é necessário dar um peso um pouco maior à força VGF do que às forças de continuidade e curvatura, mas manter a gama de VGF num nível baixo.
- Um elevado peso dos valores de intensidade da imagem serve para impôr um comportamento correto nos nós da malha que foram inicializados dentro do objeto de interesse. Esse peso precisa de ser maior que o do VGF, já que os nós dentro dos objetos não devem ser atraídos pela força do VGF. Em vez disso, eles devem ser distribuídos perto da localização inicial e manter uma estrutura estável graças às forças de continuidade e curvatura. Este cenário pressupõe que os objetos presentes nas imagens são claros e o fundo é escuro. No entanto, isto pode ser facilmente modificado sempre que o cenário da aplicação o requeira.
- O peso do parâmetro energia do detetor de arestas precisa de ser ajustado ao valor mais elevado, uma vez que servirá para corrigir permanentemente a posição dos nós que atingem as margens dos objetos de interesse.

Durante a validação de (6) observou-se também que o modelo WMD proposto prova ser robusto e não muito sensível a alterações nos valores dos parâmetros numéricos, desde que respeitem

(6). Cada cenário de segmentação tem uma certa escolha de valores ótimos dos parâmetros, mas na maioria dos casos com uma margem de 2.5% dos valores ótimos não foi possível verificar qualquer alteração no resultado obtido. A margem de 3.5% introduziu pequenas alterações, mas ainda fornece resultados corretos e precisos.

Reconhecimento das Partes Indesejadas da Malha

Tal como se pode ver na fig. 1, no fim do processo de segmentação alguns nós vão ser eliminados. Estes correspondem às partes da malha representadas fora de qualquer objeto presente na zona de interesse. Como mostra a fig. 1, o pretendido é que os nós se comportem de forma a manter as posições iniciais (ou perto delas) e desligar gradualmente das partes da malha que são atraídas para os contornos do objeto. Isto pode ser obtido usando a capacidade de alterar a topologia do modelo WMD. Assim que o processo de otimização terminar, as partes indesejadas da malha seriam reconhecidas e eliminadas do resultado (como mostra na fig. 1, imagem da direita inferior). Para isso, a malha é dividida em sub-malhas isoladas umas das outras, usando a informação sobre as ligações que são marcadas como quebras pelo mecanismo de alteração de topologia e termo de flexibilidade. Para cada sub-malha são calculados os seguintes valores:

$$\sigma = \sqrt{\frac{1}{n}\sum_{i=1}^{n}\left(I(\nu_i) - \overline{I(\nu)}\right)^2} \tag{7}$$

$$N_E = \sum_{i=1}^{n} N_i : Edg(\nu_i) = 1 \tag{8}$$

onde σ representa o desvio padrão dos valores de intensidade da imagem da sub-malha e N_E representa o número de nós finalizados nas arestas dos objetos de interesse, n é o número total de nós na malha, $I(V_i)$ é o valor de intensidade da imagem de entrada no ponto ocupado pelo nó V_i e $\overline{I(\nu)}$ é o valor de intensidade média para toda a imagem de entrada. As partes que se pretende descartar do resultado final possuem valores muito baixos, obtidos através das equações anteriores, já que a maioria dos nós nessas sub-malhas estão colocados sobre uma área de fundo. Portanto, um simples procedimento de divisão em dois grupos é suficiente para separar as partes relevantes das irrelevantes.

Modelo de Alteração de Topologia Dinâmica

O modelo WMD proposto requer um esquema preciso e eficiente para a alteração de topologia. Isto deve-se ao fato de algumas partes da malha serem irrelevantes durante o processo de segmentação, e como consequência há necessidade de separar estas da parte relevante e descartá-las. Para fazer face a esta necessidade foi desenvolvido um mecanismo de alteração de topologia como componente do modelo WMD. Isto permite alterar a topologia da malha durante o processo de segmentação e criar descontinuidades na estrutura da malha durante o processo de otimização. Sempre que for necessário a reconfiguração da malha isto será feito durante o processo de otimização, e o modelo deve reagir da forma pretendida e começar a criar descontinuidades na estrutura da malha. Por outro lado, a alteração de topologia deve ser limitada em todos os momentos pela função de energia da malha, o que garante que não

ponha em causa a sua estabilidade. Esta dupla dependência entre dois processos vai assegurar o comportamento correto da malha e uma progressão estável no sentido da sua forma ótima. Isto é realizado em contraste com o método de VTA, em que a tarefa de alteração de topologia é um passo separado de todo o processo de segmentação [BP05, BPAR08].
Em princípio, a alteração de topologia é realizada através da remoção de ligações entre os nós da malha. Durante o processo de otimização, cada nó da malha pode mudar a sua posição devido ao processo de minimização de energia e, como resultado, o comprimento das as ligações com os vizinhos também é alterado. Segue-se a inicialização do mecanismo de alteração de topologia de modo a verificar se alguma descontinuidade deve ser criada na malha. Isto é feito determinando o comprimentos das arestas entre o nó dado e os seus vizinhos e é encontrado da seguimte forma:

$$|L_n| \leq \frac{G_x + G_y}{2} \times flex \tag{9}$$

onde $|L_n|$ representa o comprimento da aresta atual, G_x e G_y são os comprimentos das arestas da distribuição inicial da malha e $flex$ é o parâmetro de flexibilidade, que é definido automaticamente após a execução de segmentação no intervalo de:

$$flex \in (1.8; 2.1) \tag{10}$$

tendo em consideração o tamanho das descontinuidades da imagem de entrada. Este intervalo foi estabelecido experimentalmente usando 30 imagens artificiais como entrada. Sempre que uma determinada ligação não satisfizer a condição (9) esta é marcada como quebra. Podemos assumir seguramente que este processo é realizado apenas quando desejado já que a malha é definida para ter uma estrutura rígida e estável e, consequentemente, a maioria das ligações da malha estende os seus comprimentos apenas para valores baixos, durante todo o processo. Quando uma quebra de ligação ocorre, sabemos que é resultado de atrair o nó a um contorno de um objeto presente na zona de interesse e, assim, a rutura de ligação deve ser chamada.
A ligação quebrada deixa de ser considerada no cálculo do termo de continuidade da função de energia na próxima iteração. Como resultado, o nó demonstra um comportamento como se a ligação não tivessse existido e vai progredir longe da sua posição atual de forma mais livre. Isso geralmente causa extensão e, possivelmente, quebra das ligações dos seus vizinhos, como se pode ver na fig. 2.
Este tipo de reação em cadeia é muito desejado uma vez que vai desencadear o movimento de nós e quebras de ligações numa pequena vizinhança. Estes, por sua vez, conduzem a uma deteção bem sucedida de toda a descontinuidade na estrutura da malha. Tal processo é interrompido em localizações corretas, isto é, onde os nós da malha encontram os contornos dos objetos de interesse. Isto é garantido definindo a energia do detetor de arestas com um valor elevado, o que vai parar a progressão de nós.

Implementação paralela

O modelo WMD foi projetado desde inicio com o objetivo de ser executado em arquiteturas paralelas. Foi implementado um algoritmo de segmentação paralela da imagem usando este modelo. Este é capaz de tirar partido das várias unidades de processamento, dividindo a tarefa de segmentação em partes iguais, que seriam efetuadas pelas referidas unidades simultaneamente. Num tal cenário, a distribuição de carga é realizada da seguinte maneira: todos os nós

da malha são divididos em tantos grupos quanto unidades de processamento disponíveis. Cada uma das unidades terá acesso total aos dados de entrada de modo a permitir a deformação completa da malha e evitar a situação em que o nó não é capaz de se mover para fora de uma região específica, porque a sua unidade de processamento não mantém qualquer informação sobre os dados da imagem. Naturalmente que esta abordagem impõe a desvantagem de tempo necessário para propagar os dados de entrada entre todas as unidades de processamento, mas os testes com um grupo de computadores têm mostrado que neste momento não é muito significativo em termos da totalidade do tempo de segmentação. Num cenário em que o ambiente de execussão é um computador multi-unidade, este seria ainda menos considerável.

A ideia em geral do algoritmo paralelo é seguinte. Cada unidade de processamento vai criar um conjunto temporário de variáveis a usar durante o progresso da segmentação. Esses valores representam o estado atual do modelo na unidade de processamento e não são partilhados nem sincronizados com outros participantes. Isto é feito para eliminar as dependências entre as unidades de processamento e evitar a necessidade de sincronização, o que poderia aumentar drasticamente o tempo necessário para a segmentação. A possibilidade de realizar a otimização de uma forma independente, é garantida pelo facto de que a maioria dos cálculos efetuados quando minimizando a função de energia são realizados usando apenas os dados locais. Os únicos valores que são definidos como globais de todo o modelo são a média das distâncias e os ângulos entre os nós da malha. No entanto, numerosas experiências demonstraram que, devido à alta rigidez da estrutura da malha WMD, os seus valores são ligeiramente modificados durante todo o processo de segmentação e, assim, não há necessidade de controlar as alterações de forma tão precisa. Portanto, é seguro assumir que o valor calculado localmente descreve bem o estado de toda a malha.

A unidade de processamento realiza a otimização simultânea da malha e testa a equação (5) de modo a decidir quando concluir a segmentação.

é importante notar que no caso do VTA a distribuição igual de carga não seria tão simples como dividir os nós em dois grupos iguais. Essa possibilidade, neste modelo, é o resultado da falta de divisão entre nós internos e externos e a aplicação da alteração de topologia dinâmica.

Graças a essas características, como indicado anteriormente, o tempo necessário para realizar a segmentação com este método depende muito pouco do conteúdo da imagem de entrada. Como consequência, este tempo é muito uniforme para diferentes partes da malha. Por outro lado, no caso de VTA, a distância que os nós externos devem viajar durante a tarefa de segmentação é altamente dependente do conteúdo de imagem, o que resulta numa grande variação dos tempos de segmentação para diferentes partes da malha. Esta é a razão pela qual este método é muito mais adequado para a paralelização do que o VTA ou qualquer outro método com base no conceito de evolução do contorno.

Modelo Estendido da Deformação da Malha Completa

O primeiro método automático de segmentação tem funcionado de maneira semelhante à segmentação manual feita por um médico, ou seja, em cortes individuais separadamente. Esta abordagem tornou o processo de segmentação muito demorado, bem como sujeito a erros. Por esta razão, o desenvolvimento algorítmico foi focado no processamento dos dados da imagem em 3D, onde os objetos de interesse são representados como volumes 3D ao longo de todo o processo. O modelo WMD na sua formulação original provou ser uma solução muito promissora,

uma vez que é capaz de fornecer resultados precisos em tempos de execução muito competitivos e é altamente adequado para paralelização. No entanto, tem carecido da capacidade de deformar a malha num ambiente 3D completo, uma característica importante.

Processamento 3D versus Semi-3D

O modelo WMD foi desenhado segundo o conceito de Modelos Deformavéis e do Método de Volumes Topológicos Activos ([BP05], [BPAR08]) como fundamento. O processo de segmentação é realizado através da construção de uma malha de estrutura tri-dimensional que cubra toda os dados de imagem de entrada. Em seguida, a malha é deformada, move os nós, a fim de detetar os objetos presentes no local de interesse. Os nós da malha foram distribuídos usando as seguintes regras:

- As distâncias entre os nós nas direcções X e Y são definidas pelo utilizador durante a execução da tarefa de segmentação. As distâncias menores resultam numa maior densidade da malha e maior precisão do resultado final. Estes valores podem ser escolhidos livremente pelo utilizador, correspondendo às suas necessidades e ao cenário de segmentação.
- A distância entre as camadas da malha no sentido Z é definida pelo número de imagens de corte no volume de entrada. Cada corte de entrada corresponde exatamente a uma camada de nós da malha e a distância entre eles (em voxels) não tem que ser transmitida como um parâmetro pelo utilizador. Portanto, a distância real entre as camadas da malha é de facto definida no momento da aquisição da imagem de entrada com o dispositivo de exploração, quando o utilizador define a densidade da digitalização no plano Z.

Durante o processo de segmentação os nós estão autorizados a circular livremente nas direções X e Y, de modo a explorar as informações disponíveis nas imagens de entrada. O movimento em direção a Z não é permitido, porque a progressão de um só pixel nessa dimensão significaria sair da imagem de entrada, e, portanto, perder o acesso a qualquer informação de imagem, que é a única fonte de dados para os cálculos de energia externa.
Embora essa abordagem mostre um bom trade-off entre a precisão e o tempo de segmentação, existem algumas situações em que ele pode vir a não ser bom o suficiente. Para superar esta limitação, o modelo WMD foi ampliado com a funcionalidade do movimento do nó na direção Z.

Movimento 3D dos Nós

Na formulação original do WMD os nós circulam apenas nas direções X e Y. De modo a permitir que os nós também se movimentem na direcção Z foi necessário enriquecer a função de energia original de WMD com o seguinte termo:

$$N_{t+1} = (x_{n+k}, y_{n+l}, z_{n+m}) \tag{11}$$

onde $m \in \{-1, 0, 1\}$ é a combinação de k, l, m correspondente ao valor mais baixo possível da função de energia. Neste caso o valor de m pode significar a distância de um voxel entre os planos consecutivos Z, que geralmente têm cerca de 10 a 20 voxel entre eles. Como podemos ver, a extensa área de movimento vai ser construída a partir de 27 em vez de 9 pontos e o nó

vai mover-se na vizinhança mais próxima nos planos X, Y e Z. Do mesmo modo, a posição com a menor energia será escolhida como a nova posição. Estas etapas vão ser repetidas para cada nó da malha até que a regra final seja atingida.
O processo de segmentação no modelo WMD 3D completo vai funcionar de forma semelhante à formulação original do WMD. A função de energia do modelo, que orienta o processo de segmentação, é definida de forma a assumir os seus valores mínimos quando o posicionamento dos nós na malha se sobrepõe à forma de interesse. A função de energia consiste nas forças internas e externas, que tem a mesma função que o modelo formulado originalmente Whole Mesh Deformation Model (WMD), ou seja, eles são responsáveis, respectivamente, por preservar a estrutura dos objetos e para a aplicação das características das imagens de entrada.
Uma vez que o processo de otimização tem sido significativamente modificado, a função de energia e seus parâmetros numéricos precisam ser devidamente atualizados, para reforçar o comportamento correto da malha. No comportamento pretendido alguns nós da malha movem-se na direcção Z, de modo a construir uma superfície mais suave entre os planos do volume de entrada e, assim, criar um resultado da segmentação mais realista. A fim de reforçar tal comportamento na malha, podem incluir-se os seguintes mecanismos no sistema de deformação malha:

- As ligações da malha devem mostrar uma tendência de encolhimento subtil. Isso irá atrair alguns dos nós e afastar do plano Z em situações em que os nós vizinhos estão localizados junto dos contornos dos objectos de interesse.

- A flexibilidade das ligações da malha deve ser ligeiramente aumentada permitindo a extensão para comprimentos maiores antes que eles sejam interrompidos pelo mecanismo de alteração de topologia. Isto ajuda a atrair os nós a assumir as suas posições entre dois planos Z, onde normalmente permanecem se as ligações deles com os vizinhos for quebrada.

Com a aquisição das características acima mencionadas no modelo WMD, o comportamento pretendido é que alguns dos nós se posicionam entre os planos originais Z criando uma nuvem de pontos, o que vai ligar os contornos dos objetos nos cortes da imagem vizinha e criar uma superfície lisa de transição entre elas.

Cálculo da Energia Externa Fora das Imagens de Entrada

De modo a permitir que os nós da malha se propaguem fora do seu plano Z original, é necessário fornecer um novo modo de cálculo da energia externa, já que os nós deixam de assumir as posições que os dados da imagem de entrada descrevem. A fim de proporcionar esta funcionalidade, os valores para as componentes da energia externa são calculados da seguinte forma:

$$I(N) = I(N_{x,y,z_1}) \times s_1 + I(N_{x,y,z_2}) \times s_2 \tag{12}$$

onde $I(\nu_{x,y,z_1})$ e $I(\nu_{x,y,z_2})$ representa os valores de intensidade das imagens de entrada com as coordenadas x, y, z_1 e x, y, z_2 respetivamente, z_1 e z_2 representa as coordenadas de Z de dois planos entre os quais o nó está localizado, s_1 e s_2 representa os pesos de ambos os valores de intensidade que são calculados considerando o seguinte valor:

$$s_i = dist_s(N_t(x, y, z), N_t(x, y, z_i)) \tag{13}$$

Como podemos ver, as equações (12) e (13) determinam o valor da intensidade do nó $\nu_{x,y,z}$ usando os valores correspondentes aos nós ν_{x,y,z_1} e ν_{x,y,z_2}, que são ponderados de acordo com a distância do nó atual no plano Z aos dois planos que o rodeiam.
Para os restantes dois tipos de imagens utilizados no cálculo de energia (VGF e o detetor de arestas), a situação seria semelhante: para os valores de intensidade calculados entre dois cortes de imagem veríamos uma progressão de graduação dos valores de um corte para o outro. No caso do detetor de arestas de imagens a situação é ligeiramente diferente, porque essas imagens são interpretadas da seguinte forma: um valor diferente de 0 representa uma aresta e as restantes áreas são representas por 0. No entanto, este mecanismo continua ainda a decorrer desejavelmente, uma vez que marca toda a área entre os dois cortes como uma área "não aresta" e, portanto, permite que as duas componentes de energia externa restantes modelem o comportamento do nó nestas zonas.

Mecanismo de Alteração da Topologia Dinâmica Extendida

Com a introdução do movimento 3D dos nós o mecanismo de alteração de topologia foi ligeiramente adaptado para permitir alterações de topologia também eficientes em ambiente 3D completo. Isto incluiu ajustar 1) a estimativa do parâmetro de flexibilidade, e 2) a maneira como o termo de flexibilidade é verificado. Isso foi feito com as seguintes etapas: os comprimentos das ligações entre o nó e a sua vizinhança são verificados da seguinte forma:

$$L_n \leq \frac{G_x + G_y + G_z}{3} \times flex \tag{14}$$

onde $|L_n|$ representa o comprimento da ligação atual, G_x, G_y e G_z são os comprimentos das ligações da distribuição inicial da malha e $flex$ é o parâmetro de flexibilidade.
O parâmetro de flexibilidade é definido automáticamente durante a execução de segmentação no intervalo de:

$$flex \in (1.9; 2.6) \tag{15}$$

tendo em consideração o tamanho das descontinuidades nas imagens de entrada. Este intervalo foi estabelecido experimentalmente, da mesma maneira como na formulação do modelo original WMD. Sempre que um determinada ligação não satisfizer a condição (14) é marcada como quebra.

Conclusão e Trabalho Futuro

Neste resumo alargado foi apresentado um novo modelo de segmentação de imagens em 3D, chamado de modelo de deformação de malha completa. Este método demonstra ser altamente eficiente, dando bons resultados de segmentação em períodos de tempo curtos.

Em comparação com outras abordagens semelhantes, como VTA, o processo de segmentação ganhou uma melhoria significativa em termos de execução. Este é o resultado de uma nova abordagem, que foi utilizada no que diz respeito à representação das formas de interesse, bem como o processo de deformação. Usando esta nova solução, foi possível atribuir uma maior parte dos recursos disponíveis para o processo de deteção de arestas, o qual é uma parte essencial do processo de segmentação.

Todos os componentes do processo de segmentação ficaram mais previsíveis e estáveis. Isto significa que é mais fácil estimar o comportamento do processo de segmentação e prever o tempo de execução e distribuição de carga ao longo do tempo. Esta é uma característica fundamental, pois permite uma paralelização muito eficiente, o que, normalmente, seria muito difícil de obter com outros métodos conhecidos com base na framework de Modelos Deformáveis. Uma paralelização eficiente é uma característica muito atraente, devido às tendências atuais no desenvolvimento de hardware - a introdução de computadores multi-unidades a preços acessíveis, capazes de lidar com 4, 8 ou 16 processos em paralelo, e a introdução de processamento utilizando unidades de processamento gráfico, que são na verdade arquiteturas de processamento paralelo em escala muito grande.

As formas de interesse presente nas imagens de entrada são representadas com uma malha volumétrica, compostas por nós interligados com contornos. Esta malha pode ser definida com diferentes níveis de densidade (mais nós por largura ou altura da imagem de entrada) e quanto maior a densidade mais preciso será o resultado obtido. Normalmente, em soluções semelhantes o aumento da densidade da malha significaria um aumento significativo no tempo de segmentação. No entanto, com o modelo WMD o tempo de segmentação é praticamente independente da densidade da malha. Esta é uma característica muito desejável e também única neste método, uma vez que permite a obtenção de resultados de elevada qualidade, sem a desvantagem de aumentar o tempo de segmentação.

O tempo de segmentação depende também muito pouco do conteúdo da imagem de entrada. Isso refere-se ao facto de que, em cenários típicos de aplicação para algoritmos modernos de segmentação de imagens, o conteúdo das imagens analisadas pode ser imprevisível e os objetos de interesse podem ser distribuídos de forma desigual. Usando a abordagem tradicional dos Deformable Models (DMs) o algoritmo de segmentação tem de expandir ou retrair as imagens de entrada de modo a incorporar todo o objeto de interesse. Isto também significa relocalizar o modelo deformávelda sua área original de inicialização, que significa que, para várias imagens da mesma resolução e tamanho os tempos de segmentação podem ser completamente diferentes. Este não é o caso para do modelo WMD - esta abordagem ao processo de deformação na vizinhança mais próxima de cada nó resultou na quase completa independência do tempo de execução a partir do conteúdo das imagens de entrada.

A dependência entre a interacção do utilizador e a inicialização da segmentação é muito baixa, significativamente menor do que nas abordagens utilizando o mesmo conceito de segmentação baseada na malha volumétrica.

A execução num ambiente de unidade de multi-processamento é simples e oferece um ganho de desempenho quase linear.

Tendo em conta todas as características atrativas listados acima, e também testes em imagens reais, podemos concluir que esta solução pode funcionar muito bem em aplicações médicas. Tem sido capaz de detetar e segmentar objetos em TC, RM e Raios-X de diferentes partes do corpo humano. O modelo WMD pode ser implementado em qualquer plataforma multi-unidade, como computadores pessoais ou portáteis, o que o torna uma solução fácil de aplicar em qualquer consultório médico.

A continuação direta do trabalho realizado com o modelo WMD passa por melhorar as características atualmente implementadas. A otimização das alterações topológicas ou do movimento 3D dos nós pode aumentar a capacidade do modelo WMD para obter resultados precisos em períodos de tempo curtos.
No entanto, devido à elevada extensibilidade do modelo de WMD, também é possível aumentar a capacidade aplicando novas características. Um grande conjunto de novas possibilidades de métodos de segmentação de imagem encontra-se na capacidade de incorporar conhecimento prévio no processo. Isto refere-se ao uso de soluções como Modelos de Forma Ativa [CTCG95], [LU09], [SS12] ou Modelos de Aparência Activa [CET01], [BC10], [TM12] para representar as características típicas de objetos presentes na zona de interesse. Isto permite aumentar bastante a robustez do processo de segmentação a falhas como o ruído ou dados incompletos para aumentar a qualidade global do processo de segmentação. Portanto, a incorporação de conhecimento prévio é um tema muito interessante para a investigação nos futuros desenvolvimentos do modelo WMD.

Contents

List of Figures

List of Tables

Acronyms

DMs Deformable Models. xi, 1–5, 7, 22, 27, 29, 37, 41, 87, 88

FMC Fuzzy C-Means. 25

KNN K-Nearest Neighbor. 14

MAP Maximum a Posteriori. 14

MRF Markov Random Fields. 14

SMAP Sequential MAP. 14

TAV Topological Active Volumes. 4, 5, 7, 37, 87, 88

WMD Whole Mesh Deformation Model. 5–8, 37, 39, 41, 87, 88

Chapter 1

Introduction

1.1 Thesis Focus and Scope

For over three decades medical practitioners over the world have been exploring the advantages of digital image processing applied to medical solutions - and it has proven that is has a lot to offer. The numerous benefit that have been widely used include in particular improvement in the interpretation of examined data, full or nearly-full automation of performed tasks, better precision and repeatability of obtained results and also possibility of exploring new imaging modalities, leading to new anatomical or functional insights. Nowadays it is no longer possible to imagine modern medicine without the support of personal computers and algorithms supporting the physicians in their work.

One of the most important steps involved in the process of medical image analysis is the segmentation procedure. This refers to the task of partitioning an image into multiple regions and is typically used to locate and mark objects and boundaries in images. After the segmentation step the image represents a set of data far more suitable for further algorithmic processing and decision making, which involves tasks like locating tumors and other pathologies, measuring tissue volumes, computer-guided surgery, diagnosis and treatment planning, and so forth.

Since its introduction in the early 80's the branch of image processing applied to medicine has evolved significantly. The earliest solutions have been based on pattern recognition methods and applied almost entirely to two-dimensional (2D) image datasets. This generation of algorithms included solutions like Region Growing and Thresholding. In the following generation we could witness the influence of knowledge-based approaches and application of image models and optimization methods. When these ideas have been explored, methods like Graph Partitioning, Classifiers, Clustering and DMs have emerged. The direction taken in next generation of image processing solutions, which has begun in the early 90's, shows the interest in exploration of knowledge incorporation. Atlas-Based Segmentation, Shape Models and Appearance Models represent the most popular solutions of that period.

One very interesting family of image segmentation algorithms, that has been gaining a lot of research focus, is called the DMs. This group of algorithms is based on the common concept of placing a geometrical object in the scene of interest and deforming it until it assumes the shape of objects present in the input image. This process is usually guided by several groups of forces, which can originate in mathematical functions, features of the input images or other constraints of the deformation process, like object curvature or continuity. DMs represent a range of very desired features, which include a high capability for customization and specialization for different tasks and also extensibility with various approaches for prior knowledge incorporation. This set of characteristics makes the DMs an efficient approach, which is capable of delivering results with good quality of segmentation, robust to noisy and incomplete data. The first work about that subject has been presented by Kass et al. [KWT88a]. These authors have described a method called The Snakes, which proposed placing a single contour in the scene of interest and then subjecting it to deformations until it assumes the shape of the objects present in that scene. The deformations have been constrained by the external and internal energies, which

described the features of the scene and of the contour itself, respectively. This idea has caused a lot of interest in the field of image segmentation in general and in relation to medicine.

The trends in development of image segmentation methods have always been tightly connected with the progress of capabilities of computer hardware and medical acquisition devices. With the improvement of available equipment new possibilities were always emerging, but also new challenges to overcome. After the three generations described above it is possible to see that the current research efforts have been surrounded on 3D medical images, produced by the modern medical scanners. Those devices have advanced through such technologies in 2D imaging as pulsed Doppler [Bak70], real-time B-mode [EJ75] or Digital beamforming [Tho96]. The concept of 3D ultrasound imaging has been introduced in 1950s [HPCH56] as a solution to limitations imposed by the 2D imaging, like the difficulty in analyzing structures lying in planes other than the original planes of acquisition. During 1980s and 1990s the technology in that field has been greatly improved but still stayed limited mostly to research settings due to time consuming acquisition and reconstruction, not optimal image quality, and lack of a clearly demonstrated added diagnostic value. In the last fifteen years the progress in computer architecture and semiconductor technology has finally allowed to support better 3D visualization algorithms, reconstruct volumes as they are acquired and provide visualization at interactive rates. This has initiated a new spectrum of research devoted to 3D/4D image processing and helped adopting these solutions in medical practice [MT99b, MKA+96, DHI92] . In contrast to the 2D segmentation solutions, they allowed to incorporate all information present in the 3D input volume at one instance of the segmentation task and therefore to take better advantage of the available data and produce a more accurate result. They have also allowed to include the available medical knowledge about the dimension and shape of different anatomical parts in the segmentation process.

Before successful application of image segmentation algorithms to 3D volumes, they have been analyzed by a trained expert, who delineated the boundaries of anatomical structures in consecutive slices of 3D images. Also the first algorithmic segmentation methods have operated in a similar manner, namely they have analyzed individual slices in an independent way. This approach made the segmentation process time consuming as well as error-prone. In the absence of feedback in 3D, contours traced in subsequent slices have become mismatched, resulting in unnatural jagged edges that pose a difficulty to applications such as shape analysis [YPH+06]. For this reason the focus in algorithmic development was placed on true 3D processing of medical data, where the objects of interest are represented as three-dimensional volumes throughout the whole process [CKS95a], [MT99a], full or nearly full automation of the process based on probabilistic models of image intensity, atlas deformation, and statistical shape models.

However, processing such large sets of data, like the 3D medical images, presents new challenges in terms of required computational power. At the same time it was possible to note a new trend in the current advances in the field of microprocessors. No longer are we witnessing significant growth of possibilities of single processing unit, but rather a trend towards multi-unit processing and parallelization of the workload. This fact has been such a significant change that the branch of software development devoted to processing on multi-unit architectures has gained a lot of importance and in fact all computationally-demanding algorithms had to be, and still have to be, redesigned in order to take advantage of the available computational power in the modern computers. This stand also true for the medical image processing algorithms.

1.2 Problem Definition and Objectives

The work described in this thesis aims at addressing the problem of modern image segmentation, which we can define as the combination of above-mentioned factors: the significant growth of image volumes sizes, the growth of complexity of image processing algorithms, coupled with the change in processor development and turn towards multi-processing units instead of growing bus speeds and the number of operations per second of a single processing unit.
As said in the previous section, the DMs offer a very good set of features and are a very promising base for the research work in this area. They have gained a lot of research focus and have been already successfully applied in real-world applications. However, despite the large amount of work carried out in this area, they still suffer from a number of drawbacks. Those that have been gaining the most focus are:

- sensitivity to the initial position and shape of the model - without a proper initialization the model might get trapped in local minima and thus not reach the objects of interest or not detect some of their features correctly;
- sensitivity to noise in the input images and to flawed input data;
- problematic topology changing - whenever the scene of interest includes more than one object or when the objects present in the scene contain discontinuities, the DMs need to change the topology of their shape. This is not straightforward in the parametric formulation of the method and requires specific algorithms;
- the need for user supervision over the process.

Some of the above drawbacks have been successfully addressed in an interesting work that has been presented by Barreira and Penedo in [BP05] and further described in [BPAR08]. They have formulated a model called the TAV which has been introduced as a general model for automatic segmentation of 3D scenes. The model has differed from the first methods based on DMs. In TAV the deformed shape was represented with a 3-dimensional mesh, with some nodes being responsible for describing the boundaries of objects and others for modeling their interior structure. The mesh was initialized over the entire image and then converged towards the objects present in the scene. Thanks to the mesh structure the TAV model was able to describe segmented scenes with more detail and more resemblance to the real-world objects. It also showed a very good potential for the topology changing capabilities and solved the issue of initialization thanks to the presence of the nodes in the entire image.
However, the initialization of the mesh was not solved in an optimal way, as it has simply covered the entire input image. Although this assures covering all the objects of interest, it also introduces disadvantages, like starting the segmentation process from the the most distant location possible and also risking the local-minima trap.
TheTAV model is also not well-suited for the execution on parallel infrastructure. This is the result of the composition of the segmentation process and organization of the task in several stages, which need to be executed separately, with every stage beginning only after the previous one has ended. This causes the need for strict synchronization of the workload at several points of the task (namely at the end points of individual stages of segmentation process) and decreases severely the performance gain on multi-processing unit platforms. This problem is very common with numerous solutions (from the image processing area and also others), which have been designed without the consideration of execution on a parallel processing architecture.

In this thesis we present our innovative model for volumetric image segmentation, called the WMD. When designing and implementing the WMD we have set the objective to successfully address the requirements described in previous sections: eliminate completely any reliance on the initialization of the process, allow efficient topology changes and show low dependence on user interaction. Comparing to the TAV solution we wanted to improve also such characteristics as performance, high suitability for effective parallelization and better solution to the initialization problem. By choice of a flexible and parametrized implementation of the energy function the WMD model can be also easily extended with further possibilities, like the ability to incorporate prior medical knowledge using e.g. statistical models.

1.3 Thesis Organization

This thesis is organized in seven chapters.

Chapter 1 introduces the scope of this work. In this part we define the problems to tackle, namely the issued arising from the concept of segmentation modern volumetric images. Later we present our ideas and approaches for addressing those problems.

Chapter 2 presents a thorough review of the most prominent approaches in the image processing field, starting from the early application in the 80's, following the developments of the ideas in the following years, and ending with the ideas developed most recently. This chapter is finalized with a comparison of the most interesting solutions according to the most important features, like the complexity and execution times, sensitivity to noise and incomplete data, ability to perform topology changes, and several others.

Chapter 3 presents the description of the Whole Mesh Deformation model, starting with the background ideas and what it inherits from its sources, namely the DMs family and theTAV. The chapter describes the definition of the main concepts and which innovation the model brings comparing to the original ideas. This includes in particular: the new idea for shape respresentation, the innovative scheme for handling of the deformation process, and the dynamic topology-changing mechanism.

Chapter 4 presents how can we perform a parallel implementation of a segmentation algorithm based on the WMD model and process the workload with several processing unit, assuring an efficient execution and good scalability of the method. As it was stated before, efficient execution in parallel environment was one of our main goals when we have designed the WMD model. In this chapter we present how it is possible to achieve and in which way is it better comparing to other approaches.

Chapter 5 describes in detail a very important feature of the WMD model, the Topology Changing Mechanism. In this chapter we describe the significance of this feature, explain the construction of the idea, the benefits that it offers and how different it is from the solutions presented in related image segmentation techniques.

Chapter 6 introduces an advancement in the WMD model, the ability of full 3-dimensional movement of the nodes in the mesh constructing the segmentation model. This possibility introduces

a better way to interpret the contents of the input medical image and to represent the scenes of interest. We mention again all the main components of the WMD model and describe how they have changed in the poroposed new extension. We also elaborate on the drawbacks of the said feature, which is mainly the extended execution time of the segmentation process.

In Chapter 7 we present our segmentation experiments using the WMD model. We use two types of images for this procedure:

- artificial images used to show the capabilities of the proposed method that are desired in 3D segmentation, namely handling numerous discontinuities in the objects of interest, complex shapes, objects inside of other objects, or uneven distribution of object in the input image,
- real-world volumetric images of high resolution. We use the medical images as a representative test case, as they are particularly challenging and demanding.

Chapter 8 presents the conclusions of this thesis, in which we evaluate the results of our experiments and compare them to related work in the field of image segmentation. We also summarize the scientific contributions of our WMD model and we present the ideas for future work.

1.4 Main Contributions for the Advance of the Scientific Knowledge

The first contribution of this work is the summary and analysis of image segmentation techniques, starting form the very early approaches and ending up at the very latest developments, which have been gaining significant research focus and made their way in real-world applications of medical laboratories. The most important solutions are then summarized in a table and compared with regard to several important features. This work has been published as a book chapter in an IGI-Global series [LPFF11b].
The work presented in the following part of this thesis composes a novel model for 3D image segmentation. It is very well-suited for processing of the modern 3D volumes, like particularly demanding modern medical images, which are characterized by high resolution in all three dimensions and therefore present a very high amount of data to process. This method is based on the concept of DMs and inherits the organization of the model from the TAV solution. However, our solution shows the following desired features, which have not been successfully applied in related work before:

1. The crucial procedure of the segmentation process, namely handling of the deformations of the model, has been redesigned with respect to the model, which was the main inspiration to the WMD model, namely the TAV model. In the segmentation procedure more nodes are allocated into the boundary detection process and to their more optimal distribution. Therefore our method shows a very significant performance gain comparing to other similar solutions. The principle concepts of the WMD model have been described in a conference paper [LPFF09a].

2. The segmentation procedure is predictable and stable. Similarly to the performance gain, this is a result of the redesigned method of shape deformation handling. Such feature allows a very efficient parallel implementation of the segmentation procedure, which would not be possible to obtain with the majority of popular methods based on DMs framework. The parallelization of the workload has been described in two conference papers[LPFF08], [LPFF09c]. The former one presented a description of a initial model for workload paralelization suitable for image segmentation methods based on Deformable Models. The latter paper has already included an implementation of the WMD model and first experiments with its parallelization capabilities.

3. The segmentation time presents a small dependence on the level of detail that we want to achieve by choosing the spacing between the nodes of the mesh. This is a very desirable and also unique feature of our method, as it allows to obtain high quality results without the drawback of increased segmentation time.

4. Segmentation time also presents a small dependence from the contents of the input image - the only factor that defines the time in a noteworthy manner is the resolution of the input image, but also that has much less impact on the segmentation time than in the case of similar solutions.

5. The dependency on user interaction and on initialization of segmentation is very low. This is a result of, aside to the already mentioned new method of shape deformations handling, a very effective method for topology changing. This important feature has been described in a conference paper [LPFF09b].

6. Execution on a multi-processing unit environment is straightforward and offers nearly linear performance gain.

7. An extension of the WMD model has been designed and implemented that allows to process the input images in true 3D environment. This extension has been described in a conference paper [LPFF11a].

The above-mentioned conferences are considered as major conferences in the field of image processing that are organized by the IEEE Signal Processing Society.
Furthermore, the WMD model has been described in two journal articles. One of them introduces the WMD model and provides a description of all its main characteristics [LPFF13]. The second article describes the Extended WMD model, capable of and is currently under review for a journal indexed by the ISI.

Chapter 2

State of the Art Review

Over the last three decades the branch of image processing has evolved significantly and various publications have been presented with the goal of summarizing and evaluating this progress. Several methods for assessing the quality of computer aided segmentation (automatic or not) have been presented in [CK97]. An early work published in 1994 by Pun and Gerig [PGR94] has presented an outline of typical tasks involved in image processing, describing also common problems of such and attempts that had been taken to address them. Approaches that have been presented and discussed include the processing pipeline, image pre-processing [LPP91], filtering [FVB81], early attempts of image segmentation by edge detection [Mar92], [tHRFKV91] and region extraction [JF90], [Mal89], [OD92], matching [AGzN94], [CTWA92] and recognition [KBP+92],[PHA+88]. Similar work, published considerably later, has been presented in [JN00] by James and Nicholas. Authors have described accurately each step of the segmentation process, with its own difficulties and challenges and with various attempts undertaken by respective researchers to overcome them. They also elaborated on key challenges that are still to be overcame and new possible application areas for the field of computer vision. The document has been structured chronologically and researched efforts characteristic to given time period have been described. Those include in particular: era of pattern recognition and analysis of 2D images until 1984 [Alb76]; [YIT80], influence of knowledge-based approaches in 1985 - 1991 [CO07], [KWT88b] and the development of 3D imaging and integrated analysis in later years, which incorporated more specifically: image segmentation [CSD96], [MSV95b], [SD96], [SKBG95], image registration, analysis of structure and morphology, analysis of function (including motion and deformation) and physics-based models. In a recent publication by Withey and Koles [WK07] the authors have presented their classification of most important image segmentation methods in three generations.

In [OS01] Olabarriaga and Smeulders have focused on the automation property in the image segmentation process, discussing on the level of user interaction required by various methods and presenting the progress and trends in this area. This feature is commonly considered to be very important, as one of the main incentives of image segmentation techniques applied to many fields is the minimization of the need for human intervention.

In this chapter we will present and evaluate some of the most important image segmentation methods, starting with the ones presented around the year 1980 and followed with the ideas that have emerged in the last few years. Many of the presented methods have been introduced as solutions for medical image processing. We will also focus mainly on this field, as it is a very challenging one, with image data constantly growing in size and delivering higher and higher amounts of data to analyze. Also the need for precise results and repeatability of the outcome makes this field a very interesting and demanding target of application. Our focus will be directed towards the methods that seem promising to significantly influence the future direction of development for the image processing. The methods will be described and their most noteworthy features will be extracted and compared, using a relative scale to grade their effectiveness in terms of those features. This will help to understand better the current needs in this area and possibly predict which directions should be kept and which should be avoided

when discussing new ideas for the evolution of image segmentation.
This chapter is divided into 5 section. In the next 3 sections we present a summary of 3 generations of image segmentation methods, according to the classification by Withey and Koles [WK07]. We find this classification a very good one, as each of the generations shows a significant level of advance comparing to its predecessor. The first generation encapsulated the earliest and lowest-level methods, including very little or none prior information. Methods based on image models, optimization methods, and uncertainty models composed the second generation. The third one surrounded in general the algorithms capable of incorporating knowledge. The following section presents a group of most recently developed image segmentation solutions, namely those presented after the classification from [WK07] was published. In this section we present the most advanced methods, which were developed as a hybrid approach between two or more previously developed methods, and other variations on modern image segmentation techniques. In the last section we present a comparison of the most interesting image segmentation methods using a set of representative features, like the segmentation speed or the need for user supervision.

2.1 First Generation

Following the classification from [WK07], this group refers to the approaches presented in the early 1980s. A particular characteristic of most of the work carried out during this period was that the researchers were primarily thinking in terms of analyzing two-dimensional (2D) image datasets. Only two significant families of image segmentation methods can be distinguished and described in detail in this generation, as they were the only ones that have delivered compelling results and have influenced the following generations.

2.1.1 Thresholding Methods

This branch describes a group of segmentation methods based on a function that assigns individual pixels to one of two groups based on their intensity value and some predefined threshold value. Hence, as a result a binary image is given, whose one state will represent objects of one group of interests and the other state would stand for the second group. This method serves quite well for the tasks in which used images have their intensities clearly distinguished between objects of interest and the rest, usually referred to as the background. From this basic formulation a significant number of ideas has been developed and the thresholding methods have proven to deliver solutions for various medical problems. The following classification of the threshold methods was proposed in ([MB04]).

Methods that analyze the shape properties of the histogram to determine the optimal value for the threshold. In [WR78] the authors present an example for this method by examining the distance from the convex hull of the histogram, using as the input data a set of infra-red images, not related to medicine. In [Sez85] by Sezan we can see a method based on the analysis of p̈eaks and valleysöf the histogram.

Clustering-based methods, where the gray-level samples are subjected to clustering functions with the number of clusters being always set to two. An important example for this method was presented in [Ots79] where the authors have suggested minimizing the weighted sum of within-

class variances of the foreground and background pixels to establish an optimum threshold.

Entropy-based methods are based on the concept of exploiting the entropy of the distribution of the gray levels in a scene, for example the entropy of the foreground and background regions [KSW85], the cross-entropy between the original and binarized image [LL93], etc.

Methods based on attribute similarity search a measure of similarity between the gray-level and the binarized images, such as edge matching shape compactness, gray-level moments, connectivity, texture or stability of segmented objects [HS88], [Yin95].

The spatial methods use not only gray value distribution but also dependency of pixels in a neighborhood and/or higher-order probability distribution [KR79].

Locally adaptive thresholding methods define the threshold value for each pixel according to the local image characteristics, like range, variance or surface-fitting parameters of the pixel neighborhood [NR79].

2.1.2 Region Growing

Region growing segmentation is initiated with a seed location in the image, which is then enlarged gradually with adjacent pixels by checking them against a predefined homogeneity criterion. Pixels that meet the criterion are included in the region. Continuous application of this rule allows the region to grow, defining the volume of an object in the image by identification of similar, connected pixels.
Ideas exploiting this method include [HK98], where authors have presented an idea for region growing by pixel aggregation with interesting similarity and discontinuity measures. That method was applied to segmentation of MR images of human brain. In [AB94] the authors have presented a region growing based algorithm for segmentation of intensity images which was free of any tuning parameters. The method, however, required the input of a number of seeds, either individual pixels or regions, which would control the formation of regions into which the image will be segmented. An algorithm that combined region growing and region merging was presented in [TB97]. It started with the region growing process which was based on criteria that took into account color similarity and spatial proximity. The resulting regions were then merged on the basis of a criterion that took only color similarity into account. An interesting method was presented in [PL90], where authors have exploited the region growing method together with the edge detection algorithm. The method started with a split-and merge algorithm where the parameters have been set up so that an over-segmented image results. Region boundaries were then eliminated or modified on the basis of criteria that integrated contrast with boundary smoothness, variation of the image gradient along the boundary, and a criterion that penalized for the presence of artifacts reflecting the data structure used during segmentation.

2.2 Second Generation

In the middle of 1980s the research subjects started to surround the area of automatic image segmentation, driven from the low level methods with the introduction of uncertainty models and optimization methods as well as a general will to avoid heuristics. Efforts have been taken

to overcome the main segmentation problems but segmentation results still remained highly dependent from the input data.

2.2.1 Graph Partitioning

In order to perform segmentation with graph-search methods the image is modeled as a weighted unidirectional graph. The image pixels are used to form nodes of the graph and are interconnected to neighbors using the corresponding pixel associations in the image. The cost value of each interconnection is calculated using the measure of similarity between the pixels. Then, the algorithms from combinatorial optimization are used to obtain minimum-cost solutions. A graph cut is a set of interconnections between nodes in a graph which, when removed, partition the graph into two distinct sets. Examples of graph-search based methods include Fuzzy Connectedness [US03], [US96] and the Watershed Algorithm, which has received a high level of interest and numerous works have been presented using variations of this approach. Some of them we present in the following section.

2.2.2 Watershed Algorithm

The watershed transform is a popular segmentation method coming from the field of mathematical morphology. The first attempts to segment images using the watershed segmentation methods have been taken in the early 1980s. The method was created by Buecher and Lantuejoul in their work [BL79], where they presented a possible application of watershed to micrography of fractures in steel and bubbles detection in radiography. But its popularity has risen significantly only around the year 1990, because of the work published in [VS91] (examples of application included segmentation of human vertebral column images) and also due to significant improvement in computational power of machines available in those days. The idea behind the first implementations of this method can be described as follows: taking a 2D grayscale image as the input let us interpret it as if it was a hypsometric map, with the bright parts being the regions of high altitude (hills) and the dark parts being the regions of low altitude (valleys). If we now imagined flooding the region with water, we could observe that it gathers in the valleys and rises until it meets one or more neighboring valleys. Now, we would like to prevent the water from flooding from one valley to another, so we construct a dam of one pixel width and high enough to prevent the water from spilling at any point of the process. This process is repeated until the water rises until the height of the highest hills of the image. If we now consider the dams that we have constructed during the process, they will be representing the segmentation of our image data. The method has been further developed to include prior knowledge incorporation [GMA+04] or operate on 3D data [AR99]. In the modern application it has been also adapted to work aside other methods to solve problems like medical image segmentation. Examples include combining watershed together with graph theory [ZC10], contourlet transform [LLL+11] or active contours [EAUC13].

2.2.3 Statistical Pattern Recognition (Classifiers-Based Methods)

This family of segmentation methods operates by modeling each of the given image pixels as belonging to one of a known set of classes. The decisions are taken based on a training set, which in most cases needs to be manually created as a prerequisite to the segmentation process itself, thus the classifiers-based techniques are considered as supervised. Application of

the training set can be obtain with a number of approaches. The Bayesian classifiers method is among the most commonly used ones, with its functioning based on the Bayes' theorem. Many early approaches to Bayesian image segmentation have used Maximum a Posteriori (MAP) estimation in conjunction with Markov Random Fields (MRF), like the solution presented in [The83], used for terrain image segmentation, and some of more recent solutions included replacing the MRF model with a novel multiscale random field (MSRF) and the MAP estimator with a Sequential MAP (SMAP) estimator derived from a novel estimation criteria [BS94]. Another commonly encountered classifier is the nearest-neighbor method, where pixels or voxels of the image are grouped in the same classes as a representative of the training set with the most similar intensity. The K-Nearest Neighbor (KNN) classifier generalizes this approach, classifying the pixels according to the majority vote of the closest training data.

2.2.4 Clustering

The functioning of clustering methods can be defined as determining the intrinsic grouping in a set of unlabelled data in an unsupervised manner. It is typically carried out by using some measure of difference between individual elements to determine which ones should be grouped into a cluster [WZW+06]. As it can be seen, it differs from the classifiers-based methods because it does not require a training set. This is replaced by iterating between the process of segmentation of the input image and characterization of properties of the each class. In a sense, clustering methods train themselves using the available data.
The k-means methods [CA79] performs clustering of the input image pixels or voxels into a given number of groups, with the objective of minimal intra-cluster variance of the attributes. The process is iterative and it is started with the initial division of the input into sets, which can be done either randomly or using some heuristic data. Then, each of the data sets have its mean point (centroid) calculated and the previous step is repeated, meaning the input pixels are reassigned to the groups, which have the calculated mean point the nearest of their own feature value. These steps are usually repeated until a convergence condition is met.
In the fuzzy c-means clustering method [CP11] the assignment of input pixels to the groups follows a fuzzy-logic formulation, meaning their assignment is expressed with a degree of belonging rather than being assigned completely to one cluster. The segmentation process is performed similarly to the k-means method: each pixel of the input data is assigned randomly to a group, with a random degree of belonging (alternatively, those values can be chosen with some pre-defined method). Then, the centroid for each group is calculated and used to calculate a degree of belonging for each of the pixels, for each of the clusters. The mentioned degree is defined as the inverse of the distance of the pixel from the cluster. Similarly as the k-means method, the algorithm continues until convergence, usually defined as the degree of coefficients change in single iteration. Some important research around this method includes ([WY02]), [SD13] or ([Dun73]).

2.2.5 Neural Networks

We can describe neural networks as massively parallel computing systems constructed from a very large number of processing units of rather big level of simplicity, interconnected with each other with numerous links. The neural network models approach problems presented to them by using organizational principles, namely learning, generalization, adaptivity, fault tolerance and distributed representation, and computation. Those methods are applied in a

network of weighted directed graphs in which the nodes are artificial neurons and directed edges (with weights) are connections between neuron outputs and neuron inputs. The main characteristics of neural networks are that they have the ability to learn complex nonlinear input-output relationships, use sequential training procedures, and adapt themselves to the data [JDJ00]. When trained with suitable image data, neural networks can be used for image segmentation. The basic concept of neural networks segmentation can be usually described as an attempt to simulate the human vision skill, which has the benefit of being very robust to noise and corrupted data. The segmentation task itself can be approached as either classification or clustering problems [BG02]. Modern application of neural networks include approaches like combination with genetic algorithms [mLS08] or experimenting with the The Competitive Layer Model (CLM) [ZZ10], which is an important neural network architecture introduced in 1990.

2.2.6 Deformable Models

The idea of image segmentation using Deformable Models was started by Kass and Witkin in the late 1980s [KWT88b]. The first implementations of that idea included a single contour that was placed in the scene of interests and then subjected to deformations in order to segment the objects present in the scene. The deformations have been constrained by the external and internal energies, which described the features of the scene and of the contour itself, respectively. The external energy was usually calculated using characteristics like image intensities, image gradient or edge detection algorithms, while the internal energy was based on the bending and shrinking/growing capabilities of the deforming shape. This idea has showed to be a very attractive solution that delivers very promising results and at the same time could be modified and extended with new ideas. For that reason it has caused a lot of interest in the field of image segmentation in general and in medical image segmentation in particular. Numerous authors started to propose their modifications from the original formulation, including the geodesic active contours formulation [CKS95b] (applied to brain MRI images) or active contours for segmentation objects without strictly defined edges [CV01b] (tested only on artificial images and pictures) among the most noteworthy ones. The former solution introduced a new way to represent the deformable models themselves and to avoid the need for parametric description of their shape. Instead, the authors proposed describing the model as the zero level set of a higher-dimensional function. This implicit representation solution practically eliminated the restrictions to the shape of the models described in an explicit way and allowed segmentation of complex shapes or detection of more than one object in a scene. The drawback was the increased computational demand of the method.
Solutions derived from the original method formulated by Kass in [KWT88b] used variatonal calculus to determine the solution, more specifically it usually involved solving an Euler differential equation using numerical techniques. A different approach has been presented by Amini and Tehrani in their early publication [ATW88a]. The authors started a discussion about some drawbacks of the analytical solution, which included instability of the evolving contour and its tendency to shrink and to distribute unevenly its discretized domain along the contour line. As a new way to approach the subject the authors proposed a solution based on dynamic programming. They argued that it could address successfully some of the mentioned disadvantages, but unfortunately it also suffered from new drawbacks. The method allowed an introduction of new type of constraints, called hard constraints, describing rules that could not be violated. It also guaranteed the numerical stability of the solution, thus addressing a serious disadvantage of the Kass method. Until then, the iterations that formed the intermediate steps of execution showed

a large level of instability and for the final solution they had to be considered meaningless. In the Amini method the contour approached the final shape in a smooth manner, introducing a larger level of stability and predictability. As for the drawbacks of new solution, it introduced a big overhead in means of memory requirements and execution times. The complexity of the algorithm was at the level of $O(nm^3)$ where n is the number of points in the discretized domain of the contour and m is the size of the neighborhood of each point which is examined for more optimum position in each step. The authors have tested their methods with a set of images of household objects, not related to medicine.
The idea of algorithmic approach was further examined by Williams and Shah in [WS92b]. Instead of using dynamic programming they have proposed a greedy algorithm approach and also introduced some advances regarding the energy function estimation. A greedy algorithm delivered a significant improvement in terms of execution time and memory needs, as by the definition it considers only local information in each iteration. Each point representing the contour is placed in a number of positions and using each of these positions a new value of the total contour energy is recalculated. Then the position that corresponds to the lowest value of energy is chosen as the new position of the point. Note that this approach does not guarantee that the resulting solution will be the globally lowest one. However, authors argue that the tests of their method have proven its ability to deliver results very near to those of the dynamic programming version and the performance gain compensates those lacks. The tests have been also performed on images not related to medicine.
Authors have also analyzed the original formulation of the energy function and discussed about possible improvements. In their opinion the continuity terms have been formulated in a way which causes the contour to shrink and to become irregular, because the points tend to gather around specific locations instead of being evenly distributed along the contour. Moreover, when introducing their greedy algorithm to operate on the original formulation they discovered that the unwanted effects tend to become even stronger, because of the nature of the greedy algorithm, namely considering only local information in each iteration. This motivated them to propose a new formulation for the continuity terms, which instead of relying on difference between each two points in the contour, calculated the difference between this distance and the mean distance between all the points in the contour. This introduced a behavior of even distribution of the points and eliminated the shrinking tendency of the contour. To improve the precision of the contour on its sharp edges the authors have introduced new methods of curvature estimation (they propose five different solutions in their paper [WS92b] and used them to detect locations to which the points should be attracted. This was achieved by relaxing the second-order continuity constraint at high curvature points. The results of experiments performed by the authors have showed that in terms of execution times the greedy algorithm performs better than the dynamic programming method, reaching execution times near of those of the variational calculus, while maintaining all of the advantages of the Amini method, being stable and flexible for introducing hard constraints.

2.3 Third Generation

The second generation of image segmentation methods has provided a rich field of ideas and experiments. The results, however, were still not sufficiently accurate and reliable to allow for a wide incorporation of these methods in real-world application. In the early 1990's this started to change thanks to the growing influence of the knowledge-incorporating image segmentation

methods.

2.3.1 Atlas-Based Segmentation

Atlas-based segmentation methods applied to medical images take advantage from the similarities between matching anatomical parts of different individuals. However the variation of shapes and sizes exists, still the corresponding organs will always show a set of common features and allow their classification under a single label. This allows describing them with a set of characteristics that would allow in turn recognizing them in medical image data.
Atlas-based segmentation is usually based on a reference set of contours or volumes that roughly represent the objects of interest. This atlas data is applied to the image data and subjected to global and local transformations which lead in the end to adjustment of the initial shape to fit the objects present in the medical image data and therefore to segment the desired objects. In the global transformation stage the entire reference data from the atlas is modified using the spatial information (i.e., relative positions) of various parts of an atlas. In this step the similarity [DHT+99] and affine [RLVC+02] transformations have been used in previous publications (applied to heart and head MR images). In the local transformations part usually an iterative optimization of the atlas objects using various types of representation is performed to describe their shape and deformations. Examples include the affine transformations and 2nd-order polynomial transformations published in [CJPM+96] and applied to segmentation of MR brain images, or the B-splines and thin-plate spline constraints used in [HBM03] for segmentation of abdominal images. The data represented in the atlas can be described either in a probabilistic or non-probabilistic way. The probabilistic solution can characterize more accurately the variation between the shapes of organs of different individuals but it requires a training set. After the registration step also a classification procedure can be performed, assigning each pixel to a most probable anatomical part, enforcing the overall precision of the segmentation process. This is usually desired, as the registration procedure itself is usually not accurate enough. However some unwanted results can be imposed by the classification procedure, as sometimes in this step it is not possible to distinguish various regions of similar intensity and texture.
Authors in [DLW05] have presented an interesting solution, able in their words to segment 3D CT volume images using a single 2D atlas. Their method used an atlas containing a set of closed contours, representing various human body parts. The atlas was constructed manually, from reference CT scans. The global transformations step was performed by first constructing a target contour with straightforward contour tracing from the acquired image data. Next, the data from the atlas image was compared with the result, the correspondence between the reference and target shapes was considered and the transformation matrix was computed. Applying this matrix to the target image would transform the target shape in a way making the centers of the reference contours fall within the corresponding body parts in the target image. Then, the local transformation was performed by searching in an iterative manner the local neighborhoods of reference contour points to find possible corresponding target contour points, using features that are invariant to image intensity.
The final step was the contour refinement using the Snakes method [KWT88b] enriched with Gradient Vector Flow [CJ97]. The results of this three-step segmentation technique are promising, as the authors have stated in their paper. The accuracy of the segmentation was measured in terms of the area of intersection between the target body part (that was obtained manually) and the segmented regions. The results of particular experiments depended on the number of

slices participating in the segmentation process and on the part of body that was being segmented, as these two factors can define how much the slice images differ from the reference image present in the atlas. The method executed on liver was showing the similarity index on the level around 0.95 and around 0.9 for the spleen, which proves it to be successful. As for the execution times, the authors have not stated them in their document, but analyzing the construction of the algorithm we can assume with high probability that they showed rather good performance. These results are also very promising when considering the approach that the authors have taken, namely performing segmentation of 3D images with only 2D atlas information. Only single reference shape is required to perform segmentation of a large number of slice images and considering the results published by the authors, it is done with high success rate. The mechanism is constructed in a way that uses the same reference shapes for the initialization step and only differs in the deformations stage to fit to different image slices. Naturally, this means that the success rate will be smaller in those slices, which vary more from the reference images.

2.3.2 Shape Models and Appearance Models

A solution called the active shape model (ASM) was developed on a foundation of DMs, extending it with a powerful mechanism of prior knowledge incorporation. It takes advantage of the fact that the medical image segmentation task often includes repeating the same processes on very similar sets of input data. For example MRI images of human brain will always show features similar to each other, not regarding the acquisition device or the individual that served as the scanned object. Those similarities will be even stronger if we will consider a single acquisition device used on a number of different individuals. This is why an important possibility to improve the outcome of the segmentation task lies in incorporation of prior knowledge about the expected features of the segmented object.
The methods based on active shape models usually describe the objects of interests by identifying a set of marker points on the edges of an object and examining the differences in their distribution between all the representatives across a set of training images [THCH93]. This process results with creation of a statistical representation of the given object's features, which in turn allows discovering these objects in a scene. Another important advantage is the enforcement of the deformation process, because the shape changes are restrained to the boundaries of the statistical model.
In [SD92] by Staib and Duncan we can find a method of knowledge incorporation with an elliptic Fourier decomposition of the boundary and placing a Gaussian prior on the Fourier coefficients. Their method was tested both on synthetic and on MR cardiac images. In [LGF00] Leventon proposed incorporating shape information into the evolution process of Casselleśgeodesic active contours, what they have applied to segmentation of three dimensional models of seven thoracic vertebrae. Cootes and Beeston [CBET99] in turn incorporated the prior knowledge about shape and texture for segmentation of MR brain images via deformable anatomical atlases. Extending the active shape model with further information, namely not only about the shape of the object, but also about its intensity, the active appearance model (AAM) was created [TGC01]. An interesting idea was introduced in [YD03] by Yang and Duncan. The authors have examined a rather general feature of 2D MR brain images, namely the gray level variation. The model was based on a MAP framework using the shape-appearance joint prior information and the segmentation was formulated as a MAP estimation of the object shape. The need for finding point correspondences during the training phase was avoided by using level set representation

of the shape.
In [GFL04] Grady and Funka-Lea have presented a semi-automatic method of medical image segmentation using Graph-Theoretic Electrical Potentials applied to CT cardiac data and MR brain images. It assumes that the input information apart from the medical imaging data would include a set of seed points, pre-defined by the user and a set of labels, describing those points. Using this information it would be possible for each unlabelled voxel of the image to estimate a certain value expressed as follows: taking current voxel in account and assuming that a random-walker algorithm would start from this location, what would be the probability that it first reaches each of the labeled seed points? This probability would be obtained with theoretical estimation, with no simulation of random walk. For each voxel of the image a vector of probabilities was then assign, including the above described likelihood for each of the existing labels. The segmentation was performed by assigning each voxel to the label with the highest possibility of encountering. The authors have tested their method on CT cardiac data and MR brain images. The results show that the rather simple assumptions taken by the authors when formulating their method have led to a set of very desirable features, like the ability to detect weak object boundaries and respect the pre-labeling choices of the medical practitioner. Also, the method proved to guarantee that the segmentation will be smooth, with no pixels left out without a classification to one of the existing labels and no discontinuities will be encountered. There was however no information about the execution times of the algorithm.
In [SSP05] Shen and Shi have suggested that the level of precision offered by standard shape models is far from desired and the problem is rooted in its formulation. Because it usually uses a training set of sample segmentations to construct the statistical model, the solution has to apply some type of averaging mechanisms to describe the set of features of our interests. This leads to loss of high-frequency information, like sharp edges and similar details. In order to improve the possibilities of shape models the authors have introduced a method which uses a mean shape template to describe the general features of objects of interest and a separate parametric model to describe high level features, like intensity edges, ridges, and valleys along with information about their location. Performing some experiments on high-contrast CT images of complex organs the authors have obtained a good segmentation, matching in high level the reference samples provided by a human expert.
Shape Models and Appearance Models are used widely in modern image segmentation problems. Lee and Elgammal have used non-linear factorised shape and appearance model for facial expression analysis and tracking [LE12]. Ayman et. al. [EBG08] have described a very interesting method that combines DMs, Markov-Gibbs random fields for the appearance prior and a linear combination of vectors of distances for the shape prior. The evolution of the Deformable Model is based on solving an Eikonal partial differential equation. The resulting method has been applied to segmentation tasks of various medical images and shows a considerable performance gain comparing to other known geometric and parametric models.

2.4 Most Recently Proposed Solutions

After the Third Generation of Image Segmentation Methods we could see a trend towards increasing complexity and implementation of advanced methods, which could take advantage of the modern image acquisition devices and powerful processing units as the execution environment.

2.4.1 Marker-Based And Knowledge-Based Watershed

The simplicity of the Watershed Algorithm has been one of its main advantages, as it allowed performing a relatively successful segmentation without the need of any parameters, prior knowledge or user interaction. However, with the growth of demand for precise segmentation the drawbacks of this approach have started to be more noticeable. Since the segmentation process depended strictly on the image data any flaws in those would have to be automatically imposed on the segmentation results, thus the high sensitivity to noise and incomplete image data. Also, the very high tendency for over-segmentation was often criticized. As said before, introducing some level of prior knowledge into the segmentation process can help counter these limits and increase the accuracy of the results.

One of the first successful mechanisms to incorporate knowledge in the Watershed Algorithm was the introduction of markers, resulting in the Marker-Based Watershed. This general name refers to an approach where the user provides information about the desired number and possibly location of regions in the segmented image by placing some markers in the scene [JFSD92]; [VS91], [LPW12]. Further extending the method with spatial prior knowledge resulted with Knowledge-Based Watershed algorithm [Bea06] which introduced a way to constrain the growing of the markers through the use of structuring element-based distance functions. Thanks to these improvements the mentioned methods managed to deal with noisy or incomplete object boundaries. In a recent publication [Lef07] Lefévre has introduced a new formulation for the marker introduction based on a feature calculation and pixel classification. Their method has s performed well, segmenting color images of size 481x321 pixels in about 15 seconds, with significant improvement in the quality of obtained segmentation comparing to the traditional methods. The tests however are rather poor in their nature, as they have been performed with images not related to medicine, using a portable computer. In [DET07] the authors have combined the Watershed segmentation and the Active Contour Model known as Balloon Snake, introducing a new image segmentation technique called Water Balloons.

2.4.2 Two Stage Methods - Based On a Coarse Approximation and Refinement

The method based on minimal paths algorithm used together with 3D deformable models targets in improving the performance and segmentation precision of DMs. It was presented by Ardon and Cohen have in [ACY05] and then further described and extended in [AC06] and [ACY07].

Following the assumptions of the authors, the method requires some user interaction in the first stage of the process. For each sequence of slice images it is necessary to manually segmented two of them, so the interaction of an expert is required for each case of segmentation. As a simple example the authors have presented in their document a 3D shape of a vase, which was described with two curves - one on the top and one on the bottom. The possibilities are however wider, for example the two slices can be perpendicular to each other, usually delivering more information about the object to segment and introducing the chance to segment more complex objects. Those two manually segmented slices will deliver then the information to construct the constraining curves for the object to segment. Between those curves a network of paths will be created using gradient descent technique. Those paths will be following the object of the segmentation. To create them the constraining curves are discretized to a finite number of points and for each point in curve c_1 a minimal path between itself and another point in curve c_2 is found. Those paths are minimal with the respect to a potential that takes small values on the object's boundaries[AC06]. The main idea is to produce a path that maintains a balance

between reducing its own length and following the points of low values of the cost function (so in fact following the shape of the object in question). When the search for minimal paths is finished they are then used to construct a surface through interpolation of the network.
As it is possible to see, the above described method assumes a high level of simplification and approximation of the surface in question. It results in good performance and low execution times, but presents a poor segmentation precision. That is why the authors propose next to adjust the segmentation with the application of level set method. In fact, the minimal paths method can be simply perceived as the solution to the initialization problem for deformable models. With its application the resulting model, which will be subjected to the level set method, is already a very near approximation to the final shape. This can improve very significantly both the execution times and the precision of the results comparing to the original idea, which assumed commencing the deformation process from a basic shape, like a sphere or a cylinder. Authors show in their experimental results that in fact both this goals have been obtained - they managed to minimize significantly the number of iterations that were necessary to obtain a stable state of the model and they minimized the chance of obtaining a local minima error, because the model is always initialized very near to its final position. They also managed to successfully segment some scenarios that have failed when subjected to segmentation with a cylinder as the initial shape. This included for example a complex shape consisting of three s-shaped tube objects placed one inside another. The initialization with a single cylinder shape resulted in wrong segmentation, although the level set formulation is capable of topology changes and it detected more than one object in the scene. The result was still quite far from the desired after 150 and after 500 iterations, whereas using the 3D minimal paths solution for the initialization the authors obtained a precise segmentation only after a few iterations of the level set model. Another example of application presented by the authors was segmentation of the left ventricle from the 3D ultrasound images.
The advantages of this initialization method over traditional initialization can be clearly visible. Its main drawback is probably the need to perform two manual segmentations for each scenario.

2.4.3 Parallel Genetic Algorithm Refinement Method

Another two-stage approach for the segmentation problem, including steps of a quick approximation and then shape refinement with more precise method was presented in [FJD02] by Fan and Jiang. As we can see, this is similar to the 3D Minimal Paths approach presented by Ardon and Cohen, although only the general concept is analogous. The quick approximation method involves using a dynamic equation based on finite differences method. Formulation of model energy is enriched with a temporal parameter and thus reconstructed into an evolution equation, in which an estimated surface is used as initial data. Solving that equation results in a fast but coarse descriptor of the object in question. A series of those is then used to generate an initial population to the next step, which is namely surface refinement using a parallel genetic algorithm. Again, we can see a similarity with the idea introduced in [InBSP06], although the genetic algorithm is formulated in a slightly different way.
Authors have used an idea of a parallel genetic algorithm presented in [MSB91], which is a relatively recent addition to the evolutionary algorithms family. It has however proven to be a strong optimizer, capable of delivering results superior to the traditional genetic algorithm. Broadly speaking its main new feature is the fact that several populations are evolving in an independent manner and migration operator is defined to assure the exchange of information between those populations. The usual scenario assumes that the healthiest individuals are

chosen to be transferred to neighboring population and likewise the healthiest are received to replace the worst ones. Experimental results since the introduction of this concept have shown promising abilities of this formulation. Authors have tested their solution on brain images obtained from the Brainweb project [CZK+98]. In another publication by Kanungo et. al. [KNG10] the parallel genetic algorithm has also been used to perform image segmentation by optimal thresholding.

2.4.4 Hybrid Methods

Numerous solutions proposed by different authors have been based on attempts to combine the possibilities of region-based and boundary-based methods. Those are generally referred to as the hybrid methods and they usually consist of a model formulation to represent the shape and the features of the object in question and of a set of object characteristics to improve the segmentation process [MT04], [ODJG98], [RPM06], [TWMM07]. This is however a generalization, as the attempts to combine the advantages of several segmentation methods have been taken frequently and with many various approaches.

Metaxas and Chen in [MT04] have pointed out that the integration of region-based and boundary-based methods is usually difficult because the region-based methods developed at that time offered very limited possibility to incorporate the information provided by the boundary-based methods. With their research started in [CM00] and continued in [MT04] and [CM03] they tried to address this issue using the following scheme: a Gibbs Prior Model was prepared from the MR brain image data and default parameters, serving as a base boundary information. Next a 3D mesh was constructed from a series of those 2D masks, using the marching cubes method. Finally, the structure of the 3D mesh was sculptured more precisely using the Deformable Models and this final model is used to estimate the parameters for the Gibbs Prior Model, which would replace the default parameters used in the first iteration. This method used a combination of 3D and 2D data to construct its outcome, which could impose some level of inaccuracy because of frequent transitions between two and three dimensional scope. In [RPM06] Rui and Metaxas have suggested a new method with a similar idea and the same input medical image data, but using a fully 3D definition of the Deformable Models, which resulted in a much more robust smooth surface segmentation.

Yifei and Shuang in [YSGD07] have proposed a solution created from a combination of the morphological watershed transform and Fuzzy C-Means (FMC) classifiers. Thus, like most common hybrid solutions, the proposed method integrates the edge-based and region-based techniques. The advantages of the watershed technique applied to medical image segmentation are its simplicity and intuitiveness. It can be also parallelized easily and it always produces a complete segmentation of the image. It is however rather sensitive to noise, it has problems with successful detecting of thin objects and the delivered results are often over-segmented. On the other hand, the FMC algorithm classifies the image by grouping similar data points in feature spaces into clusters. This unsupervised technique that has been successfully applied to feature analysis, clustering, and classifier designs in the fields such as astronomy, geology, medical imaging, target recognition, and image segmentation. Its disadvantage is the fact that it does not deal with the problem of intensity inhomogeneity.

The method proposed by the authors operates in three steps. First, the original image is subjected to dilation-erosion contrast enhancement. This allows obtaining well defined object borders, which can help greatly to improve the outcome of the watershed algorithm. Next, the watershed algorithm with internal and external markers is applied. The result returned

by it is then subjected to a post-processing stage, namely applying a 4-connectness pattern, which helps to get rid of some misleading boundaries. At this point the image represents a set of regions, which are subjected to fuzzy c-means clustering, in order to connect them and eliminate the over-segmentation effect of the watershed transform. The authors have tested their implementation over 80 lung images and compared the results to the ones obtained by the watershed and the c-means algorithms, used apart from each other. The segmentation obtained with the hybrid algorithm has shown a much better level of similarity to the manually performed reference segmentation. There was however no information about the possible overhead in execution times.

Another recent publication presented a slightly different approach to the concept of hybrid methods. The authors in [HY05] have introduced a two step method of medical image segmentation, which they have applied to MR brain images. In the first step a coarse approximation of the shape would be done using the fast sweeping evolution method based on the image gradient information and the result of this initial segmentation would be enlarged to a local region zone using morphological dilation. In the second step a dual front evolution model would be used to achieve the final boundary.

2.4.5 Implicit and Explicit Deformable Models Representation

As mentioned in the previous chapter, the idea of Deformable Models has been well received amongst the researchers and various ideas about possible improvements have been suggested. One of the most significant subjects has been the discussion about the way in which they are represented. The mechanisms used to describe the segmented shape always influence in big part the segmentation process, as they are responsible (fully or in some part) for features like the ability to perform topological changes, the speed of deformations, the flexibility of the object and some others. In the original formulation of Snakes [KWT88b] and in other publications [TWK88] the parametric representation was introduced, which assumed describing the curve with a set of points, holding information about their coordinates. It was a simple and effective approach but in some solutions the offered possibilities have been not sufficient and representing a shape with a high level of detail required using a big number of points, which was not effective. Different explicit approaches to deformable models representation include the methods based on a B-spline [PB02], which allowed describing even shapes of high complexity in a precise and smooth manner and with a limited number of points. That method has been applied to complex scenes segmentation, such as live images from video cameras.

A very important effort to improve the possibilities of shape representation has been taken by Caselles and Kimmel in [CKS95b] by introducing the Geodesic Active Contours. This solution was based on an implicit deformable models representation, namely the levelsets. The implicit representation was later adapted in a number of successor works [CK96]; [MBMC01], [SR09], [MPP12] and became an important milestone in improving the possibilities offered by the Deformable Models. The features offered by the implicit and explicit representations have been summarized and compared in a number of publications [GLBr99], [MD00] and in recent publication by Lingrand Montagnat [LM05] a comparative study of implicit and explicit deformable model based methods was performed using authors' own implementations and concrete examples of data, illustrating the differences between the two approaches.

2.4.6 The Active Nets

In contrast to active models based on contour evolution in [TY89] Tsumiyama and Sakaue have proposed a solution that used active nets. This idea was then further researched and developed by Ansia and Lopez in [ALPM00]. This solution assumed that instead of evolving a contour the image would be covered with a discrete mesh. The nodes of this mesh would be incorporating the whole image and each node would have the ability to move in a predefined neighborhood, thus evolving the shape of the whole mesh. Based on the boundary information all nodes would be classified into two categories, internal and external. The former ones model the inner topology of the object while the latter perform more similarly to the active contours, trying to fit to the edges of the object in the image.

This solution had the goal of combining together the features of region-based and boundary-based segmentation techniques. It managed to give an answer to some fundamental issues of DMs, like the initialization problem and the ability to change shape topology. The latter feature allows to segment more than one object in the scene and to detect holes and discontinuities in object bodies. Similarly to the original formulation, the model deformation was controlled by an energy function, which was defined in a way to acquire minimum values when the mesh was placed over the objects of interests. The internal energy depended on first and second order derivatives of the energy function, which controlled contraction and bending features respectively and they were estimated using the finite differences technique. The external energy was described as representation of the features of the scene that guided the deformation process. As a broad outline, in the original formulation the adjustment process consisted of minimizing those functions with a greedy algorithm. The energy of each point of the grid was computed in its current position and its nearest neighborhood; the position with the lowest energy was then chosen as the new position of the point. When no point could be moved to a more optimal position in its nearest neighborhood the algorithm was stopped.

As it can be seen, using a greedy algorithm to solve the optimum finding problem introduces the risk of stopping at a local minimum instead of the global one. This issue was further examined in [InBSP06] by Ibánez and Barreira and new optimization techniques were introduced, namely a genetic algorithm. Authors have used a standard approach for genetic algorithms presented in [Gol89], introducing their own solutions for crossover, mutation, spread and group mutation operators. They also enriched the original energy function with a new term for external energy calculation. It took into consideration the distance of the node from the nearest edge of the object in image. Running experimental segmentations the authors have decided to perform them in a very precise way, using large population sizes, thus the resulting execution times have shown to be very large comparing to the greedy algorithm version. Authors have however obtained a very significant improvement in terms of reliability of their method. It managed to successfully segment objects in scenes (using images of artificial shapes) with which the greedy algorithm has failed completely due to bad initialization, bad parameters for the energy function or to highly noisy images. Recently the authors have presented the Extended Active Nets [BIC13], enriched with the Scatter Search - a global search internal energy term, which improved the previously local-only search abilities of the Active Nets.

2.4.7 Topological Active Volumes

Topological active volumes model was proposed in [BPMA03] by Barreira and Penedo as an extension of the active nets model into 3D world, applying it to the task of segmenting CT slices

of the femur. The authors have again emphasized the valuable features of active nets that solve some inherent problems of deformable models, namely the insensitivity to bad initialization and integration of region and boundary information in the adjustment process. Also the ability to perform topological changes was considered as a valuable feature, allowing the TAVs to detect two or more objects in the scene, model holes and discontinuities in the objects and also adjust themselves to the areas where greater definition is required. With these characteristics the topological active volumes have been a promising solution for the 3D segmentation.

A topological active volume (TAV) has been defined as a 3D structure composed by interrelated nodes where the basic repeated structure is a cube [BPMA03]. Therefore the TAV model is based on a mesh structure, which is a 3D equivalent of a net and is commonly used for 3D shape representation for in numerous areas [PA02], [Del94]. Similarly to the Topological Active Nets, the deformation process was governed by an energy function, with internal and external energies responsible for characteristics of the model and of the scene, respectively. The internal energy estimation has been performed using the finite differences technique in 3D. Also the external energy definition did not change comparing to the topological active nets formulation and also the structure in question was described with internal and external nodes.

The authors have performed their method tests also on artificial noisy images. The behavior of the model was organized as follows: covering the entire 3D structure with the volume; detecting the number of objects of interest; adjustment and description of the objects with energy minimization using local information. In contrast to the active nets model, here each node of the mesh was tested in 26 of its neighbor locations for optimal energy as a natural consequence of operating in a 3D environment. Once the mesh had reached a stable situation, the process of readjustment of the mesh began, the connection breaking was performed and the minimization was repeated. Authors state that the model is fully automatic but on the other hand they formulated its cost function to be dependable from six different parameters, so actually some level user interaction is required. The results obtained for images with the size of 256x256x80 included about 20 minutes of segmentation time. If we compare it to the results obtained with active nets in [InBSP06] we could see that the execution time is significantly larger. The results obtained with active nest using a greedy algorithm, which was also used with active volumes, have varied from 5 seconds to 60 seconds. It is difficult to compare the complexity of the images used in both cases, because in [InBSP06] the authors only refer to the images that they have used as simple ones (giving about 5 seconds execution times) and complex ones (giving 30-60 seconds execution times).

As we can see, with the introduction of 3D images we can see a significantly worsened performance. This is due the fact that not only we need to process significantly larger datasets, but also we have to operate in a 3D environment and perceive the scene as a volume, not a flat image. The result of this can be seen starting with the fact that no longer we operated on 8-pixel environment for each node of the mesh, but 26-pixel one. Also the estimation of the energy of the model becomes more complex, as we need to consider a significantly larger model, with more nodes and more values to calculate. If we take a look at the results obtained in [InBSP06] using genetic algorithm, we could predict that probably porting that solution into 3D would result in even larger execution times. Authors have however agreed that future work with their method should include experimenting with more advanced optimization techniques, which should help to shorten the execution times. They have addressed this matter in [NBPS12] by presenting a new optimization method of the segmentation model that uses Differential Evolution as an alternative evolutionary method that minimizes the decisions of the designer with respect to others such as genetic algorithms. Also a hybrid method was presented that com-

bined Differential Evolution with a greedy algorithm approach, to integrate the advantages of global and local searches and at the same time improve the segmentation speed. Most recent work on this model includes [BPAR08], where the authors have presented an updated version of the topology-handling mechanism, and [NSP13], where they performed a combination of differential evolution and a multiobjective approach for the optimization of TAV.

2.4.8 Deformable Organisms

As it can be seen in [MT96b]-[MLM+05] the problem of prior knowledge usability has been addressed in numerous publications. It has been proven that using information about certain features that are common to a group of objects of interest and are know before the segmentation process, can give a broad view over the problem and help in deciding which encountered characteristics are desirable and which are not. This can significantly improve the robustness and precision of the segmentation process, making it less vulnerable to corrupted or incomplete input data. Typical solutions for prior image incorporation include calculating vectors of characteristics or formulating statistical models describing the features of interest [MD00], [FS06b].

In [HMT01] the authors have proposed a different perception of how the DMs can be influenced to behave in a desired way and to take advantage of the prior information about the structures of interest. They have constructed the Deformable Organisms model, which combined the classical approach to deformable models with a decision making mechanism based on the solution of same authors called the Artificial Life [Dem99]. The idea was to significantly improve the automation of the segmentation by eliminating the need for human supervision over the whole process.

The model that they proposed was a layer-based architecture, where the higher-level layers had the knowledge about the state and control over the low-level parts. This means that each layer was responsible for some primitive functions, which could be managed by the layer above it. This relation has been repeated recursively over the following layers, resulting in a well-defined and manageable hierarchy between them. At the base of this model authors used a geometric modeling layer to represent the morphology and appearance of the organisms. Following, the physical modeling layer incorporated some principles of biomechanics to control the geometry and simulate biological tissues. Next, the motor control layer, which was responsible for internal muscle actuators in order to synthesize lifelike locomotion. The following layer controlled the behavioral and perceptual capabilities, to provide reactions to environment conditions and other organisms. At the top of the scheme we could find the cognitive layer, responsible for simulating the deliberative behavior, ensuring that the organism is aware about itself and other organisms in the environment, how it acquires and responds to knowledge and how its reasoning and planning processes can help to reach its destination [HMT01].

As we can see, the model was defined as far more complex, than in case of traditional deformable models. Comparing these two approaches we can see that the traditional model included only the definition of the geometric and physical modeling layers. In more complex solutions we can see also the introduction of prior knowledge, which can successfully constrain the shape during segmentation process, to better correspond to the actual objects. However, this solution still lacks the awareness ability, meaning the deformable models do not have the knowledge about their position in the scene and also their actions are always guided by local decision making. This means that the decisions cannot be seen as parts of a global intelligence but only as simple choices that do not directly affect the following decisions or the decisions of

other models in the scene. Organisms created by the authors in their study have been called the deformable worms. As the name suggests, they have been imitating simple bodies, described by four medial profiles. Those profiles described respectively: the length, the orientation, the left thickness and the right thickness of the body. Using this features the authors described a way of controlling their shape using the multilevel scheme described above, defining for example the following operators: for the basic geometric representation - bending and stretching; for the motor system - moving a bulge on the boundary, smoothing the boundary, stretching/bending at certain locations; for the perception system - sensing image intensity, image gradient, edge detecting; for the behavioral system - finding specific regions of other body of the organism, latching to specific parts of other organisms, thickening right or left side of the body.
Authors have released the deformable worm into a 2D MRI brain image and argued that it progressed successfully to achieve its goal. They present images of the segmented structures and point out that the precision is very satisfying and their framework performed just like it should. Unfortunately, they do not present any execution times, so it is unknown how effective this method is in terms of execution times.
Recent references to this idea include [MH06a] and [MH06b] by McIntosh and Hamarneh. In those publications the authors have introduced artificial life forms called vessel crawlers and spinal crawlers, respectively. Those deformable organisms have been constructed for the purposes of segmentation particular human organism parts, meaning the vasculature system and the spinal column. They were build upon a 4-layer based system for artificial life representation, including the geometrical, physical, behavioral and cognitive levels. Both those solutions have been constructed in a way to incorporate information about the body parts of their interests, namely the geometrical properties of the tubular structures (for the vessel crawlers) and the human spinal cord (for the spinal crawlers). The results produced by those methods has shown that thanks to their high configuration capabilities it is possible to define their behavior in a very precise manner and obtain very promising results in situations where segmentation is a complex procedure (spinal column and vasculature system both fall into this category). The spinal column segmentation has been compared to a level-set method and has proven to be more effective, resulting in 10 minutes execution times for a 256x256x60 MRI volume with a very low level of user interaction. The same volume required 30 minutes and a significant level of user interaction using the level-set method. As for the vasculature system segmentation, the authors have focused on presenting the capabilities of their solution to operate with such a complex, branching structure. Comparing to other solutions, the vessel crawlers have presented a great improvement in terms of proper object detection and the precision of results.
In [PJT+11] Prasad et. al. have used the Deformable Organisms to perform segmentation of brain from non-brain tissue within magnetic resonance images of the human head, also known as skull-stripping. The method has performed very well at delineating the area around the medial longitudinal fissure (the groove separating the two hemispheres of the brain) and the anterior part of the parietal lobe when compared to the other algorithms like the Brain Extraction Tool (BET) and Hybrid Watershed (HWA).

2.5 Evaluation of Selected Methods

In this section we present a detailed comparison of a selection of methods described in sections 2.1 - 2.3. The choice of methods has been performed in the way to present all the noteworthy models and ideas, that have proven to deliver good segmentation and at the same time have

inspired in large part the development of next generations of segmentation models. Of course we needed to limit the selection to the methods, which were presented in enough detail to be able to take some conclusions regarding their features.

2.5.1 Selection of Features

The selected methods described in sections 2.1 - 2.3 have been characterized using a set of features described below. Those have been selected in a way to allow proper definition and evaluation of the most important characteristics of a given method, which in turn would allow an evaluation of the whole method and provide some level of comparison between different methods.
This selection of features has been performed considering the most common way in which the respective authors describe their methods in existing publications. Usually a description of this kind involves a set of experiments and a presentation of the results with careful examination and explanation of the outcome. Observing those we could notice that the features that guarantee the best evaluation are composed from similar to the below presented selection:

Sensitivity to parameters - this describes the reliance of segmentation result from a good selection of parametric values for the method. Those values typically describe the deformable features of the model, like stretching and bending capabilities, its behavior under specific circumstances, etc. High dependability from the parametric values, as well as big number of values to define, are undesirable, as this introduces the need for high level of user interaction.

Sensitivity to initialization - describes the reliance of the result from a good choice of initial shape for the model. Usually the initial stage is assumed to be significantly far from the final, desired shape, being for example a primitive shape, like a circle or cylinder. Ability to perform successful segmentation using such simple initial shape is desirable, because it eliminates the need to perform manual initialization.

Sensitivity to noise - describes the ability of the method to operate on noisy data (robustness of the method). High sensitivity to noise is not desirable.

Topology changes - describes the ability of the method to successfully detect changes of the model topology during the segmentation process. This allows to detect features like holes and discontinuities in object contour/surface or to detect more than one object in the scene.

Segmentation precision - describes an overall quality of delivered results not considering the errors originating from above described problems (noise, bad parameters, bad initialization), so this feature actually describes how well is the segmentation performed if all the circumstances are advantageous.

Execution times - describes the time necessary to perform the segmentation process, which originates in the complexity of the algorithm.

Each feature has been rated in a comparative scale, choosing values from the following: very low, low, medium, high, and very high. All assumed values are chosen in a relative way, that is to present best their correspondence to each other and they should not be considered as

absolute. The results of our evaluation are presented in Table 1.

2.5.2 Comparison

As it can be observed, the effectiveness of image processing applied to computer aided diagnosis has evolved significantly through the last two decades. New possibilities arose with numerous improvements applied to the original ideas of thresholding, graph partitioning or deformable models, but also with the possibility to use computers with radically larger processing power. It is however possible to see that some authors have focused on improving the method's efficiency only together with enlarging its complexity, which in turn diminishes the improvement in processing possibilities of currently available computers and results in ever growing execution times of those algorithms. This is further extended by the fact that modern image processing methods operate on massive amounts of image data, acquired from medical scanners offering high resolutions and dimensionality of three or more (for example four-dimensional images, being temporal sequences of three-dimensional images). This is not necessarily a worrying fact, as we are currently witnessing a popularity growth of a new approach to expanding the possibilities of computers, namely parallelization. Distributing the workload of an algorithm between a number of processing units is becoming more popular, delivering new possibilities for development of image segmentation methods, decreasing the need for such a high regard for its complexity. The solution based on the active nets enriched with genetic algorithm optimization present a set of very impressive features. It seems to be virtually insensitive to bad parameters, bad initialization nor noise. It performs well in complex scenarios thanks to the topology change ability and their segmentation precision proves to be very good. These valuable characteristics take their origin from the formulation of active nets and from the nature of genetic algorithms, which makes them a very powerful optimization tool. Thanks to their ability to automatically favor the best solutions and to self-adapt to different conditions of operation they deliver an answer to a lot of issues of the medical image segmentation problem. Unfortunately, these valuable characteristics result in relatively high execution times. However, as it was mentioned before, the authors in [InBSP06] have assumed a very specific approach of high precision and big population sizes for their experiments. The high flexibility of the genetic algorithms promises a large field for improvement for this method and the possibility to reduce the execution times.
Similarly good set of features can be also seen by the solution based on artificial life framework, the deformable organisms. The approach to the segmentation problem, taken in this case, is quite different from the one described above. Instead of relying on the natural selection mechanisms, authors use a highly configurable, hierarchical model as the base for deformable organisms, thus allowing them to introduce a high amount of knowledge to the model. This information can successfully serve as guidance for the organisms in the segmentation process, defining their actions and responses in specific scenarios. As it is possible to see in our evaluation, this allowed developing a highly-effective segmentation method, which probably is still capable of performing better with the introduction of more research efforts. However, in contrast to the active volumes/genetic algorithms solution, this method lacks the ability of self-adaptation and thus requires a high level of user interaction in terms of method construction and development. The definition of the algorithm and the configuration of the behavioral functions for the organisms have to be precise to obtain optimal results. Also the flexibility of the method is believed to be significantly lower in terms of applying the same method to segmentation of different body parts, different types of scanning devices, etc.
The two-stage solutions, like the 3D minimal paths and the parallel genetic algorithm refine-

Method	Sens. to parameters	Sens. to initialization	Sens. to noise	Topology changes ability	Segment. precision	Execution times
Original snakes by Kass [KWT88b]	High	High (manual, near the desired contour)	High	Not capable	Low	Low
Dynamic programming [ATW88a]	High	High	Medium	Not capable	High	High
Williams greedy alg. [WS92b]	High	High	Medium	Not capable	Medium	Low
Methods based on level sets [CKS95b]	Low	High (similar to original Kass formulation)	Medium	Medium	High	Low
Ardon's 3D Minimal Paths [ACY05]	Medium	Medium (partial manual segmentation required)	Not tested by the authors, probably Low	High	High	Low
Active Nets (greedy alg.) [TY89]	Medium	High when combined with noisy images	Medium	Very high	High	Low
Active Nets (genetic alg.) [InBSP06]	Very low	Very Low	Low	Very high	Very High	High
Topological Active Volumes (greedy alg.) [BPMA03]	Medium	High when combined with noisy images	Medium	Very high	High	Very High
Parallel genetic algorithm refinement [FJD02]	Low	Low	Not tested by the authors, probably Low	Very high	Very high	Medium
Hybrid methods [MT04]	Low	Low	Medium	Medium	High	Medium
Deformable Organisms [MH06a]	High	Low	Low	Very high	Very High	High

Table 2.1: Comparison of different segmentation methods using a selection of representative features.

ment, benefit richly thanks to a very natural idea of initializing the segmentation process very near its final, desired shape. What is worth noticing is that this solution delivers a very good and effective method to obtain that goal. A quick approximation of the shape to be segmented is performed at the beginning, assuming a high level of simplification and gaining high performance advantage. This step would occupy relatively little time and deliver an initialization position for the deformable model far better than a primitive shape representing absolutely no knowledge about the scene. Because at this point no connection exists between this initialization scheme and further processing with the DMs method (those steps are independent), we consider this idea strictly as a solution to the initialization problem, which offers significant improvement and can be applied before any other segmentation scenario, not just the one proposed by the authors. It is a good idea, which can possibly bring improvement in segmentation precision and execution time applied to any segmentation solution.

Chapter 3

Whole Mesh Deformation Model

In this chapter we describe our proposed image segmentation method called the WMD. It is a powerful image segmentation model based on the DMs idea and includes a new approach for shape optimization. It is characterized by a very effective and precise segmentation capability, which makes it a very good choice for applications demanding efficient and accurate processing of large amounts of data. The proposed WMD model uses a 3-dimensional mesh instead of a contour or a surface to represent the segmented shapes of interest, which allows exploiting more information in the image and obtaining results in shorter times, independently of image contents. The model also offers a good ability for topology changes and allows effective parallelization, which makes it a very good choice for large datasets.

3.1 Motivation

The WMD model has been designed using the ideas of the DMs and the TAV method as its foundation. The differences between the two mentioned approaches can be summarized in the following way:

- In the original DM the segmentation was performed using a single contour (in case of 2-dimensional images) or a surface (in case of 3-dimensional images). Only the boundary information from the input data has been used and the result included a description of the shape of the objects of interest.
- In the TAV model the deformed shape was not described as a contour or a surface, but instead it was based on a volumetric mesh constructed with nodes interconnected with links (or edges). Some were responsible for describing the shape of the objects and others for modeling their interior structure. Thanks to this the TAV model was able to perform the segmentation taking advantage of both boundary and region data present in the input images and to deliver the result describing both the shape of the segmented object, as well as their interior.

In the WMD model the segmentation process is based on similar structure of volumetric mesh as in the TAV model. There are however some significant differences between the TAV and the WMD models in the way in which the mesh is defined and the assumptions on which the process of handling the deformations is built upon.
Fig. 3.1 presents an outline of an exemplary segmentation using the TAV model. The mesh has been initialized over the whole volume with all the nodes divided into two groups: internal and external ones. The external nodes are initialized on the superficial layer of the volume and during the segmentation process they progress towards the edges of object present in the input image. The vital part of the segmentation process is performed by the external nodes of the mesh, which were distributed only over the superficial layer of the volume. The internal nodes would be distributed between the boundaries set up by the external nodes and their function

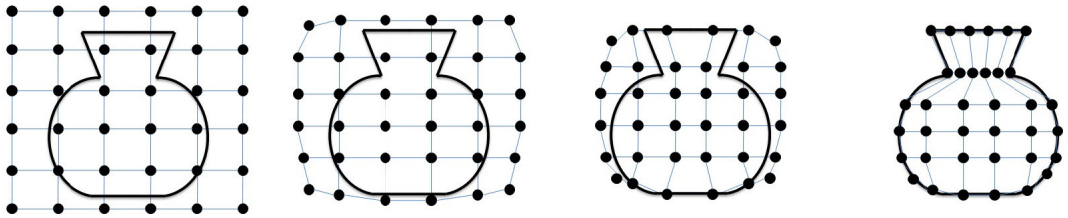

Figure 3.1: Visualization of concept of the TAV segmentation method.

was reduced to model the internal structure of the objects by maintaining an even distribution between one another. We consider this approach to be not optimal for the following reasons:

1. The number of nodes that segment the boundary of the object is usually significantly lower than the number of nodes which model their interior structure. This might not be the case in the exemplary image given on Fig. 1, but in real-world scenarios the density of the mesh is significantly higher, resulting in different proportions between the external and internal nodes. Because of the mesh structure every augmentation of the number of external nodes would result in an even bigger increase of the internal nodes number. As a result, the computational power is not efficiently used, because distributing the internal nodes inside of objects of interest is a trivial task and the most precision is required at the boundary detection part.

2. The segmentation process is completed not sooner than when the external nodes place themselves on the borders of objects of interest. This is a very inefficient approach, because the distance that the external nodes need to travel during the segmentation process is relatively large. The mesh is always instanced in a way to cover the entire image (or volume) and the external nodes are instanced on the edges of the mesh. This puts them in the most distant location possible from the objects of interest, which in turn results in longer segmentation times.

3. The shapes present in the scene of interest are approached from image borders with a single layer of external nodes. This makes the segmentation time highly dependent on the contents of the image, because the distance which the nodes need to travel can be varying in different images or even in different parts of a single image. This makes the segmentation time very difficult to predict or to control. That is a much undesired characteristic if we want to perform a parallel implementation of the algorithm or to segment a 3-dimensional volume composed of a number of slice images. Without the possibility of predicting the segmentation time for each part of the image it will be very hard or impossible to guarantee an even distribution of workload and overall segmentation time in these cases will always be longer than necessary.

In order to take advantage of the great potential of the TAV method but also to cope with the above-described drawbacks, we have proposed the WMD, which uses a different organization of the mesh in order to process the scene of interest.

3.2 General Concept of the Whole Mesh Deformation Model

In order to illustrate the new ideas that compose the WMD model we have depicted an exemplary segmentation using the ideas of our model on Fig. 3.2.

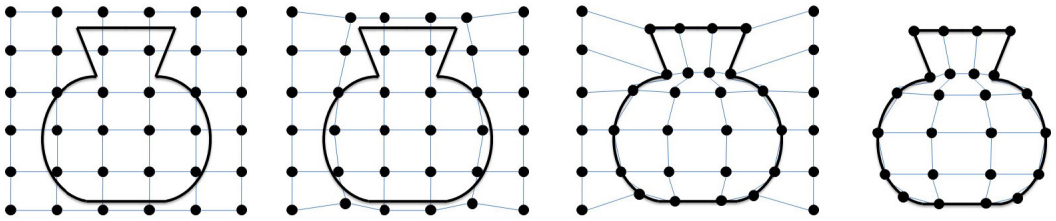

Figure 3.2: Visualization of concept of the WMD segmentation method.

More specifically, the WMD model has been designed with the following principles:

1. The nodes of the mesh are not divided in two groups, but rather they are all equal and their behavior is controlled with a single function. As described above, the TAV model has used two functions, one for each type of the mesh nodes.

2. The behavior of the nodes, however, remains in line with the one in TAV model - a part of the nodes is responsible for detecting the boundaries of the objects of interest, the rest of them is responsible for describing their interior structure. This is achieved by simulating the behavior of both types of nodes from the TAV model, but without dividing them strictly in two groups at the beginning of the procedure. During the segmentation process each node should discover by itself which behavior should it carry out. Furthermore, this behavior should be allowed to change during the process, namely a node which has been modeling the interior structure of the object can at some point detect the boundary of the object and vice versa.

3. Since a single function is used to control the behavior of the nodes during the segmentation process, the decision on acting as internal or external nodes depends solely on the image features in the nearest neighborhood of the given node.

As a consequence of the above-described characteristics of the WMD model, the behavior of the nodes can be described in the following manner:

1. Only the nodes, which have been initialized in the proximity of an object, begin to progress towards them. This is enforced by detecting edges of objects in the scene of interest and creating a vector field near them, which attracts the nodes of the mesh towards the objects.

2. The nodes of the mesh which have been instanced within objects of interest, but that do not reside near any boundaries of those objects, will show a tendency to maintain equal distances from one another and 90 degrees angles between the edges of the mesh. They will of course be subjected to a certain amount of stretching and/or bending, but the regularity of the whole structure will be preserved.

3. The nodes of the mesh which have been instanced away from any objects of interest will detach from the mesh during the segmentation procedure and in the end they will be discarded.

With the introduction of above-described changes no functionality of the TAV-based segmentation method is lost. The WMD model maintains the ability to model the boundaries as well as the interior structure of objects of interest and to describe segmented scenes with high detail and great resemblance to the real-world objects. The change in segmentation approach on the other hand offers a very good potential for the topology changing capabilities and independence of initialization. Enforcing the correct behavior on all nodes of the mesh without dividing them strictly in two groups is obtained with an innovative formulation of the energy function of the mesh, which is described in detail in Section 3.3. This energy is the main component of the model that guides the segmentation process. It is calculated taking the current shape of the mesh as the input and expresses the difference of the current state of the mesh from the desired result. Therefore, it should be defined in a way to assume its minimal values when the nodes of the mesh position themselves on the shape of interest. Therefore, the segmentation task can be seen as iterative optimization task, where the deformed shape is changed in every iteration so that it resembles more the desired result.

The task of defining a single energy function that could incorporate all necessary behaviors and perform a correct segmentation is naturally more complex than in the case of two energy functions, but only in terms of the algorithm development - the calculation cost during the segmentation procedure remains the same. As a result it opens a possibility to address all of the above described disadvantages of the TAV model and offer a significant performance improvement.

3.3 Formulation of the Energy Function

The energy function of the WMD model is described as follows:

$$E(\nu) = E_{int}(\nu) + E_{ext}(\nu). \tag{3.1}$$

where ν represents the current state of the model. As it can be seen, it consists of two groups of forces:

- Internal energy, which is responsible for preserving a regular structure of the objects.
- External energy, which is responsible for applying the features of input images.

The division of the energy function into two forces has a purely organizational purpose and it takes its origin from the first publications about the DMs [KWT88a]. It doesn't have anything to do with the division of the nodes of the mesh into internal and external ones, which was introduced in the TAV model and, as mentioned already, doesn't exist in the WMD model.

In order to calculate energy for a given model state, the domain [0, 1][0, 1][0, 1] is discretized as a regular mesh defined by the internode spacing Gx, Gy, Gz and each of the contributing forces is calculated using the appropriate function. These function corresponding to internal energy and external energy are described in Sections 3.3.1 and 3.3.2 repectively.

3.3.1 Internal Energy Formulation

The internal energy is composed of two forces, namely of continuity and curvature [KWT88a], and it is defined as follows:

$$E_{int}(\nu) = \alpha \sum_{n=1}^{k} |m_n - \overline{m}| + \beta \sum_{n=1}^{k} \left| \arctan \mu_n - \frac{\pi}{2} \right| \tag{3.2}$$

In (3.2) the following symbols stand for:

- The parameter k stands for the total number of nodes in the mesh.
- Parameter $\overline{m}$ represents the average distance between all the nodes in the mesh - the sum of lengths of all links of the mesh divided by their number.
- The parameters m_n and μ_n are respectively the average distance and angle between the node n and its neighbors and are calculated by dividing the sum of lengths (or angles) of the links in the neighborhood of the node by their number. Only those links that are not longer than the flexibility parameter allows are considered for this step. The flexibility parameter of the links is a feature used for the task of topological changes of the WMD. This characteristic will be described in more detail in Chapter 5 of this thesis.
- The symbols α and β next to the sum expressions represent their weights and serve to balance their impact on the whole equation.

As it can be seen from equation (3.2), the continuity force attracts the nodes of the mesh to maintain equal distances between one another, whereas the curvature term attracts the nodes to keep a 90 degrees angle. This serves to preserve the initial structure of the mesh based on regular, cubic elements.

3.3.2 External Energy Formulation

The external energy is composed of three forces and is defined as follows:

$$\begin{aligned} E_{ext}(\nu) &= \gamma \sum_{n=1}^{k} (1 - I(\nu_n)) + \delta \sum_{n=1}^{k} (1 - G(\nu_n)) + \\ &\quad + \varepsilon \sum_{n=1}^{k} E(\nu_n). \end{aligned} \tag{3.3}$$

The symbol $I(v)$ represents the intensity values taken directly from the input images.
The $G(v)$ symbol stands for the Gradient Vector Flow (GVF) [XP98] values, which are calculated using the GVF algorithm over the input images. This algorithm has been presented specifically as a very efficient component for the external energy function of DMs segmentation methods. It is computed as a diffusion of the gradient vectors of a gray-level or binary edge map derived from the image. The result is a field of vectors that has a large range of influence and forces the boundaries of the DMs, or the nodes of the mesh in case of the WMD model, towards the edges of objects of interest.
The $E(v)$ symbol represents the values from the edge detector, which are defined using the Canny Edge Detector algorithm [Can86] over the input images.
Similarly to equation (3.2), the symbols γ, δ and ε represent the weights of particular components.

3.4 Proposed Optimization of the Shape of the Mesh

The WMD model searches for the global minimum value for the energy function 3.1, which implies the minimization of both internal and external energy (3.2) and (3.2), respectively. In each iteration the current shape of the mesh will be taken as the input and each node of the mesh will be moved in its neighborhood to find the new optimum location.
The process is initiated with the creation of a regular mesh over the entire volume. One layer of mesh nodes is instanced per one slice image in the 3D data set and in each layer the nodes are distributed with a certain distance from one another, which is defined by inter-node spacing parameters Gx and Gy upon algorithm execution. Naturally smaller distances offer a better precision of the delivered result but result in longer execution times. This relation is not straightforward and will be discussed later in Chapter 7.
During each single iteration of the optimization task, the following is performed for each node N of the mesh: if the coordinates

$$N_t = (x_n, y_n, z_n) \tag{3.4}$$

describe the position of the node N at the time t, then for time $t+1$ the coordinates of N would be described with

$$N_{t+1} = (x_n + k, y_n + l, z_n) \tag{3.5}$$

where $k, l \in \{-1, 0, 1\}$ and correspond to the lowest possible value of 3.1, which is the energy of the node N calculated with equations (3.2) and (3.3) at these given coordinates.
These steps are repeated for each node of the mesh until the following rule is satisfied:

$$r_n < \mu \tag{3.6}$$

where μ is a small value near zero. and the r_n expression is defined as follows:

$$r_n = \sum N : N_t \neq N_{t+1} \tag{3.7}$$

Equation (3.6) verifies the number of nodes that have changed their position in the last algorithm iteration. Whenever this number is decreased to zero (or very near to zero) the mesh is assumed to be in its stable position and the segmentation is finished.
The above-described procedure can be summarized in the following manner:

1. For every node of the mesh do the following:
   (a) Place the node in 9 positions corresponding to its current location and points of its nearest neighborhood. This is illustrated on Fig. 3.3.
   (b) In each of these positions calculate the energy of the node using the energy function 3.1, described in Section 3.3.
   (c) Choose the position corresponding to the lowest energy value as the new position of the given node.
   (d) Check the links between the given node and all its neighbors with the flexibility term. This is a function that controls if the links do not stretch over certain limit.

This serves to detect links that should be broken in order to allow topology changes. This step is described in Chapter 4.

2. If in the end of an iteration a number of nodes larger than μ have changed their position, return to step 1.

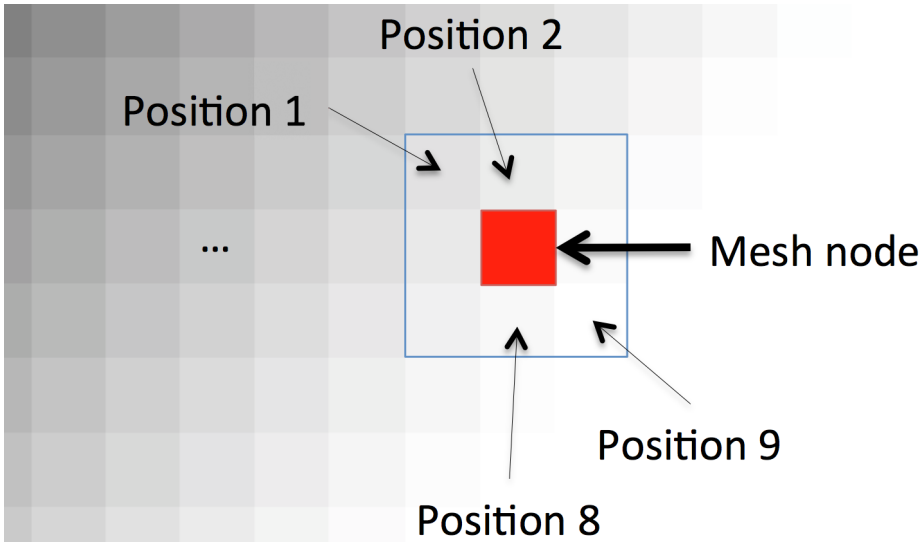

Figure 3.3: Illustration of consecutive positions in which every node of the mesh is placed in order to find the new position in each iteration.

The optimization task is achieved using the Greedy Algorithm approach. This algorithm is relatively simple and not resistant to local-minima trap, however in the case of our model this disadvantage is not relevant, because the WMD mesh maintains a stable, regular structure throughout the entire segmentation process and searching for minimal values in distant locations is not necessary. Therefore, a simple and not computationally demanding optimization method is the best choice.
At the end of the optimization step some parts of the mesh will be irrelevant for the final results. These sub-meshes would be constructed out of nodes that have been initialized outside the boundaries of any objects of interests. At the end of the optimization step it would be important to locate and discard them from our results. This step will be described in Section 3.7.

3.5 Complexity of the WMD Model

The proposed WMD model follows a pattern of greedy algorithm optimization for all the nodes of the mesh. The steps performed in that pattern include:

1. calculation of the Internal Energy (eq. 3.2) and External Energy (eq. 3.3) in all the neighbor locations of a given node;

2. definition of the location with the lowest energy as the new location for the given node;

3. repetition of steps 1) and 2) for all nodes of the mesh, while the overall energy continues to decrease.

From the above steps we can see that the execution time of the segmentation task depends linearly on the number of the nodes in the mesh. Furthermore, the number of necessary iterations of the algorithm depends strictly on the distance which the nodes need to travel during the optimization step. In the WMD model we have focused on decreasing this value as much as possible and as a result, the pessimistic execution time of the WMD model is very low. This will be described in more detail in Chapter 6.

3.6 Proposed Numerical Parametrization of the Energy Function

The symbols $\alpha, \beta, \gamma, \delta$ and ε next to the sum expressions in equation (3.2) and (3.3) represent their weights and serve to balance their impact on the whole equation. They are called the parameters of the energy function.
The parameters are a limitation of parametric DMs, since these models are often very sensitive to them. Because we want that the proposed model to be as automatic as possible, it needs to be less dependent from the right choice of parameters. In this section we will propose a numerical parametrization of the energy function.
A heuristic rule has been defined based on a reflection of the methods principles and supported by experiments. This rule is presented in equation 3.8. It was verified that this rule stands correct for all executed scenarios and therefore the model works correctly since the parameters obey to it. The said relation is as follows:

$$\beta < \alpha < \delta < \gamma < \varepsilon \tag{3.8}$$

The symbols starting from the left represent the weights of: curvature, continuity, Gradient Vector Flow, image intensity and the edge detector terms.
The principles for the above assumption are the following:

- The continuity and curvature terms need to be weighted with values just high enough to maintain a high regularity of the mesh. This will not decrease the quality of segmentation as the majority of nodes will have to travel only small distances during the entire process.
- The nodes that are initialized in the proximity of objects of interest need to be attracted to their borders and they should be the only ones attracted - nodes that are initialized farther should maintain their positions and regularity of the mesh. That is why we need to give the GVF force a weight slightly higher than the continuity and curvature ones, but keep the range of GVF on a low level.
- A high weight of the image intensity values serves to impose the correct behavior on the nodes of the mesh that have been initialized inside the objects of interest. The weight needs to be higher than the one of GVF, as the nodes inside the objects should not be attracted by the GVF force. Instead, they should be distributed near their initial locations and maintain a stable structure thanks to the continuity and curvature forces. This scenario assumes that the objects present in the images are bright and the background is dark. However, this can be easily modified whenever required by the scenario of application.
- The weight of the edge detector energy parameter needs to be set to the highest value, as it will serve to fix permanently the position of the nodes that reach the edges of objects of interest.

During the validation of our heuristic rule we have also noted that the proposed WMD model proves to be robust and not highly sensitive to changes in the values of the numerical parameters, as long as they follow this rule (3.8). Each segmentation scenario has a certain choice of optimal values of the parameters, but in most cases within the margin of 15% of the optimal values it was not possible to notice any change in the delivered result. The margin of 25% introduced small changes but still delivers correct and precise results.
In conclusion, we have maneged to verify that although the WMD model still has a parameter dependence, it is highly reduced when compared with most DMs that are highly parameter dependent.

3.7 Recognition of the Unwanted Parts of the Mesh

As stated before, one problem of using our assumptions for shape deformation, is the fact that some groups of nodes will be irrelevant at the end of the segmentation task and therefore should be discarded. This can be seen on Fig. 3.2. These would be the parts of the mesh that have been instanced outside of any objects present in the scene of interest. As shown in Fig. 3.2, the behavior that we would desire for them to have, would be to reside at their initial positions (or near to them) and gradually disconnect from the parts of the mesh that are attracted to boundaries of object. This is performed using the topology changing capabilities of the proposed model. As soon as the optimization step is finished the unwanted parts of the mesh are recognized and discarded from the result (as shown on Fig. 3.2, bottom right image). To do this the mesh is divided into sub-meshes that are isolated from each other. For each sub-mesh the two values σ and N_E are calculated using eq. (3.9) and (3.10) and will be used to identify the unwanted parts of the mesh. The parts that we want to discard from the final result would show very low values given by those two equations. The intensity values of these regions will be mostly representing the color of the background, so no variation of colors is possible. There will also be no edges, as they are reserved only for objects of interest.
As the final step, a simple clustering procedure into two groups is enough to separate the relevant from the irrelevant parts.

$$\sigma = \sqrt{\frac{1}{n}\sum_{i=1}^{n}\left(I(\nu_i) - \overline{I(\nu)}\right)^2} \tag{3.9}$$

$$N_E = \sum_{i=1}^{n} N_i : E(\nu_i) = 1 \tag{3.10}$$

- σ represents the standard deviation of the image intensity values in the sub-mesh.
- N_E stands for the number of nodes finalized on the edges of objects of interest.
- n is the total number of nodes in the mesh.
- $I(v_i)$ is the intensity value of the input image at the point occupied by the node V_i
- $\overline{I(\nu)}$ is the average intensity value for the whole input image.

The WMD model, introduced and described in this chapter, is a novel image segmentation method based on Deformable Models with unique solutions for the formulation of Energy Function and Shape Optimization [LPFF09a], [LPFF13]. The structure of the model and its functionality is in line with the needs of modern image segmentation problems.

Chapter 4

Parallel Implementation

As said in the previous chapters, one serious difficulty of processing images in 3D is the increased amount of data comparing to 2D images. This is further amplified by the constant improvement in the field of acquisition devices. Shorter acquisition times offer the opportunity to perform denser scanning (includes more scan images for each acquisition) and better sensors allow the registration of images in larger resolutions, allowing the perception of smaller details. Both improvements result in a major growth of data to process. The current progress in the field of computing performance lets us believe that parallelization is one of the best solutions to improve the effectiveness and shorten execution times of computation and data-intensive algorithms. This can be described in general as distributing the workload necessary to complete a given task between a number of processing units, which execute their respective operations or process some parts of data while keeping some level of awareness about the remaining processing units and communicating with them.

4.1 Previous Work

Efforts to distribute the work between a number of processing units have already been taken. In an early work presented in [HS97] the authors have noticed the growing amount of data generated by radiological imaging devices and proposed their idea of using a distributed processing environment in order to decrease the execution times of medical algorithms. The scenario that they worked with assumed a combination of several heterogeneous processing and communication devices operating together under control of a massive processing virtual machine, which was referred to as a metacomputer [KMCP94]. In [SHPA05] by Salomon and Heitz the authors have used a MIMD parallel processing computer to perform matching of 3D medical images, reducing the execution time of some medical tasks from the level of several hours to around 30 minutes using 32 processing units. Mayer and Meinzer in [MM99] have constructed a client/server application that provides high computational power to handle medical tasks. Their solution was based on a distributed system granting access to its resources by a network, performing time consuming operations on dedicated machines and returning desired results again by network back to users. In the last years the fast development of Graphics Processing Unit (GPU)s has sparkled a trend to use them for more general purposes than its original graphic related work. The high parallel computation capabilities of GPUs are welcomed by programmers who work at image processing which always have to deal with a large scale of voxel computation [PGX08]. Several authors have proposed the implementation of image segmentation algorithms using GPUs [WBKC09], [PGX08].

The above mentioned solutions have one thing in common, namely they assumed using some specialized system to perform the demanding operations of a specific algorithm. The parallelization was usually performed by applying the image processing algorithms to a very specific hardware/software scenario and thus limiting seriously the portability and general usability of developed solution. Therefore, in this chapter we propose a different approach and present

a solution that has been designed to be a very efficient parallel segmentation algorithm and thus will be able to provide its functionality without strict definition of hardware/software requirements.

4.2 The Approach for Parallel Implementation of the Whole Mesh Deformation Model

The WMD model has been designed from the beginning with the aim of execution in parallel environment. This means that at every stage of design and implementation of the model we have taken into account the need to guarantee a very efficient scalability of the segmentation model, which means the efficient utilization of available resources and decrease of the overall segmentation time. In order to achieve this we have designed the WMD model with the following principles:

- The need for inter-process communication during the segmentation sequence needs to be as low as possible. After a range of experiments we have in fact agreed that the efficiency that we are aiming for can be achieved only with no inter-process communication and no synchronization at all.
- The model needs to be able to equally share the workload between any number of processing units. This requires that the segmentation procedure is:
  - stable and predictable - we need to be able to estimate the execution time of any given sub-task
  - homogeneous - we need to be able to divide the entire segmentation process into smaller tasks of any required size

As it can be seen, we have designed the WMD model as a uniform, homogeneous task, composed out of very small sub-task units, that can be grouped to create tasks of virtually any size and execution time. It can be seen as a container of tasks that can be distributed over the available processing power in several ways. One approach is by continuous assignment of small tasks to currently available processing units, which is a good solution for parallel architectures of heterogeneous nature and without the possibility to efficiently estimate the execution time of given task on given processing unit. Another approach is to distribute the workload in units of identical sizes to all the available processing units at the beginning of the segmentation task, which would work well only on homogeneous execution platforms, where all the available processing units should process the given task in very similar times. This approach has been taken in our parallel implementation of the WMD model.

4.3 Parallel Implementation

The consecutive steps of parallel execution of the WMD model-based segmentation can be seen on Fig. 4.1. At first the 3D mesh is created in a way that its nodes cover the entire set of input images and are distributed in even distances. This task is performed by only one of the processes participating in the computation, a so-called root process. In the next step the root process verifies how many units are available to perform the computations and assigns

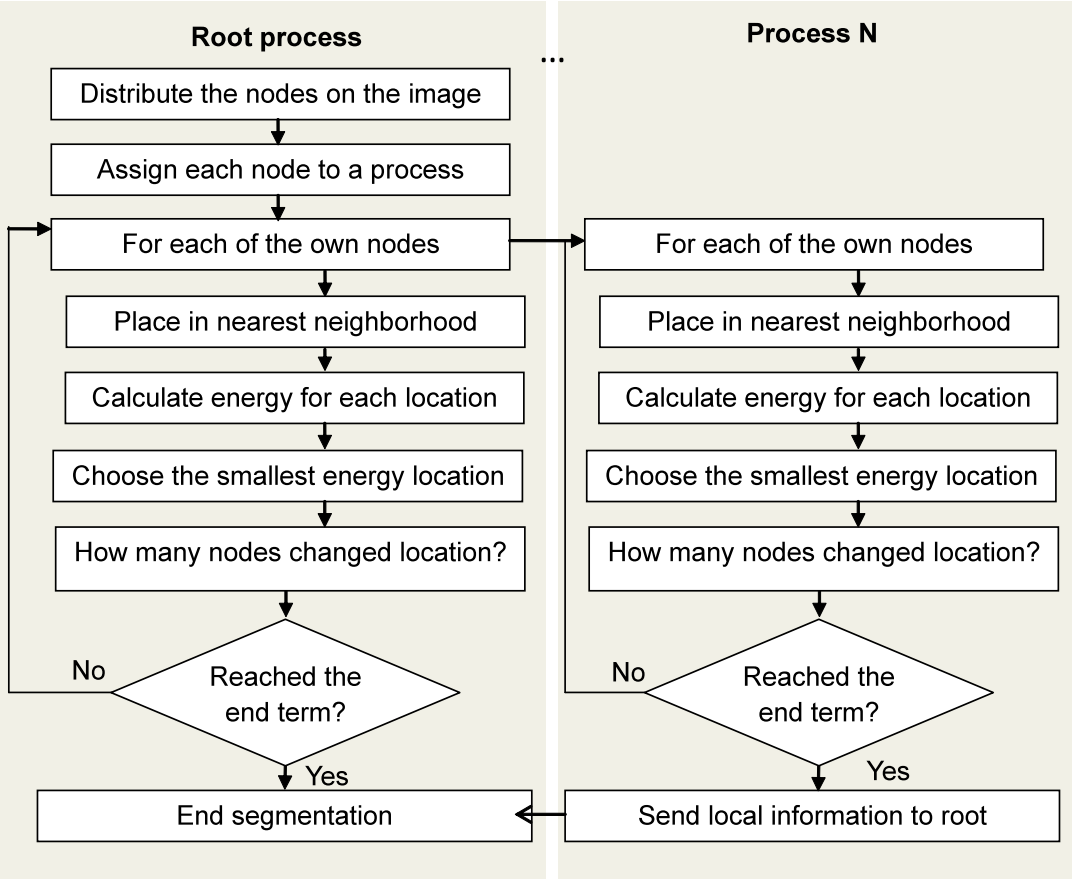

Figure 4.1: General flowchart representation of the parallel algorithm implementation.

each of the processes an equal (or nearly equal) number of nodes to operate on. Each of the participating processes will now work with its own portion of the mesh, performing the segmentation steps. The distribution of the nodes is performed as presented in the example on Fig. 4.2. This figure presents an example for a cubic mesh and an execution environment of 3 processing units. Each of the available processing units is assigned a zone, which covers an equal number of mesh nodes. In the example on Fig. 4.2 these zones are marked with A, B and C. This step can be compared to cutting out a slice of the mesh for each of the participating processes.

After receiving the range of nodes to operate on, the processes start to perform the segmentation steps, as described in Section 3. Each node is placed in nine locations corresponding to its nearest neighborhood and current position (see Fig. 3.3). The energy value in those locations is calculated using the energy function 3.1. Next, the position corresponding to the smallest energy value will be chosen as the new location for the given node. The process is repeated for the entire mesh.

It is important to notice that the steps of segmentation performed in each of the participating processes are independent from those performed in all the other processes and therefore there is no need to perform any communication between them at this step. Each of the processing units will create a temporary set of variables to use while the segmentation progresses. Those values will be representing the current state of the model on a given processing unit and will not be shared nor synchronized with other participants. This is done to eliminate any dependencies between the processing units and avoid the need for synchronization, which could severely decrease the scalability of the WMD model. The possibility of performing the optimization in an

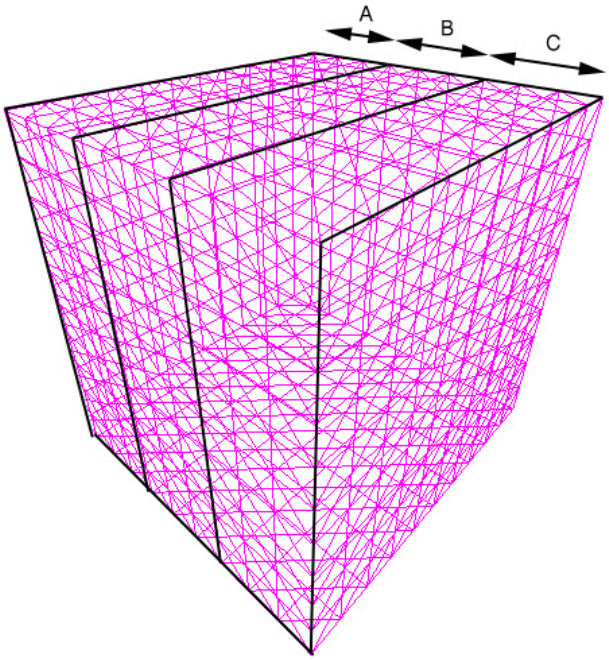

Figure 4.2: An example of how the mesh of WMD model can be distributed into 3 zones, for execution on 3 processing units.

independent manner is guaranteed by the fact that most of the calculations carried out when minimizing the energy function are performed using only the local data, taken from the input images in locations covered by the zone assigned for each of the processing units. The only values that are defined as global for the entire model are the average distances and angles between the nodes of the mesh. However, our experiments have shown that due to the high rigidity of the WMD mesh structure, their values are modified very slightly during the entire segmentation process and thus there is no need to track their changes very precisely. Therefore it is safe to assume that the locally calculated value describes well the state of the entire mesh.

When all the nodes of the mesh have been processed the root process checks how many nodes have changed their position during the last loop and based on that number the decision about finishing algorithmâs execution is taken. The data about positions of the mesh nodes is stored by each process in a local array, which has to be shared with all the other processes at the end of the segmentation. The root process again assumes control, as it can be seen in the Fig. 4.1, and calls all the processes to send him their parts of the array. It receives it in a form of two- dimensional array of the size $m * n$, where m is the number of processes participating in segmentation and n is the number of nodes assigned to each process. Using this information it constructs then a single array with the information about all the nodes of the mesh, which is the segmentation outcome.

Nodes that are assigned to a single process are not restricted to move away from the zone controlled by the given process. The assignment of mesh nodes to a given process is the same during the whole segmentation procedure, not regarding the current position of the node. This allows the mesh to deform freely, without any restrictions imposed by the parallelization.

4.4 Comparison with Existing Methods

It is important to note that in the case of most segmentation methods based on the DMs idea the equal distribution of the workload would not be as straightforward as dividing the nodes in equally large groups. This possibility of our model is a result of the approach that we have taken, namely the lack of division between internal and external nodes and by implementing the dynamic topology changes scheme. Thanks to these feature, as stated before, the time required to perform segmentation with our method depends very little on the contents of the input image. As a consequence, this time is very uniform for different parts of the mesh. In case of most DMs, the distance that the contour or mesh nodes need to travel during the segmentation task depends highly on the contents of the image, which results in a big variation of the segmentation times for different parts of the mesh. This is the reason why our method is much more suitable for parallelization than most other DMs or any method based on the concept of contour evolution.

The initial work about execution of image segmentation methods on parallel architectures has been presented at a conference and described in proceedings [LPFF08]. A second paper has also been published, that already included the WMD model and more advanced implementation of parallel execution [LPFF09c].

Chapter 5

Topology changing mechanism

The process of topology changing is a feature often encountered in the segmentation methods based on DMs. It describes the ability of the segmentation method to divide the deformed shape, so that it becomes two or more separate shapes. Two of the most common reasons to use the topology changing ability are: the need to create discontinuities in the objects of interest, e. g. to detect holes, and the presence of more than one object in the segmented scene.
In the WMD model the topology changing mechanism plays a role yet more important than in many solutions of the DMs family. The segmentation process is carried out using a 3D mesh placed over the input data. During this procedure the nodes of the mesh change their positions in a way which will results in placing them over the borders of objects of interests. This approach is similar to the general idea of segmentation methods based on the DMs family. However, an important characteristic of our model is its ability to take advantage only from the groups of nodes that are initialized in the proximity of objects of interests - the remaining nodes would not be engaged in the segmentation process and at its end they would be discarded. The topology changing mechanism in that case is used to divide the mesh into several disconnected sub-meshes, which would be later classified as either relevant, or irrelevant for the segmentation outcome. Therefore, in the WMD model an efficient ability to perform topology changes is crucial for the segmentation task. For this reason we have created the Dynamic Topology Changes (DTC) model.

5.1 Definition of The Dynamic Topology Changes Model

The WMD model has the ability to change the topology of the mesh during the segmentation process and to create discontinuities in the mesh structure while the mesh deformation progresses. This is performed in contrast to many DMs methods, where the task of topology changing is a separate step of the whole segmentation process. The difference between these two ideas is depicted on Fig. 5.1 and 5.2.
The first one shows the approach taken often in the segmentation methods, for example in the TAV method. It is possible to see that the process is organized in a sequential manner, with each step being performed separately from the remaining ones. The steps of shape optimization are always repeated until the mesh representing the scene of interest reaches a stable state, namely when its nodes will no longer show a tendency to significantly change their positions. After that the size of the mesh in terms of number of nodes is recalculated in order to provide an even distribution of the nodes in the entire mesh. As a result, the mesh can be deformed out of its optimal shape, which is why the optimization step is performed again. After this the step of topology changes is carried out. The mesh is tested for nodes placed in wrong locations, like the external nodes placed far from any surface or internal nodes placed on a background area. Those nodes, when detected, are subjected to one of the following procedures: the node removal or the link removal. The former assumes that the wrongly located node should be

discarded completely from the mesh structure; the latter assumes that only the links interconnecting the given node with its neighbors should be broken until the structure of the mesh will not show any more errors. Finally, the shape optimization step is carried out again to ensure that the mesh assumes the position with the minimal energy value.

As it can be seen, the composition of the process is modular. The respective parts are performed one by one and any step along the sequence requires for the predecessor to finalize its actions. This causes the segmentation process to be very badly suited for tasks like workload parallelization. Also, the progression of the model towards the desired result is not stable and during a major part of the segmentation process the state of the model represents data that is not useful.

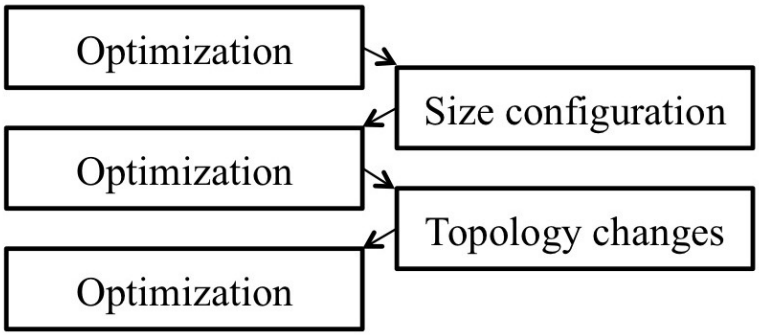

Figure 5.1: Visualization of concept of sequential approach to topology changing mechanism.

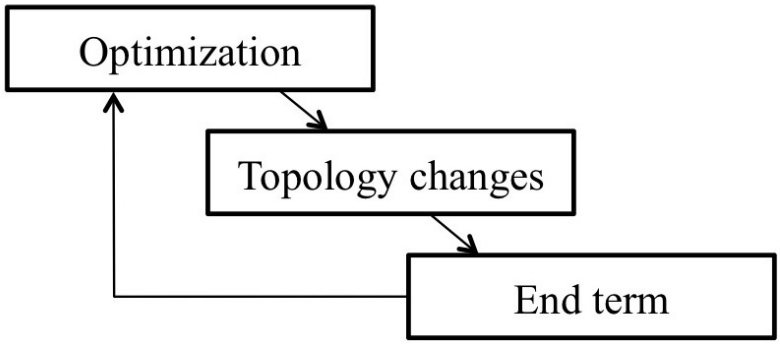

Figure 5.2: Visualization of concept of topology changing mechanism implemented in the WMD model.

The approach used as the base for the DTC model is presented on Fig. 5.2. It is constructed using a different assumption, namely to join the topology changes feature together with the optimization of mesh and carry them out along the whole segmentation process. During every iteration of the shape optimization step the need to perform a topology change is tested and whenever the need occurs, the model creates discontinuities in the mesh, therefore changing the topology of the whole mesh. On the other hand, the topology changes feature is constrained at all times by the mesh energy function, which guarantees that it will be constantly progressing towards an optimal state, namely the desired result of the segmentation task.

5.2 The Procedure of Topology Changing

As shown on Fig. 5.2, the topology changing and the shape optimization steps are constrained into one loop, which is repeatedly executed until the segmentation end term has been met. During the shape optimization step each node of the mesh can change its position due to the energy minimization process and as a result the lengths of links connecting it with its neighbors are also altered. What follows is the initialization of the topology changing mechanism in order to verify if any discontinuities in the mesh should be created. This is done with the following steps:

- The lengths of the links between the given node and its neighborhood are checked with term presented in equation (5.1),
- Whenever a certain link fails to satisfy equation (5.1) it is marked as broken.

We can safely assume that this process is carried out only when it desired because the mesh is defined to have a rigid and stable structure, as defined in Section 3.3, and as a result a majority of the links of the mesh extend their lengths only by small values during the whole process. When a link break occurs we assume that a given node has been attracted to a border of an object present in the scene of interests and thus the connection break is performed.

$$link(N_n, N_c) \leq \frac{G_x + G_y}{2} \times flex \tag{5.1}$$

In equation (5.1) G_x and G_y represent the average distance between mesh nodes in x and y directions and $flex$ is the flexibility parameter, which is defined upon segmentation execution and will be discussed later in section 5.3.

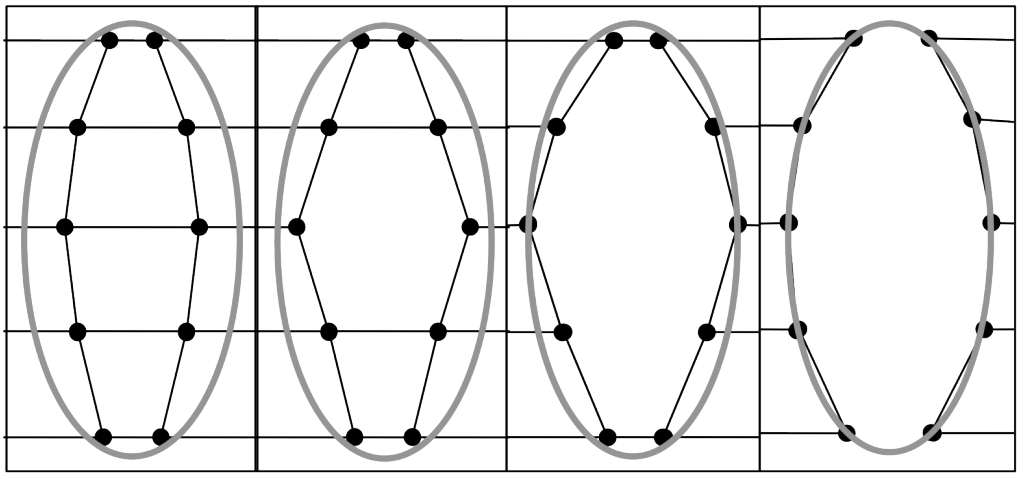

Figure 5.3: Example of a chain reaction during discontinuity detection in the structure of an object.

The broken link will no longer be considered when calculating the continuity term of the energy function in the following iterations. As a result, the neighboring nodes will show a behavior as if this link did not exist at all and they will progress away from their current locations more freely.
When a node is no longer attached from one side to its neighborhood, it will usually cause extending and possibly breaking the links of its neighbors, as shown on Fig. 5.3. This sort

of chain reaction is much desired as it will trigger the movement of nodes and breaking of connections in a small neighborhood.
The proposed approach will lead to a successful detection of the entire discontinuity in the mesh structure. Such process will be stopped at the right locations, namely where the nodes of the mesh encounter the edges of objects of interest. This is guaranteed by defining the energy of the edge detector to a very significant value, as described in Section 3.6.
The above-described process is carried out exactly in the same manner during the detection of two or more separate objects in the scene of interest. Likewise, some nodes are attracted towards an edge of the object and the links between the nodes and their neighborhoods are extended, which leads to a chain reaction and separation of the mesh into two (or more) independent parts.

5.3 Estimation of the flexibility parameter

The flexibility parameter is a value that defines how much the links of the mesh can extend their lengths without breaking. The DTC model requires the correct value of the flexibility parameter to be defined upon algorithm execution in order to perform successful segmentation. If the said parameter is defined with a too high value for the specific environment, the mesh will not be disconnected in the areas in which it should be and as a result several objects present in the scene would be detected as one. On the other hand, if the flexibility parameter is defined with a too low value, the mesh will detect discontinuities in locations where they do not exist.
Manual selection of this parameter for each segmentation task is not desired. To eliminate the need for manual tuning we propose to compute the flexibility parameter according to the current execution environment.
In order to do this we have performed a number of segmentation experiments using a set of artificial images as the input. Those have been constructed with the aim of representing several different scenarios concerning the features, which in our opinion would have an impact on the required value of the flexibility parameter. Those are namely:

- the minimum distance between the objects in the scene
- the size of the smallest discontinuity in the scene
- the width of the largest object in the scene

After performing the first round of experiments we have discovered that the distances enumerated above should be measured in a slightly different manner, namely not as the actual distance in a two-dimensional plane, but rather as two separate distances in the x and y planes individually. Then, the smaller value should be considered as relevant. The style of this measurement is depicted on Fig. 5.4. The explanation for this fact lies in the way in which the mesh is constructed. It is initialized with the links forming a regular, cubic structure and during the segmentation process the mesh tends to maintain this arrangement. As a result majority of the links would still be located in a parallel manner either to the x or y axis when they will be subjected to testing with the flexibility term and thus those distances should also be measured in a manner parallel to the x and y planes. The experiments that we have performed were carried out according to the following plan:

- A series of artificial images presented in Fig 5.5 was used.

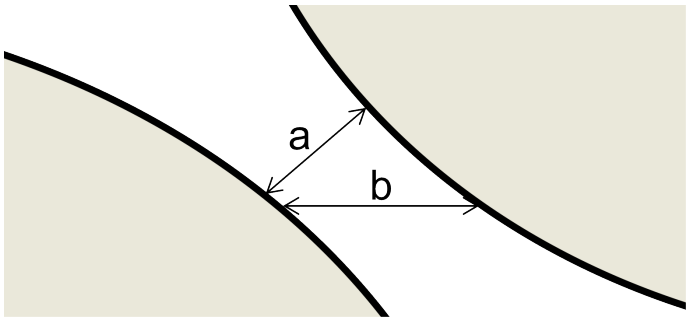

Figure 5.4: Illustration of the way in which the measurements of image features in our experiments are taken. The value a is the actual distance between the two objects in the image, the value b is the distance measured only in the X plane. The latter is considered as relevant in our experiments.

- For each of the images we have measured the three values described above.
- For each image we have performed a series of segmentation experiments using different values of the flexibility parameter and of the mesh grid size. The value that offered the best segmentation result was marked as the optimal one for the given scenario.

Using a total number of 16 images with 4 different grid sizes and 5 to 6 values of the flexibility parameter per image, we have performed 352 segmentation experiments. During these experiments it was observed that:

- A strong dependency can be noted between flexibility parameter and the initial size of the grid. The optimal value of the parameter has been kept in the range of:

$$flex \in (1.8 \times grid; 2.1 \times grid) \tag{5.2}$$

  where $flex$ stands for the value of the flexibility parameter and $grid$ is the average initial size of the mesh in x and y directions. This is a very expected behavior, as both the initial grid size and the flexibility parameter describe in a straightforward way the same feature of the mesh during the segmentation process, namely the lengths of the links.

- The exact optimal value of the flexibility parameter depends on the minimum distance between the objects in the image or the size of the smallest discontinuity, whichever was smaller. This dependency is depicted on Fig. 5.6. As it can be seen, the correlation of the both values is high and the value of the optimal flexibility parameter can be expressed as follows:

$$flex = \begin{cases} min_d & \text{if } dist < min_d \\ dist & \text{if } dist \in [min_d; max_d] \\ max_d & \text{if } dist > max_d \end{cases} \tag{5.3}$$

  where min_d and max_d stand for the minimum and maximum values from the optimal range of the flexibility parameter according to 5.2 and the $dist$ describes the smallest distance between the objects in the scene.

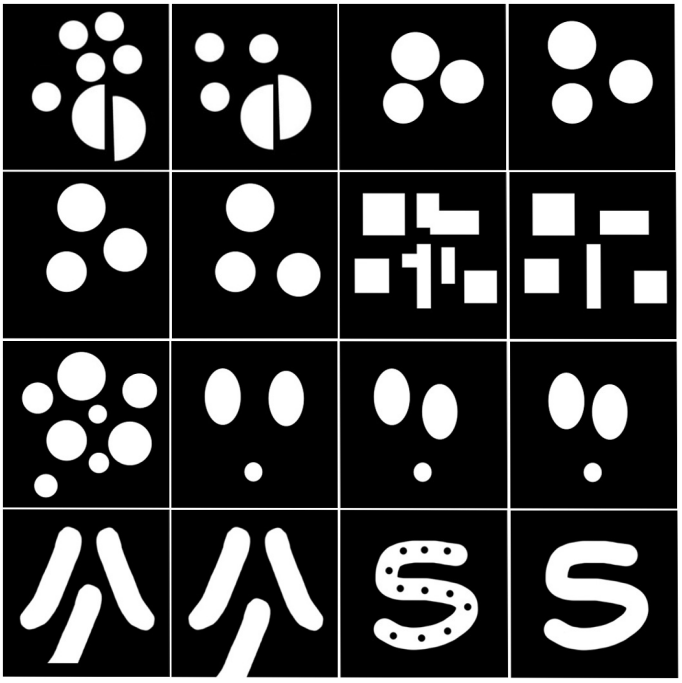

Figure 5.5: A set of artificial images used to perform our experiments on the automatic flexibility parameter estimation.

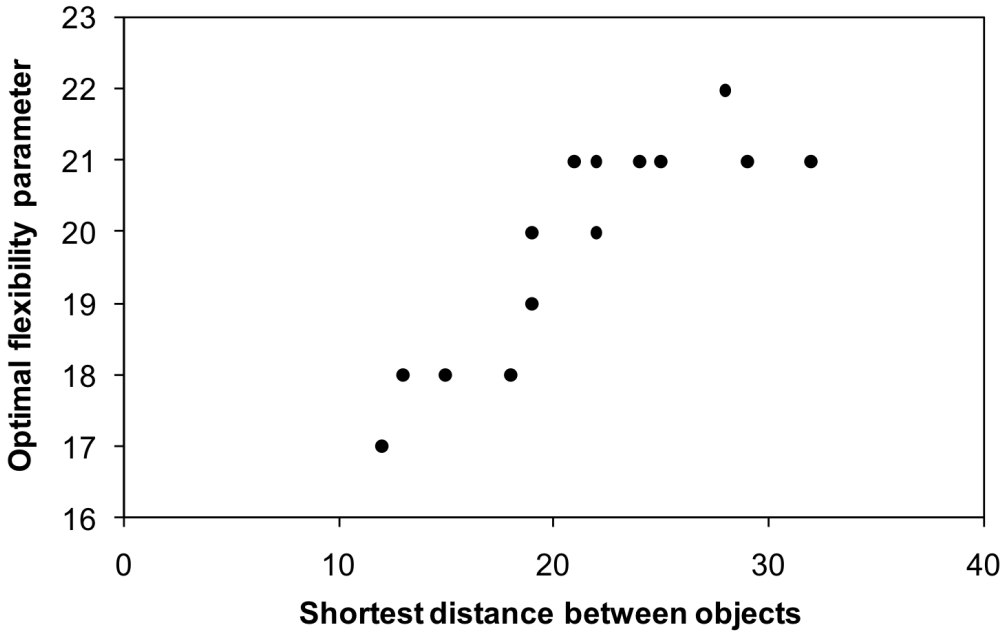

Figure 5.6: Dependency between the optimal value of the flexibility parameter and the shortest distance between objects in the scene.

- The width of the objects themselves does not show to have any impact on the optimal flexibility parameter value.
- Finally, the algorithm shows to allow some margin of error, i.e. the segmentation outcome has not been noticeably different with the flexibility parameter set to $\pm 15\%$ of its optimal value.

5.4 Validation of the topology changing mechanism and the flexibility estimation process

To assess the efficiency of our topology changing method we have performed a series of test, each presenting different type of input data. The first group was based on artificial images, not used before as the training set for the construction of the function calculating the dynamic flexibility parameter. The second group consisted of real, 2-dimensional medical images.
At the beginning of the segmentation process the input images have been subjected to an automatic measurement function that has analyzed them for the size of discontinuities in directions parallel to x and y planes. Images representing the edge detector function have been used for this purpose and since the measurement had to be taken directly in x and y directions, this process was simple and not time consuming. As the second step, the same experiments have been performed with the flexibility parameter manually chosen to an optimal value. In order to avoid any influence on this decision, this was done without the knowledge about the value chosen for this particular scenario by the automatic function. In all the cases the difference between values chosen in manual and automatic manner has been kept on a very small level of 10-15% of the value, which corresponded to 1-2 pixels. As said before, such a small difference was difficult to notice in the results and small enough to be ignored. Examples of the results delivered by the segmentation algorithm are presented in Chapter 7.

Chapter 6

Extended Whole Mesh Deformation Model

The initial attempts to perform segmentation of 3D images were carried out by a trained expert, who manually delineated the boundaries of structures in consecutive slices of 3D images. The first automated segmentation methods have operated in a similar manner to the manual segmentation performed by a physician, namely on individual slices separately. This approach made the segmentation process very time consuming as well as error-prone. In the absence of feedback in 3D, contours traced in subsequent slices may become mismatched, resulting in unnatural jagged edges that pose a difficulty to applications such as shape analysis [YPH+06]. For this reason the focus in algorithmic development was placed on true 3D processing of image data, where the objects of interest are represented as 3D volumes throughout the whole process [CKS95a], [MT99a], full or nearly full automation of the process based on probabilistic models of image intensity, atlas deformation, and statistical shape models.
The WMD model in its original formulation has proven to be a very promising solution as it is able to deliver precise results in very competitive execution times and is highly suitable for parallelization. It has however lacked an important feature, which was the ability to deform the mesh in full 3D environment. Enabling the nodes of the mesh to move in this direction implies significant changes to the way the segmentation process is carried out. This would result in the need to re-design behavior of such basic components of the model like the calculation of the energy function and the topology changing mechanism.

6.1 3D versus Semi-3D Processing

The WMD model has been designed with the ideas of Deformable Models as its foundation. As presented in previous chapters, the segmentation process is carried out by constructing a 3-dimensional mesh structure that would cover the entire input image data. Next, the mesh is deformed by moving its nodes in order to detect the objects present in the scene of interests. The nodes of the mesh were distributed using the following rules:

- The distances between the nodes in X and Y directions are defined by the user upon execution of the segmentation task. Smaller distances result with bigger density of the mesh and larger precision of the final result. These values could have been chosen freely by the user, corresponding to his needs and to the segmentation scenario.
- The distance between layers of the mesh in Z direction is defined by the number of slice images in the input volume. Each input slice corresponds to exactly one layer of nodes in the mesh and the distance between them (in voxels) has to be passed as a parameter by the user. Therefore, the actual distance between the layers of the mesh is in fact defined upon acquisition of the input image with the scanning device, when the practitioner defines the density of the scan in the Z-plane.

During the segmentation process the nodes are allowed to move freely in X and Y directions in order to explore the information available in the input images. Movement in the Z direction was

not allowed, because the progression by even one pixel in that dimension would mean moving out of the input image and therefore loosing the access to any image information, which is the only source of data for the external energy calculations and thus plays a vital part in the entire segmentation process.

This approach has proven to deliver a very good balance between the precision of results and execution times. The distribution of one Z plane for each slice of the input image is a very effective assumption, because it allows the most efficient extraction of information from the input data.

Although this approach has shown to be a very good trade-off between precision and segmentation times, there are some situations for which it might prove to be not good enough. An example of such situation can be the case of segmentation of input data with large distances between the input slices. In those situations the difference between two consecutive slices can be very significant and nodes that are fixed to a specific Z plane might not be able to properly describe the objects of interests. Two such examples are shown on Fig. 6.1. To simplify the example, the view is projected from the Y plane, so the visible planes are X and Z. The interconnected points represent the mesh and its nodes while the rectangles represent the relevant part of the input data from the slice images. The place where the rectangle ends represents the background part of the image. The left images (top and bottom) show the initial distribution of the mesh in both examples. The middle column shows the possible result of segmentation assuming that the nodes do not have the possibility to move in the Z direction. As it can be seen, the results are somewhat unsatisfactory, the differences between the consecutive slices are big and the mesh could not describe them properly. The images on the right present what could be the possible result if we assume that the nodes can move in all the directions. As we can see, the results are more precise and describe the objects of interest in a more realistic manner. Some of the nodes have assumed their positions between the Z planes in which they have been originally instanced and this allowed to create a more smooth surface of the objects of interest. These results would be much more desired in real world scenarios.

This functionality can be obtained with the implementation of node movement in the Z direction. Implementation of complex mechanism that would allow initialization of the mesh independently from the number of input image slices, is not desired, as it would result with higher computational cost of the method and it would not allow any new functionality or increased precision of the result.

6.2 Definition of Full 3D Node Movement

6.2.1 Movement of the Nodes

In the original formulation of the WMD the nodes have been allowed to move only in X and Y directions. During the procedure the following is performed for each node N of the mesh: if the coordinates

$$N_t = (x_n, y_n, z_n) \tag{6.1}$$

describe the position of the node N at the time t, then for time $t + 1$ the coordinates of N would be described with

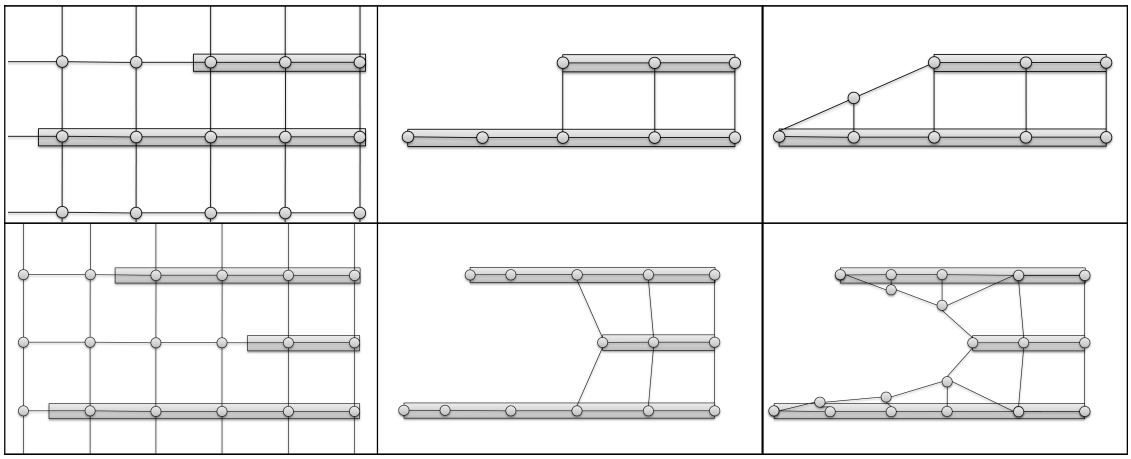

Figure 6.1: Two examples of situations in which the 2D processing of the nodes would perform not satisfactory. The top-left and bottom-left images present the initial distribution of the mesh in both examples. Images in the middle and on the right present respectively the results obtained with 2D and 3D node movement approaches.

$$N_{t+1} = (x_{n+k}, y_{n+l}, z_n) \tag{6.2}$$

where $k, l \in \{-1, 0, 1\}$ and can correspond to movement by the distance of one pixel, or no movement at all, depending what is the location with the lowest possible value of the energy function. In order to allow the nodes to move also in the Z direction we need to enrich (6.2) with the following:

$$N_{t+1} = (x_{n+k}, y_{n+l}, z_{n+m}) \tag{6.3}$$

where also $m \in \{-1, 0, 1\}$ and the combination of k, l, m corresponds to the lowest possible value of the energy function. In this case the value of m can mean the distance of one voxel between the consecutive Z planes, which usually have around 10 to 20 voxel between them. As we can see, the extended area of movement will be constructed from 27 instead of 9 points and the node will be moved in its nearest neighborhood in X, Y and Z planes. Similarly, the position with the lowest energy will be chosen as the new position. Those steps will be repeated for each node of the mesh until the following rule is satisfied:

$$r_n < \mu \tag{6.4}$$

where μ is a small value near zero. and the r_n expression is defined as follows:

$$r_n = \sum N : N_t \neq N_{t+1} \tag{6.5}$$

Equation (6.4) verifies the number of nodes that have changed their position in the last algorithm iteration. Whenever this number is decreased to zero (or very near to zero) the mesh is assumed to be in its stable position and the segmentation is finished.

6.2.2 Formulation of the Energy Function and Numerical Parametrization

The segmentation process in the fully 3D WMD model will be carrier out in a similar manner to the original WMD formulation. The energy function of the model, which guides the segmentation process, is defined in a way to assume its minimal values when the nodes of the mesh position themselves on the shape of interest. The energy function consists of the internal and external forces, which have the same role as in the original WMD model formulation, namely they are responsible respectively for preserving the structure of the objects and for applying the features of input images.

$$E(N) = E_{int}(N) + E_{ext}(N). \tag{6.6}$$

The internal and external energies are defined exactly the same as described in Chapter 3 Section 3. The energy function will be calculated taking the current shape of the mesh as the input. The state of the mesh corresponding to the minimal value of the energy function will be considered as the solution of the segmentation task.
Since the optimization process has been significantly modified, the energy function and its numerical parameters need to be properly updated, to enforce the correct behavior of the mesh. As it can be seen on Fig. 6.1, in certain situations we would like the nodes of the mesh to progress away from their original Z plane. This can be generally described as situations when two or more consecutive slices of the input volume contain objects with their edges distributed farther from each other than the distance between the nodes in the initial distribution of the mesh. This can also be seen on Fig. 6.1 where two slices on the upper example contain objects with edges that are located two mesh squares from each other. In the bottom example there are respectively two and three squares of distance between the first and the second slice, and second and third slice. The expected behavior of the mesh in these situations is shown on the middle images of Fig. 6.1. The nodes of the mesh are progressing towards the nearest edge in their neighborhood and if there isn't any present, they remain located near their initial positions.
The desired behavior is depicted on Fig. 6.1 right. Some nodes of the mesh move in the Z direction in order to construct a smoother surface between the planes of the input volume and thus to create a more realistic segmentation result. In order to enforce such behavior on the mesh we can include the following mechanisms in the mesh deformation scheme:

- The links of the mesh should show a subtle shrinking trend. This will attract some of the nodes to move away from their Z plane in situations like the ones shown on Fig. 6.1, namely when their neighboring nodes are located next to the edges of the objects of interests.

- The flexibility of the links of the mesh should be slightly increased comparing to the previous version of the WMD model. This means that they should be allowed to extend to larger lengths before they will be broken by the topology changing mechanism [LPFF09b]. Fig. 6.1 shows that keeping a larger number of links from breaking will help to attract the necessary nodes to assume their positions between two Z planes, where they would normally stay if links connecting them with neighbors would have been broken.

- Prior knowledge incorporation mechanism can be used to describe more accurately the desired result of segmentation. This includes the parts which do not hold any information

from the input images (spaces between the acquired image slices). Using such mechanisms we can include information about how the crossing between two consecutive slices should appear and thus what should be the behavior of nodes in that areas.

With acquisition of the above mentioned features into the WMD model the desired behavior is that some of the nodes would position themselves between the original Z planes and create a cloud of points, which would connect the edges of objects on neighboring image slices and create a smooth transition between them.

6.2.3 Calculation of External Energy Outside of the Input Images

In situation where we would like to allow the nodes of the mesh to propagate away from their original Z plane, we need to provide a new way of calculating the external energy, as the nodes would no longer be assuming positions which the data in the input images describe. In order to provide that functionality the values for components of the external energy are calculated in the following way:

$$I(\nu_n) = I(\nu_{x,y,z_1}) \times s_1 + I(\nu_{x,y,z_2}) \times s_2 \tag{6.7}$$

where $I(\nu_{x,y,z_1})$ and $I(\nu_{x,y,z_2})$ represent the intensity values from the input images with coordinates x, y, z_1 and x, y, z_2 respectively, z_1 and z_2 represent the Z coordinates of the two planes between which the given node is located, s_1 and s_2 represent the weights of both intensity values and are calculated taking the following value into consideration:

$$s_i = dist_s(N_t(x, y, z), N_t(x, y, z_i)) \tag{6.8}$$

As we can see, equations (6.7) and (6.8) compute the intensity value of node $\nu_{x,y,z}$ using the values corresponding to nodes ν_{x,y,z_1} and ν_{x,y,z_2}, which are weighted accordingly to the distance of the current node in Z plane from the two planes surrounding it.
Taking the above equations into consideration the interpretation of the external energy calculation would be the following: the distance of any given node from the two Z planes that are surrounding it is checked. These distances are used to calculate the weights, which are going to be used to calculate the final value of the external energy components for the given node.
Using this approach it is possible to project to a certain extend the information that would be present between the available image slices. It offers a good level of realism and approximation of the real data. This has been confirmed by analysing exemplary data, like the one on Fig. 6.3. The top row present GVF images obtained from two slice images of a CT brain scan volume. As we can see, the information in the image includes the strength of vectors surrounding the edges of the objects, represented with greyacale values. The closer the value is to 0 (black) the stronger is the force pulling the nodes of the mesh in the upward direction. Values close to 255 (white) represent vectors that pull the nodes of the mesh in the downward direction. The neutral value for these images is 125. The bottom row of Fig. 6.3 presents two images that have been obtained by combining the two images from the top row using two different values for the s_1 and s_2 weights. Those values for image bottom-left have been set to s_1 = 0.33, s_2 = 0.66 and for image bottom right: s_1 = 0.66, s_2 = 0.33. We then check the greyscale values of the point indicated on the two images by an arrow, which are: 153 on the left and 120 on

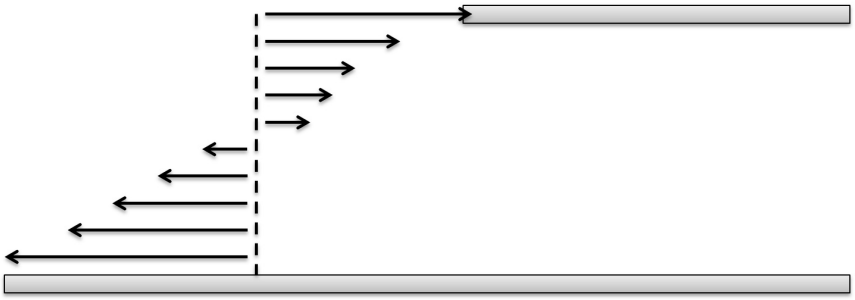

Figure 6.2: Top row presents two Gradient Vector Flow images from a CT brain scan. Bottom row presents their combinations with two sets of s_1 and s_2 weights. For bottom-left s_1 = 0.33, s_2 = 0.66, for bottom-right s_1 =0.66, s_2 = 0.33.

the right. Since the neutral value of the image is 125, we can see that the node that would be positioned in these two locations, would progress in two different directions. On the first image it would progress towards its bottom-right direction and on the second image it would progress to the upper-left. This corresponds well to the real-world explanation of this situation, because in the first case (bottom-left image) the node would be located closer to the image slice with the smaller contour and therefore it should be attracted to progress towards it. On the other hands, in the second case (bottom-right image) the node would be located closer to the larger contour and should progress towards that one.
We note that the strength of the effect that the force has on the node will be properly adjusted and simulate behavior that we can see on Fig. 6.2. That is because the closer a node is to given Z plane, the larger weight will be assigned to its energy value and the stronger will be the affecting force on that node.
For the remaining two types of images used in our energy calculation the situation would be similar: for the values of intensity calculated between two image slices we would see a graduate progression of the values from one slice to another. In the case of edge detector images the situation is slightly different, because those images are interpreted in the following way: any value other than 0 represents an edge and all the non-edge area is represented by 0. However, our mechanism would still perform desirably, as it would mark all the area between two slices as a non-edge area and thus it would allow the two remaining external energy components to model the behavior of the node in that areas.
The general assumptions of this method make it very suitable for our goals. The precision of the final result of the segmentation can be fine-tuned by the numerical parameters of the energy function.

6.2.4 Extended Dynamic Topology Changing Mechanism

With the introduction of 3D movement of the nodes the topology changes mechanism has been slightly adapted to allow efficient topology changes also in full 3D environment. This included adjusting 1) the estimation of the flexibility parameter, mentioned in Section 6.2.3, and 2) the way the flexibility term is verified. This was done with the following steps: the lengths of the links between the given node and its neighborhood are checked with the following term:

$$L_n \leq \frac{G_x + G_y + G_z}{3} \times flex \tag{6.9}$$

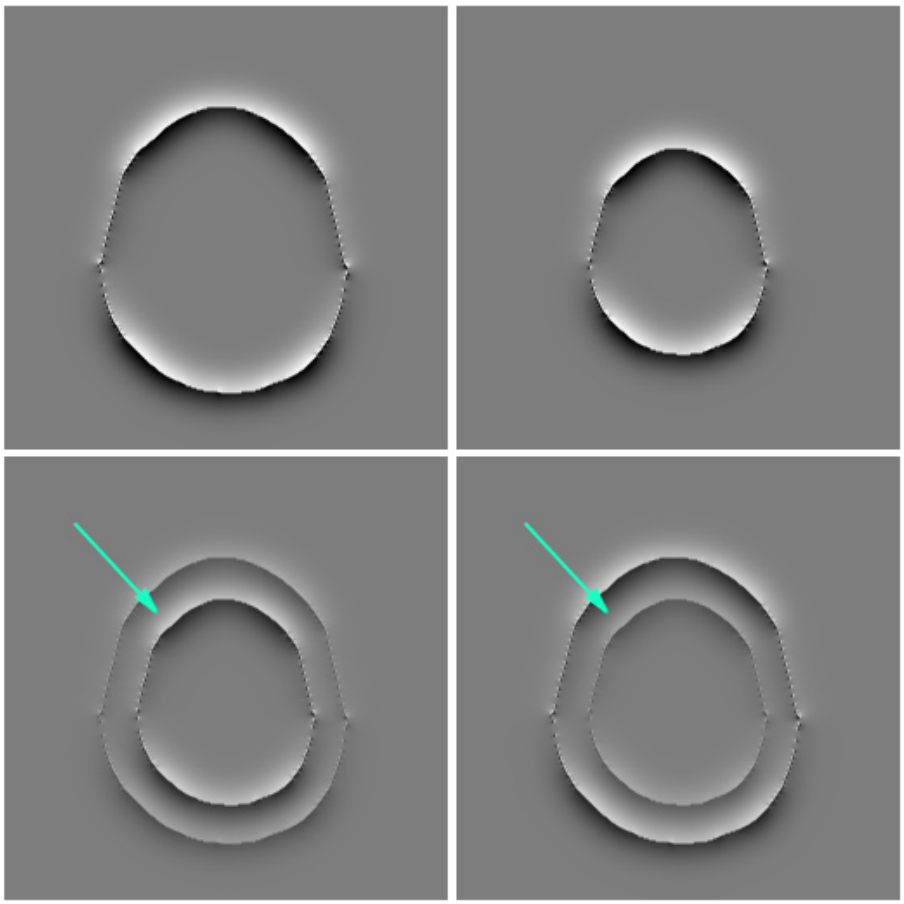

Figure 6.3: Top row presents two Gradient Vector Flow images from a CT brain scan. Bottom row presents their combinations with two sets of s_1 and s_2 weights. For bottom-left s_1 = 0.33, s_2 = 0.66, for bottom-right s_1 =0.66, s_2 = 0.33.

where $|L_n|$ represents the length of the current link, G_x, G_y and G_z are the lengths of the links in initial distribution of the mesh and $flex$ is the flexibility parameter.
The flexibility parameter is defined automatically upon segmentation execution in the range of:

$$flex \in (1.9; 2.6) \tag{6.10}$$

taking into consideration the size of discontinuities in the input images. This range has been established experimentally in the same manner as in Chapter 5 Section 3. Whenever a certain link fails to satisfy (6.9) it is marked as broken.
We can safely assume that this process is carried out only when desired because the mesh is defined to have a rigid and stable structure and as a result the majority of the links of the mesh extend their lengths only by small values during the whole process. When the situation of a link breaking occurs, we know that this is a result of attracting the given node to a border of an object present in the scene of interests and thus the connection breaking should be called.
The broken link will no longer be considered when calculating the continuity term of the energy function in the next iteration. As a result, the node will show a behavior as if this link did not exist at all and it will progress away from its current location more freely. This will usually cause extending and possibly breaking the links of its neighbors, which will lead to a topology change.

The Extended WMD model offers an increased possibility of shape deformation for the WMD model. In certain scenarios this is a very useful feature, as it allows to model the shapes of interest more freely and therefore obtain more realistic results. The work on the Extended WMD model has been presented in a conference paper [LPFF11a].

Chapter 7

Experiments and Results

The experiments described in this chapter have been performed in order to evaluate the performance and the quality of segmentation delivered by the WMD model. We have prepared and executed a range of experiments, using different input data, to test different components of our method, that have been described in previous chapters.
The values of the numerical parameters of energy function that have been used for all the following experiments are the following: α = 0.4, β = 0.1, γ = 0.7, δ = 0.5, ε = 0.9. As it can be seen, they follow the general rule specified in Section 3.6. The algorithm was implemented in C#. The execution environment included a machine equipped with 3 GHz processor and 2GB of RAM.

7.1 Input Data

As the first input data we have used a set of ten artificial shapes presented on Fig. 7.1. They have been created with the aim of representing features that are often encountered in real-world segmentation tasks, i.e. several objects present in the scene, objects placed inside one another or non-isometric distribution of objects in the image.

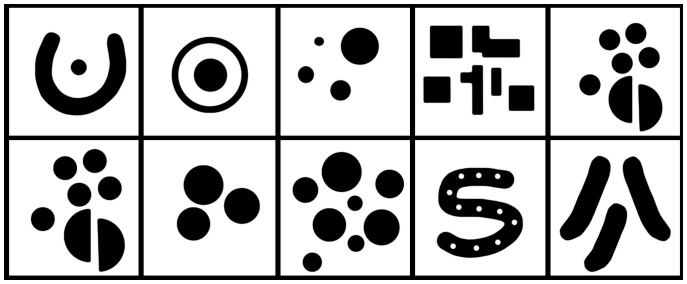

Figure 7.1: A set of artificial images used for the performance experiments.

We also wanted to assess the potency of our method when dealing with real-world images. For this purpose we have used two large 3D volumes presented in part in Fig. 7.2 and Fig. 7.3. The former volume presents a CT scan of human skull. It is composed of 320 slices, 512 by 512 pixels each. The latter volume presents an X-Ray scan of a spinal column area and is composed of 380 slices, each of them also of 512x512 dimensions. During the segmentation tasks the mesh density was defined to 8 by 8 pixels in all the scenarios.
For comparisons between the WMD model and the Extended WMD model we have used medical image volumes of a relatively small size: a 256x256x12 CT brain scan, a 472x512x16 MRI knee scan and a 256x256x16 CT brain scan, presented on Fig. 7.4.

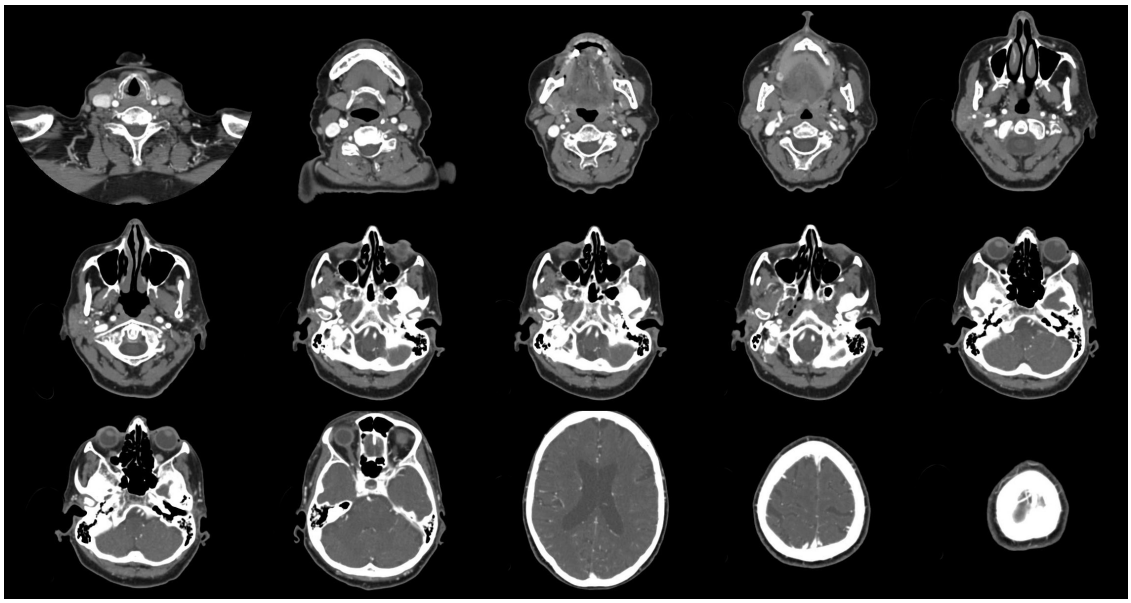

Figure 7.2: A sample of image slices from the 320-slice CT scan volume.

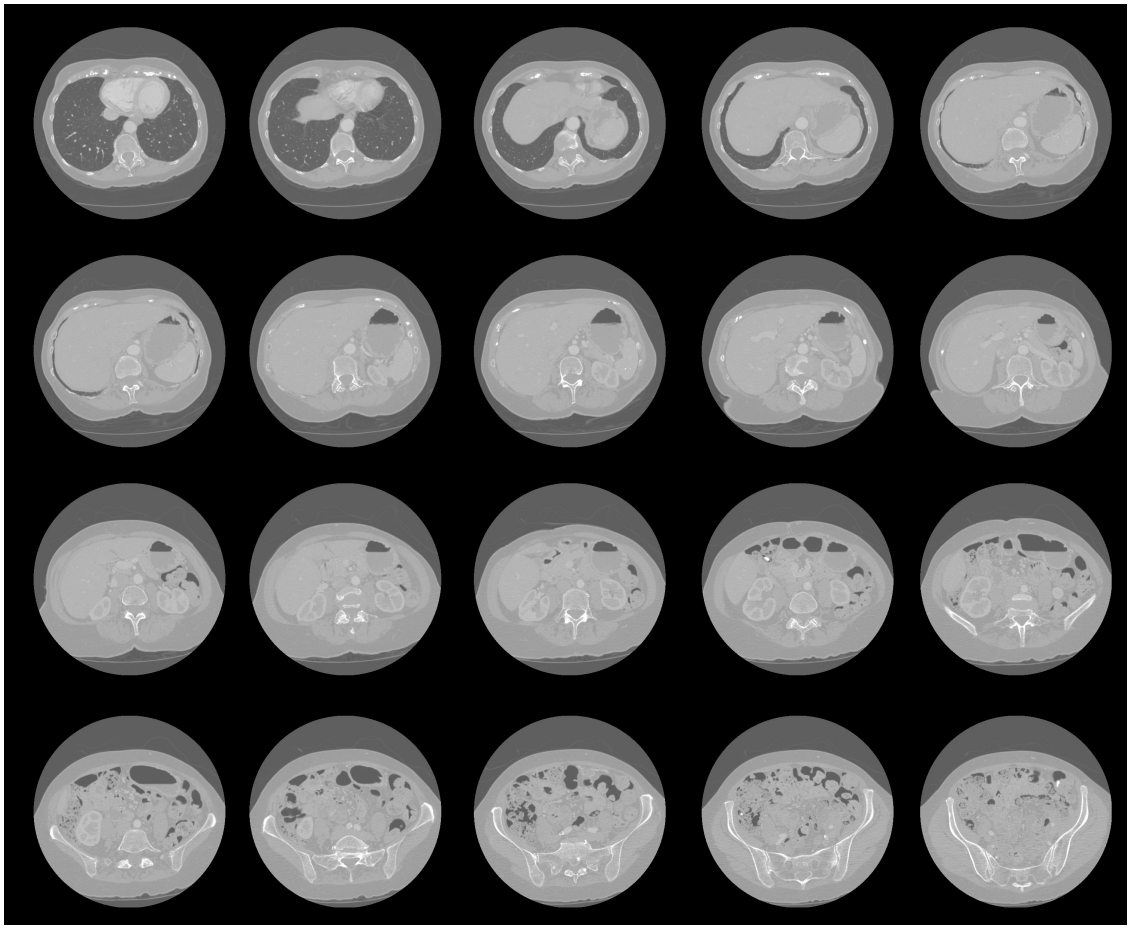

Figure 7.3: A sample of image slices from the 380-slice X-Ray scan volume.

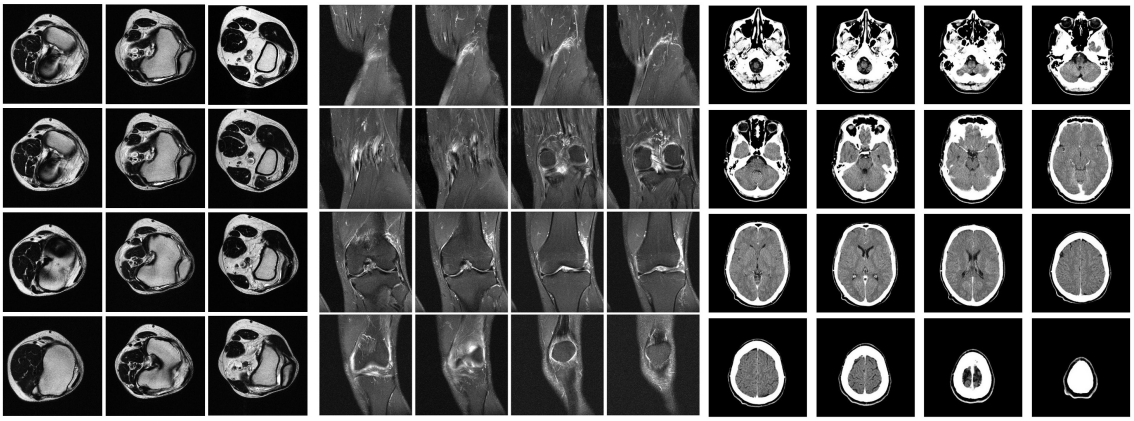

Figure 7.4: Three input volumes used for experiments with the Extended WMD model. From the left: a 256x256x12 CT brain scan, a 472x512x16 MRI knee scan and a 256x256x16 CT brain scan.

7.2 Segmentation Results

We have prepared illustrations of two exemplary segmentations with the WMD model. During the procedure several stages have been captured in order to depict the progression of the mesh deformation. These stages are depicted on Fig. 7.5, which presents segmentation of an artificial shape from Fig. 7.1, and on Fig. 7.6, which presents segmentation of a simple teapot shape. As it can be seen, the algorithm behaves in a predicted way. In the initial step the nodes that are initiated near boundaries of objects begin to progress towards them. This step can be seen on second and third image of Fig. 7.5 and on second image of Fig. 7.6. Next, the links that have stretched to lengths exceeding the flexibility parameter begin to break, which can be seen on consecutive images in both figures. Links that were broken and in fact do not participate in the process anymore, have been marked with a light grey color. After the chain reaction of breaking links and disconnecting the unwanted parts of the mesh from the part describing the object of interest, the final result can be seen on the last image on both figures.

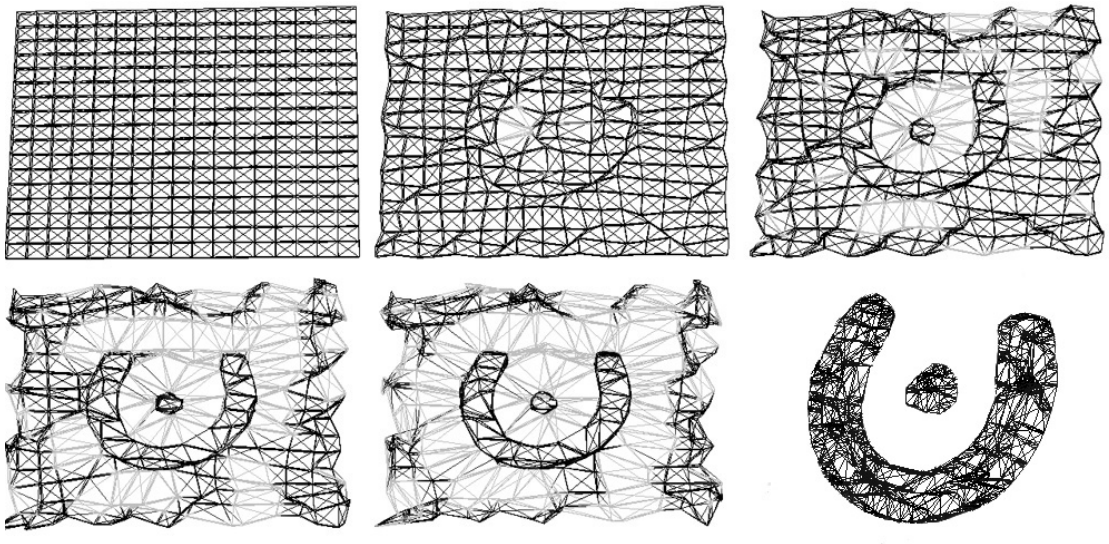

Figure 7.5: Consecutive steps of segmentation algorithm execution using an image with artificial shape as the input. The input image included Shape 1 from Fig. 7.1.

In order to present the segmentation procedure in a clear way, the inter-node spacing in these two scenarios has been set to a relatively high value, which resulted in a low mesh density. Much better accuracy of the final result can be obtained with a smaller value of the inter-node spacing.

An example of segmentation result of real medical data using the WMD model can be seen on Fig. 7.7 and Fig. 7.8, which present the result of segmentation of images from Fig. 7.2 and Fig. 7.3 respectively. It can be seen that results delivered by the WMD model are very precise and reliable, small details are detected successfully. Complex parts of the input images have been segmented correctly and described with surfaces that are smooth and without distortions.

In order to experiment with detection of different objects in the scene of interests, we have segmented the 380-slice X-Ray scan volume (Fig. 7.3) with two different setups. Fig. 7.8 and Fig. 7.9 both present the results corresponding to this X-Ray scan. The former one presents the results of bone structure segmentation, which was obtained by segmenting the brightest zone of the image, the latter presents the organs, which was obtained by setting the algorithm to segment the medium intensity ranges in the image. This result can be easily controlled

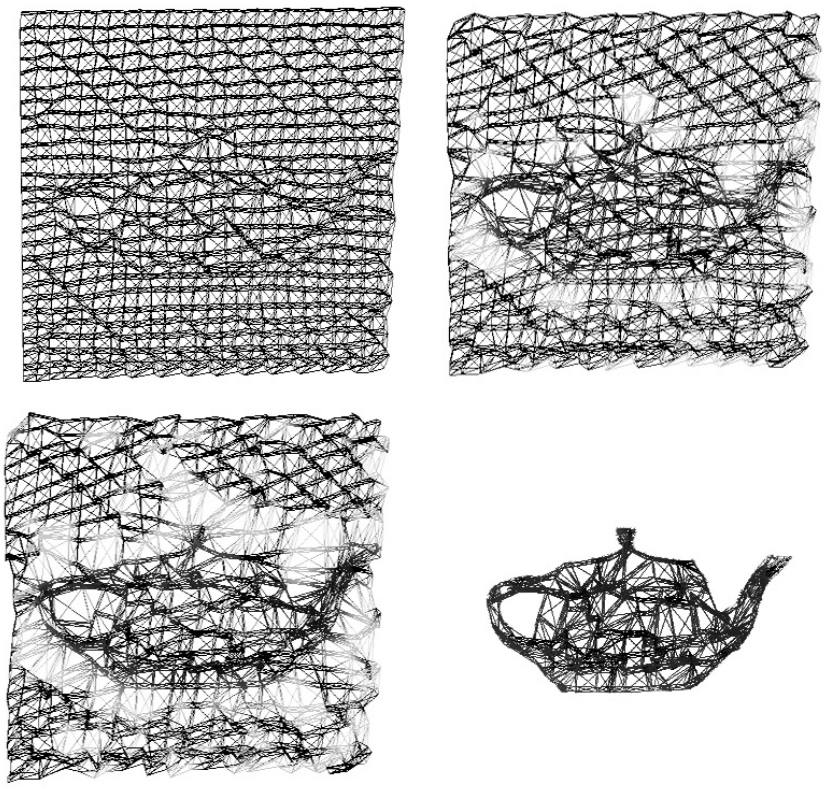

Figure 7.6: Consecutive steps of segmentation algorithm execution using an image with artificial shape as the input. The input image included a simple teapot shape.

by simple pre-processing of the input images, namely by thresholding them and discarding all the pixels with intensity value above certain level. After this step the medium intensity ranges appeared as the brightest areas in the image and the segmentation algorithm was able to detect them ignoring the bone structure.

Our segmentation experiments show that the level of detail and accuracy in detection of structure of objects is high and comparable with other popular segmentation methods. The new shape optimization scheme and other components of the WMD model do not introduce any drawbacks or flaws in the segmentation outcome, no parts of the input volumes are missing in the final results. The WMD model is also very suitable for working with very high densities of the mesh and very high resolutions of the input images, which resulted in very precise segmentation results.

7.3 Comparison with Existing Methods

In this section we compare the results of segmentation and the segmentation time of our method with the same values obtained using the TAV model. Both these segmentation methods rely on similar concepts and share some features of the model, however our changes in the shape optimization method and the topology changing mechanism can bring big improvements in the time of the segmentation process.

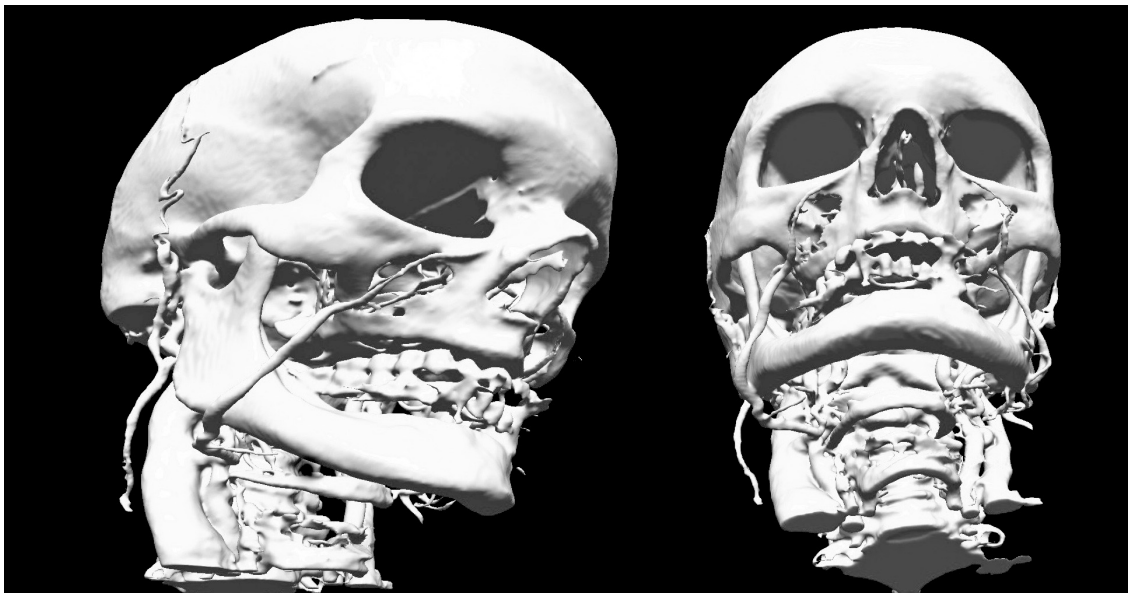

Figure 7.7: Result of the 320 slice CT scan segmentation.

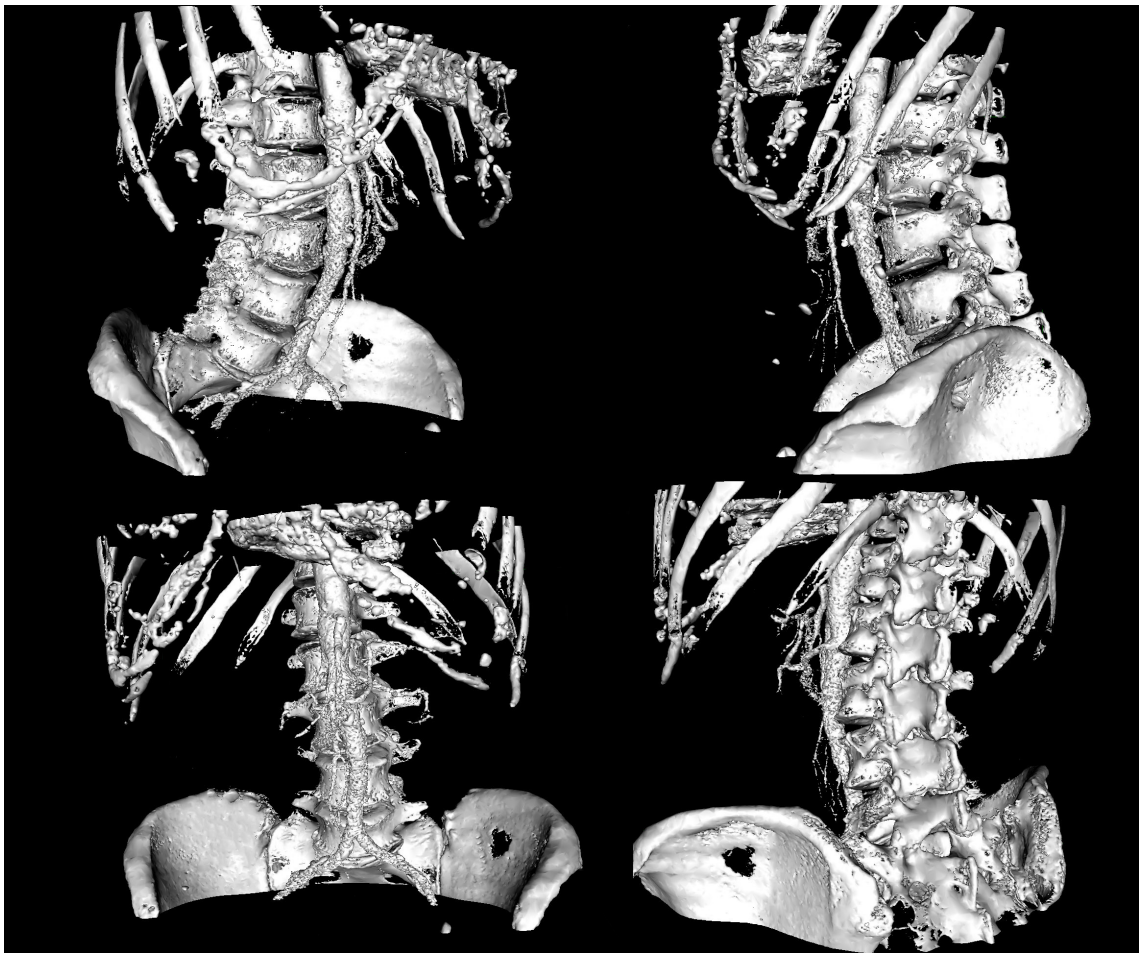

Figure 7.8: Results the 380 slice X-Ray scan segmentation.

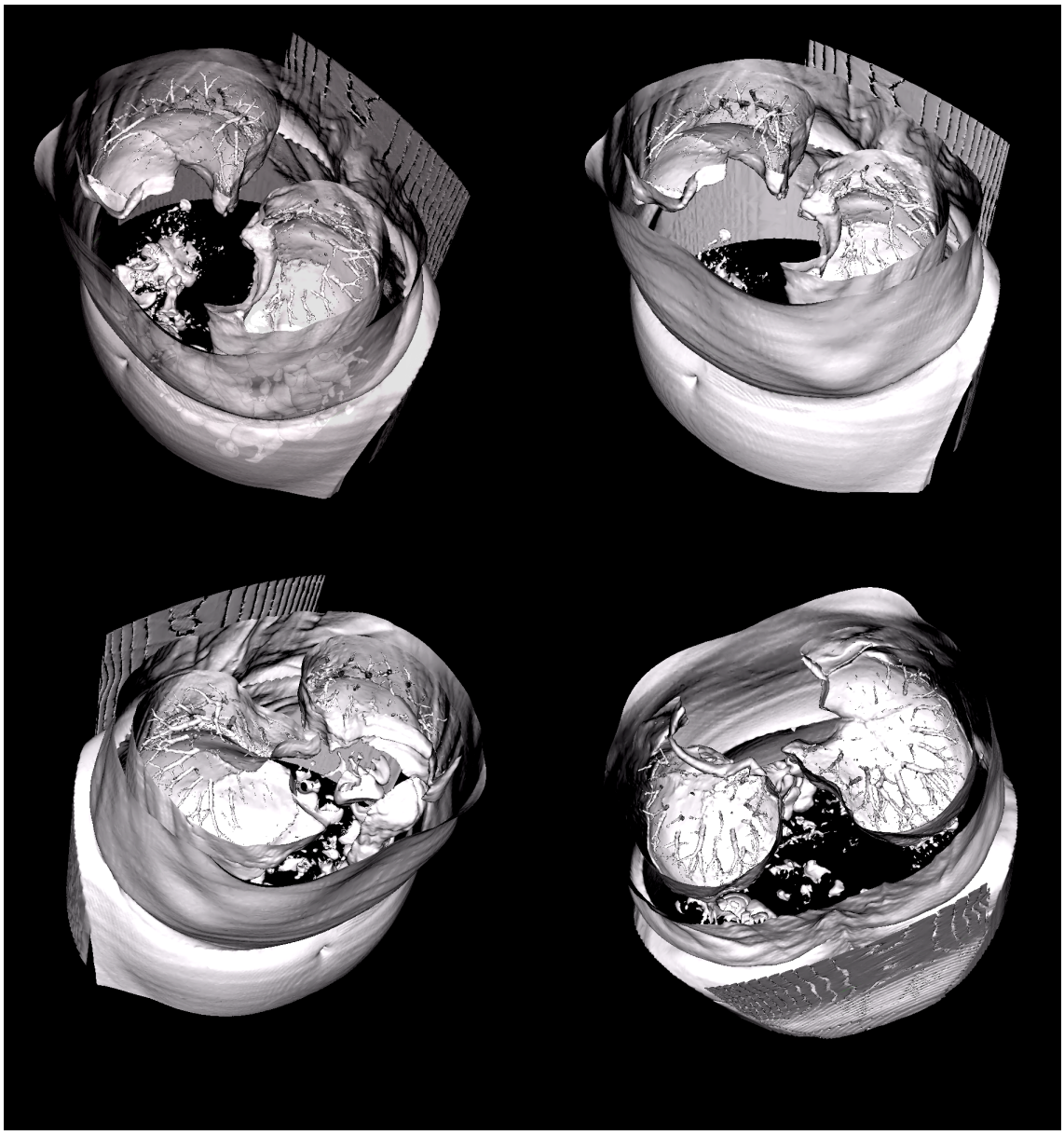

Figure 7.9: Results the 380 slice X-Ray scan segmentation.

7.3.1 Comparison of Segmentation Time

In each experiment with the artificial images the 2D image has been used twice, which resulted in a 2-slice 3D volume, which was segmented with the WMD amd TAV models. The execution times obtained in our experiments are presented on Fig. 7.10. As we can see, the Whole Mesh Deformation method shows a noteworthy improvement in the segmentation performance in all the cases. The execution time was always significantly lower than in the case ofTAV method, reaching 5.3 times improvement in Scenario 3.

This confirms our expectations described in the previous section. What is also very notable is that the WMD model delivered very similar segmentation times in all the scenarios, whereas theTAV model showed a much higher variety in this value. This shows that the segmentation time and the number of iterations are nearly independent from the contents of the images. To explain this let us consider the following:

The size of the mesh in those experiments was 16 by 16 pixels, which results in 16 pixels of

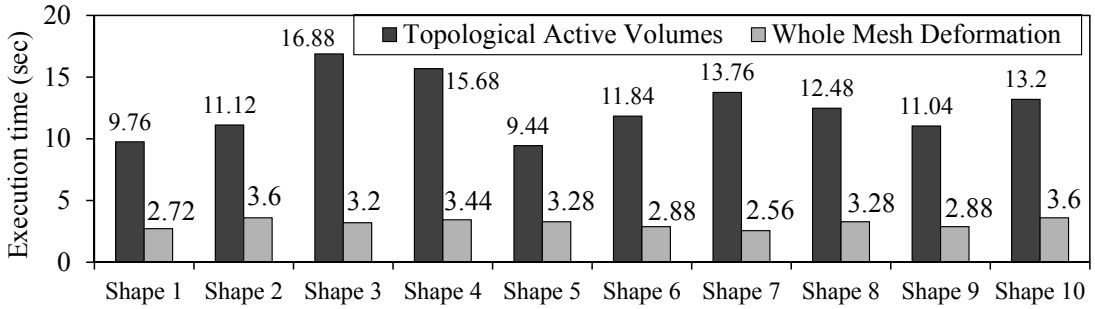

Figure 7.10: Results of the performance experiments.

maximum possible distance needed for each node to travel during the segmentation process. This is true if we assume that the segmentation parameters are chosen correctly and every given object will be approached only by the nodes initialized in their nearest neighborhood. As we can see, the maximum travel distance of a node can be estimated with high confidence without any information about the contents of the input images.

The size of the two input images was 512 by 512 pixels, which results in mesh of the size 33 by 33 nodes for each image, giving total number of 1089 nodes, constructing 1024 cells of the mesh. The number of mesh cells is relatively high, which lets us assume with high probability that at least in one of the cells a node will have to travel the maximum possible distance. And since the whole segmentation time is defined by the node that has to move for the largest distance of all the nodes, we can assume that this pessimistic scenario is the factual scenario for majority of algorithm executions. Tracing the segmentation process iteration by iteration we have confirmed that the above assumption is correct. Through the initial 16 iterations the nodes are progressing towards the object borders and after that only the step of breaking unwanted connections between nodes continues in order to finalize the topology changes and separate unwanted parts from the mesh. This part shows to be less predictable and presents some variation, which is mainly responsible for the small differences in required iterations for different scenarios. What can be seen from these experiments is that the WMD model is by definition not highly dependent from the contents of the segmented image and delivers identical results in much shorter times.

7.3.2 Dependency Between the Grid Density and Segmentation Speed

We have also compared how the two approaches perform in scenarios of different sizes of the mesh. We have executed the segmentation using Shape 10 from Fig. 7.1 together with 13 different values of inter-node spacing, namely from 20 by 20 pixels to 8 by 8 pixels (in x and y axis). As it can be seen on Fig. 7.11 (left), theTAV method requires exactly the same number of iterations to finish the segmentation, regardless the density of the mesh. In turn, the number of iterations required by the Whole Mesh Deformation method is decreasing along with the growth of mesh density. The explanation for this behavior lies in the fact that with smaller initial distances between mesh nodes the number of pixels that each node needs to travel is also decreasing, resulting in faster progression towards boundaries of objects. The optimal value of this parameter can be noticed around the initial distance between the nodes of 10 by 10 pixels. After that threshold the number of necessary iterations starts to depend more on the step of connections breaking and recognition of unwanted parts of the mesh, so further increase in the mesh density will not result in significant decrease of necessary iterations.

The values of execution times for all those scenarios are depicted on Fig. 7.11 (right). The time required to carry out segmentation using theTAV method is growing severely with the growth of mesh complexity, whereas in case of Whole Mesh Deformation we can notice only a very slight growth of the execution time. As we can see, the smaller number of iterations is balanced with the increased number of nodes to process in the whole mesh. As a result the execution times are maintained on nearly constant level until the optimal value is reached (10 by 10 pixels). Then we can see a slightly faster increase of the execution time, as the growing number of nodes in the mesh is no longer balanced by smaller number of iterations.
This low dependance of the segmentation time from mesh density is a much desired feature of the WMD model, as it allows performing precise segmentations of very complex shapes, having almost no drawback of increased execution times. With most of the known segmentation methods, including theTAV, an increase of the segmentation accuracy imposes also a significant growth of the segmentation time.

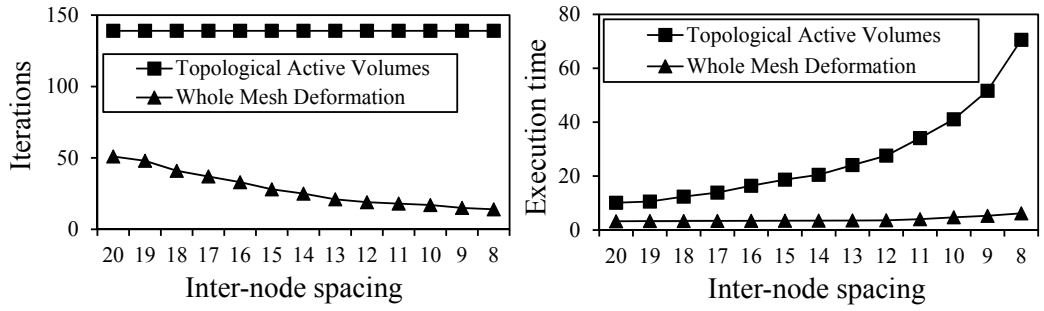

Figure 7.11: Results of segmentation experiments using different values of inter-node spacing, number of necessary iterations (left) and execution times in seconds (right).

Because of this differentiation the WMD model performs the segmentation in much shorter times than theTAV model. It also is much less dependent on the contents of the input images and on the number of nodes in the mesh.

7.3.3 Performance with Real-World Medical Images

The experiments with real medical images have been performed using the volumes presented in Fig. 7.2 and 7.3. In these images it is important to notice the large difference in the contents of the consecutive slices. In every case of 3D volume segmentation the whole execution time will be highly dependent from the slice, which requires the biggest amount of time to be processed. In our CT skull scan example (Fig. 7.2), as well as in many similar real-world medical images, we can see that the last slices of the sets contain very little data, located far from the image borders. Performing the volume segmentation using the assumptions of theTAV model we would need the nodes of the mesh to travel through nearly the entire image to reach this data. Therefore, the whole segmentation would be very time consuming. We have examined the last slice of the CT volume and found out that the longest distance from the edge of the image to object of interest is 220 pixels. This means that the number of iterations required by theTAV method to complete the segmentation should be around 220. On the other hand, our Whole Mesh Deformation method is nearly independent from the contents of the image, so the segmentation times should be almost equal for all the slices and the total segmentation time should be significantly lower.

The execution times and the number of iterations for the two test cases are depicted in Fig. 7.12 and Fig. 7.13, respectively. As it can be seen, the WMD model outperforms theTAV model significantly in all the scenarios. The segmentation time of the CT scan volume equalled 689 seconds for the WMD model and 3320 seconds for theTAV model. This results in 481% efficiency growth ratio. The number of necessary iterations for WMD andTAV models equalled 45 and 239, respectively. The very large number of iterations required by theTAV model confirms our observations about the required way that the pixels need to travel under the assumptions of this model. The results of the second experiment are of yet higher difference, the execution times equaled 818 seconds for the WMD model and 6284 seconds for the TAV model, which results in 768% efficiency growth ratio. The required iterations equaled respectively 47 and 382. The WMD model maintained a similar number of iterations comparing to the previous experiment and the increased execution time is the result of a larger input volume. The TAV model required a significantly larger number of iterations. This of course resulted in a much longer execution time, which was even further increased by the larger number of slices in the input volume. The higher number of iterations for the TAV model in the second experiment is justified again with the placement of objects of interest in the input volume. In some input slices of the X-Ray volume (corresponding to the second row of images in Fig. 7.3) we can see that parts of the bone structures are located in the lower-right regions of the image. To close the mesh and to finish the segmentation process the TAV model needed to move the nodes of the mesh from the top-left corner of the image for the distance of around 370 pixels. These experiments shows how well-suited is our model for real-world scenarios, where similar situations can occur often - the slices of a single volume can show a big variety of sizes, which can lead to unreasonably long execution times.

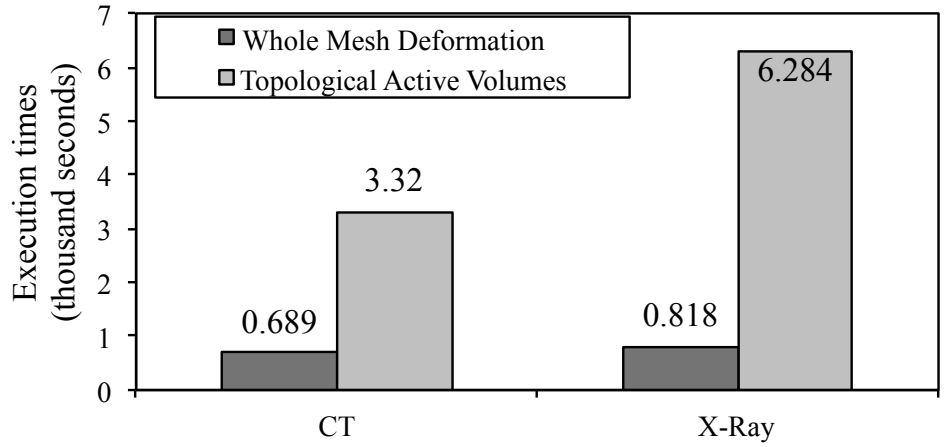

Figure 7.12: Results of the experiments with real medical images - execution times of the segmentation algorithms.

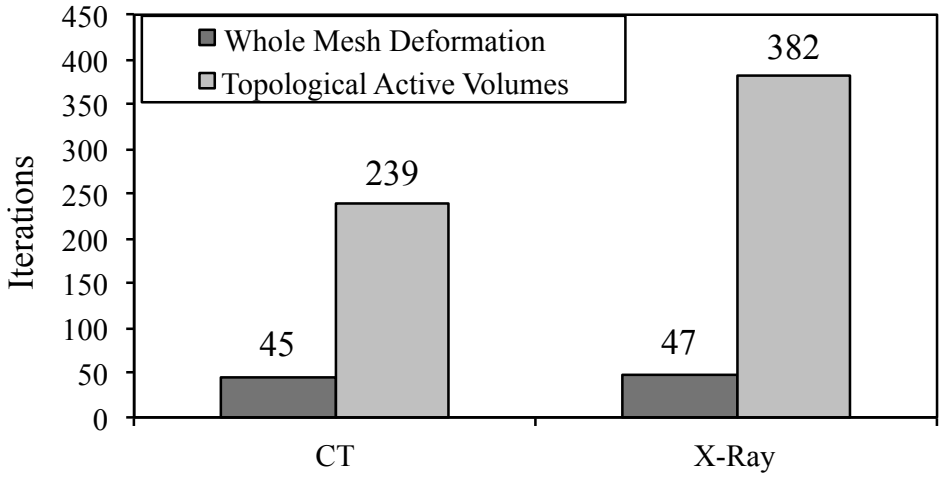

Figure 7.13: Results of the experiments with real medical images - iterations required to perform a full segmentation.

7.4 Parallel Implementation Results

The implementation of our parallel algorithm has been performed using the MS-MPI message passing interface. The experiments have been executed on a computer cluster constructed from 12 processing units of 3GHz each, running the Microsoft HPC Server 2008 operating system. As the input image we have used the CT head scan presented on Fig. 7.2. The times required to carry out the segmentation with different numbers of processing units are presented on Fig. 7.14 left. Furthermore, Fig. 7.14 right presents the speedup obtained with the parallel implementation. This metric is obtained by dividing the execution time of segmentation using single processing unit by the execution time with multiple processing units.

The charts show that the parallelization of the method is performed efficiently and the resulting performance improvement is very close to ideal. By this we mean half the execution time for 2 processing units, quarter for 4 processing units and so on. This is a result of the fact that our method does not need any synchronization or exchanging any data between participating processes and also of the fact that the segmentation process takes almost exactly the same time for any part of the input volume.

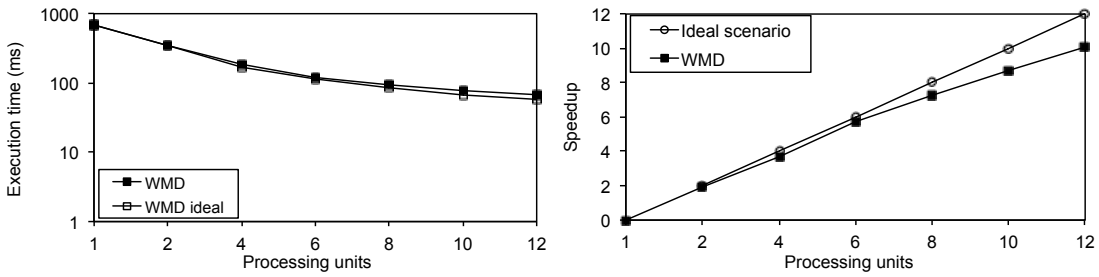

Figure 7.14: Execution times and speedup gained with execution of the parallel algorithm on multi-processing unit environment.

7.5 Extended Whole Mesh Deformation Model

The segmentation algorithm has also been implemented using the approach of the Extended WMD model described in Chapter 6. The changes included the ability to move the nodes of the mesh in the Z-direction and the modifications to the energy formulation and flexibility parameter, described also in Chapter 6.

Our initial experiments included segmentation of three images presented in Fig. 7.4. For each input volume we have carried out the segmentation process using the WMD model and the Extended WMD model with the same resolution of the mesh. This allowed comparing the exact differences between the two approaches in terms of delivered accuracy of results and the whole execution time.

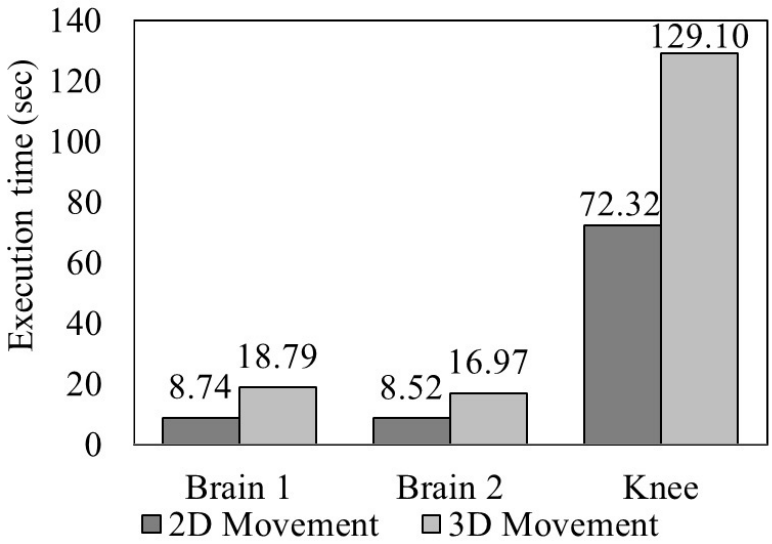

Figure 7.15: Execution times (in seconds) for 3 segmentation experiments presented in this section.

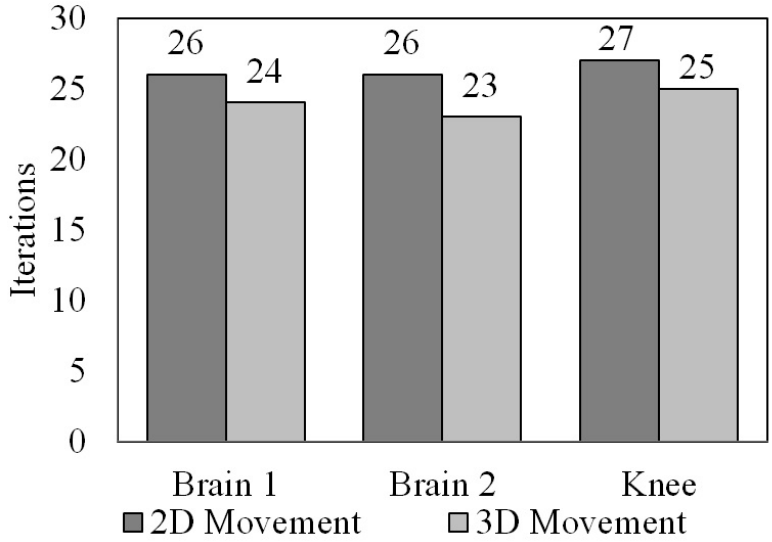

Figure 7.16: Number of necessary iterations for 3 segmentation experiments presented in this section.

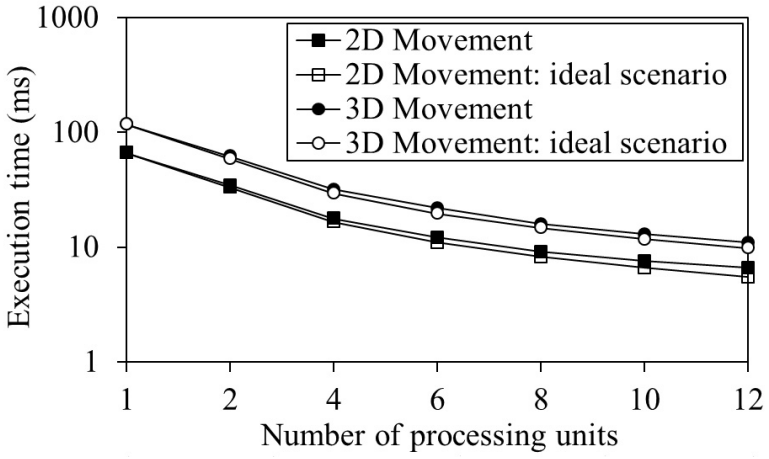

Figure 7.17: Execution times (in milliseconds, on logarithmic scale) for knee scan segmentation experiment using 2D and 3D node movement and different numbers of processing units.

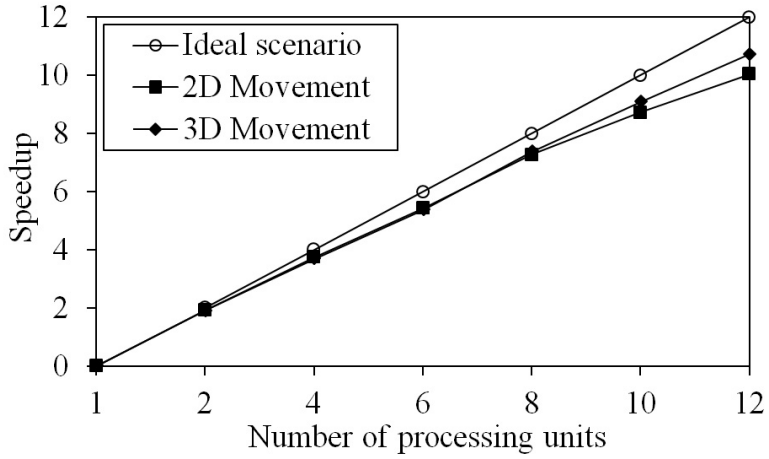

Figure 7.18: Level of speedup achieved for the knee scan segmentation experiment using 2D and 3D node movement and different numbers of processing units.

Fig. 7.15 presents the execution times for each segmentation task. As it can be seen, the first implementation of the WMD model, with only 2D movement of the nodes of the mesh, delivers the results in shorter times. This has been expected, as the deformation process in case of the Extended WMD model is carried out in 3 instead of 2 dimensions. This in turn means that each node is positioned in 27 instead of 9 locations in each iteration of the algorithm. This results in growth of the number of necessary calculations and extends the overall segmentation time, which are around 52% longer in each of the experiments. On the other hand, Fig. 7.16 present the amount of iterations that has been necessary to finish the segmentation task. As we can see, the Extended WMD model with 3D movement of the nodes the number of iterations has been slightly smaller for each experiment. This can be explained by the fact that nodes of the mesh have bigger movement capabilities and they are able to position themselves in locations that were not reachable using just 2D node movement. Therefore they are able find their way to the final location more efficiently.

7.5.1 Parallel Implementation

The WMD model has been designed with the aim of execution on parallel architectures and it has shown to be very scalable [LPFF09c]. After extending it with the capabilities of 3D movement of the nodes we have performed also the execution experiments on a parallel architecture. Given the fact that the overhead of the execution time of the 3D node movement version is due only to the increased amount of calculations, the scalability possibilities of the WMD model should be maintained or increased, as those calculations do not require any synchronization or communication carried out during the process and thus they should scale very efficiently. The computer cluster used for these experiments was composed of 6 double-core machines with 3Ghz processing units and 1GB of memory each. The operating system used was the Windows HPC Server 2008.

Fig. 7.17 presents the execution times of the algorithm using different number of processing units. It can be seen that the version capable of 3D movement takes longer to finish the task, but both versions of the model perform very similarly in terms of scalability, reaching very near to the ideal scenario. By this we mean half of the execution time for 2 processing unit, a quarter of the execution time for 4 units, and so on. On Fig. 7.18 we are able to see the exact amount of speedup obtained with different numbers of processing units for both versions of the model and this time it is notable that in experiments with up to 8 processing units both models perform in the same way, while starting from the 8 processing units the 3D movement capable version shows a better performance in terms of scalability. This is due to the following fact: the calculations increase the time necessary to finish the segmentation task and all of this overhead is treated by the processing units, giving them more work. At the same time none of the overhead becomes a part of the communication/synchronisation step. With the increased amount of workload for the processing units and no communication overhead, the scalability of the whole process is increased.

7.5.2 Segmentation Results

The 3D movement capability of the Extended WMD model is presented on Fig. 7.19. The images present the final result of segmentation using the Extended WMD model (left) and the WMD model (right). The volume is projected from the Y plane, which means that the X and Z planes appear visible. Only the nodes of the mesh are presented, the links have been hidden. As it can be seen, the 3D movement capable model has produced a volume with nodes that are distributed in all the planes. On the other hand, the 2D movement version has produced a volume with nodes restricted to their original Z coordinates. What appears to be the slight movement on nodes in the Z plane in the top and the bottom of the volume are in fact just a result of a perspective view of the volume, all the nodes of the mesh have their original Z coordinates maintained. As we can expect, this sort of result would not describe properly the real-world objects.

Fig. 7.20 and Fig. 7.21 present exemplary results obtained with the WMD model and the Extended WMD model. We have used the CT head scan volume that can be seen on Fig. 7.2, however, the amount of image slices in the volume has been decreased by half by removing every second image from the available set. In each pair of similar images the top image presents the result obtained with the original WMD model and the bottom image presents the result of the Extended WMD model. As we can see in all of the original WMD results the images present a range of certain artifacts and the surface appears not smooth. On the other hand, the Extended

WMD model was able to reconstruct the volume in a much more desired way, creating smoother transition between the available image slices.

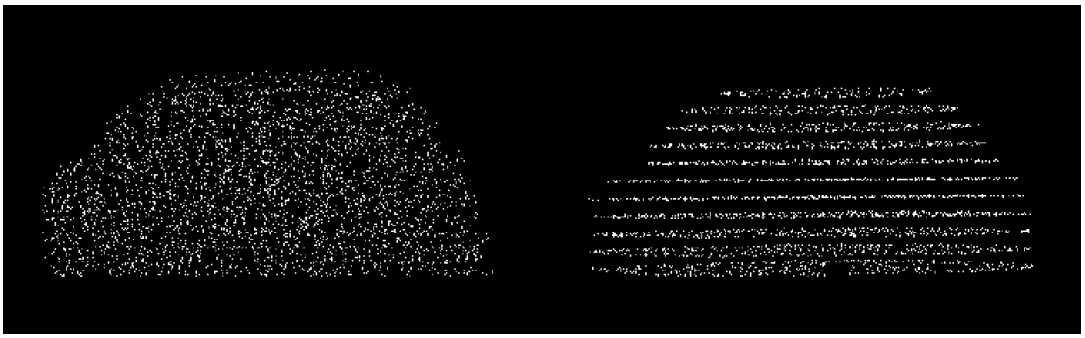

Figure 7.19: Results of the CT brain scan segmentation experiment. Left: full 3D movement of nodes, right: only 2D movement of nodes

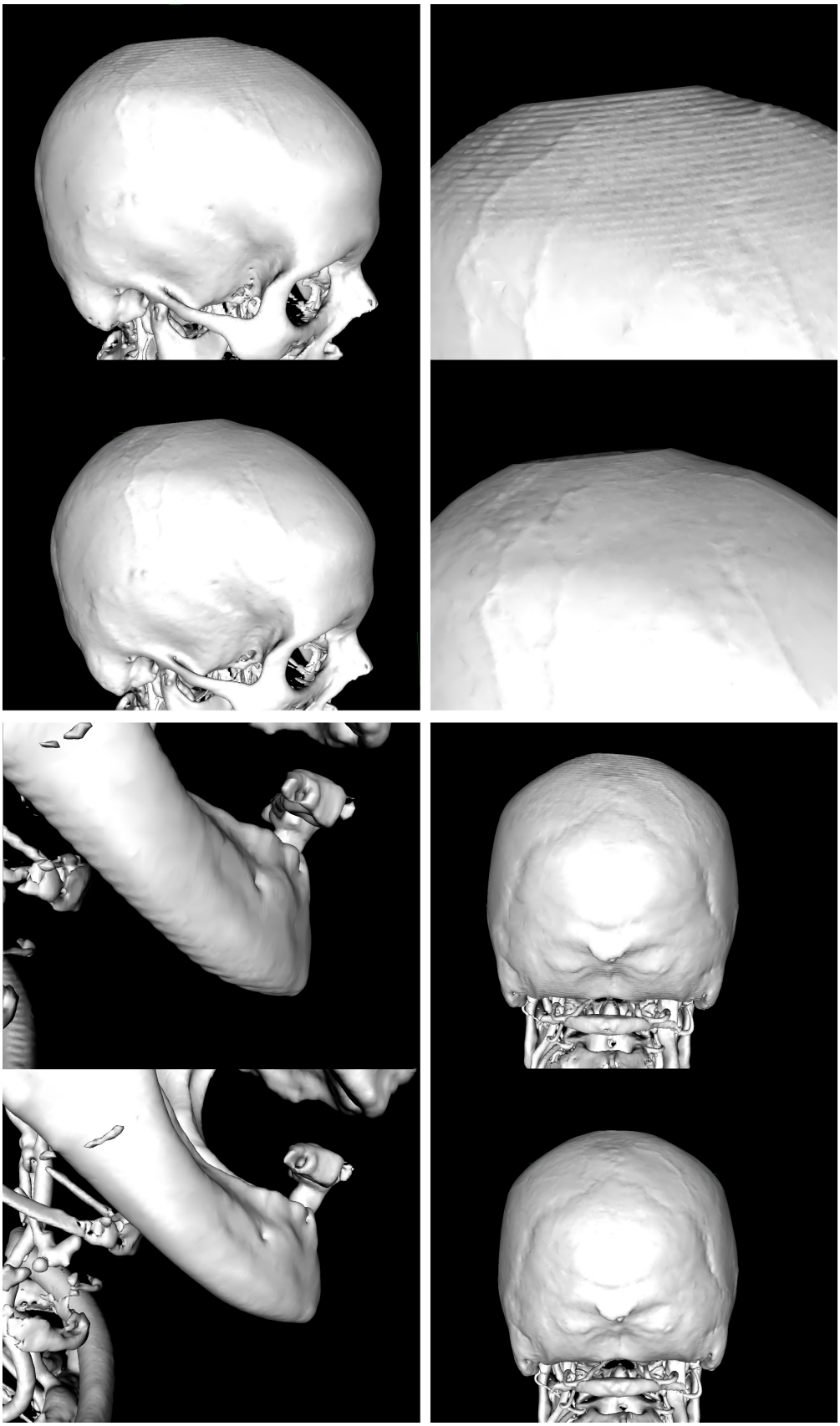

Figure 7.20: Results of the CT brain scan segmentation experiment using the WMD model and the Extended WMD model. In each pair of similar images the top image presents the result obtained with 2D movement of the nodes and the and the bottom image presents the result of the 3D movement of the nodes.

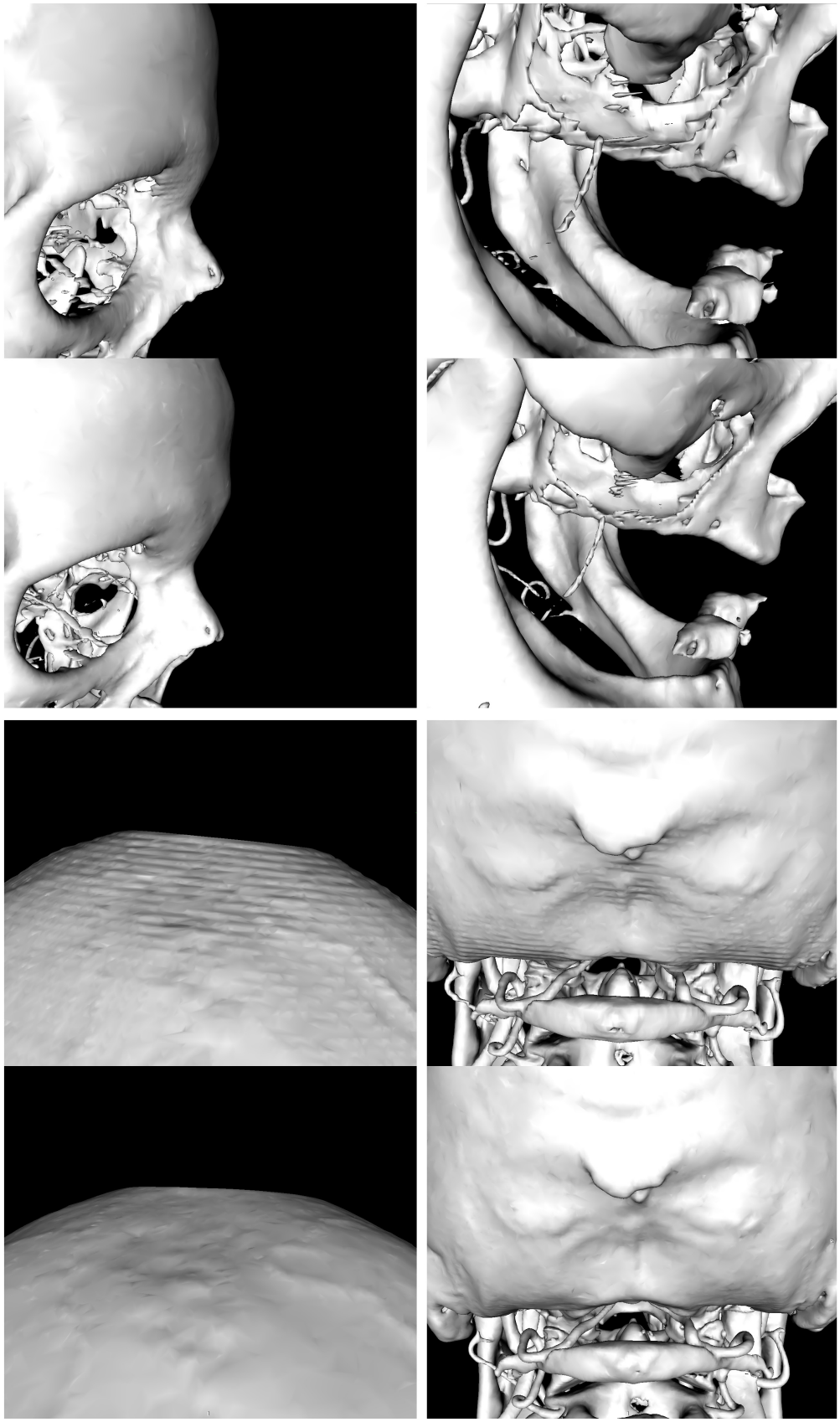

Figure 7.21: Results of the CT brain scan segmentation experiment using the WMD model and the Extended WMD model. In each pair of similar images the top image presents the result obtained with 2D movement of the nodes and the and the bottom image presents the result of the 3D movement of the nodes.

Chapter 8

Conclusions and Future Work

In this thesis we have approached the topic of modern medical image segmentation. The evolution of this field has been very interesting and challenging over the last three decades. As written before, the abilities of computers to deliver valuable segmentation results have been constantly improving and extending in that time. Until this day the added value of the medical image segmentation has grown so much that it is impossible to speak of modern health-care without mentioning the help offered by the segmentation algorithms.
The last years have brought a tremendous progress in this field and we are now capable of gathering and exploiting medical information that was never before possible. Medical devices, which perform scanning and deliver images for the medical practitioners, have expanded their possibilities and deliver data in short time, with very high resolution in all three dimensions. This means that practitioners are able to acquire more information than ever before, but it also raises a set of new challenges for the image processing algorithms and the hardware on which they operate.
In this work we have described thoroughly these challenges and problems, which included the tremendous growth of sizes of data to process, and the shift in development of computer hardware - from increasing frequencies and number of operations per second, towards multi-core architectures and parallelism.
In order to answer all of these challenges, we have presented a novel model for 3D-image segmentation, called the Whole Mesh Deformation Model. Being based on the concept of Deformable Models, a popular image segmentation algorithms family, it inherited the main components and features of typical solutions belonging to this family. However, when designing the most important parts of our model, we have taken a new approach with the specific goal in mind, namely to adapt this solution to the above-mentioned problems. Because of this the main components of the WMD model have differed notably from the original idea of DMs as well as from more recently proposed solutions, like the Level-set method, or the TAV.

8.1 Addressing the Problems

The above-mentioned assumptions have been implemented in the WMD model. They have resulted in several very interesting capabilities of the model, which address very well the problems described in Chapter 1, under Problem Definition and Objectives. In particular we can specify that the WMD model has proven to have the following features.

Perhaps the most important characteristic of the WMD model has to be the fact that the segmentation procedure shows a very good performance. The experiments performed on a wide range of input data have shown that the new methods for representation of the shapes of interest, as well as to the process of their deformation and shape optimization, which have been implemented in the WMD model, allow to allocate more of the available resources into the segmentation process and give a significant improvement in terms of the execution times. Ex-

periments have been performed with comparison to the TAV solution, which is the only currently known one that delivers comparable results to the WMD model. In every experiment the segmentation time has been significantly in favor of the WMD model, ranging between 3 to 5 times shorter exectution times for the artificial input images, and reaching a very high improvement of nearly 8 times shorter execution time with the real-world medical images. Performance improvement of this rate shows that the concepts behind the WMD model were designed and implemented in a correct way.

All the components of the segmentation procedure have become more predictable and stable. This means that it is easier to estimate the behavior of the segmentation algorithm and predict the execution time and workload distribution over time. This in turn allows a very efficient parallelization, which is very hard to obtain with other popular methods based on DMs framework. An efficient parallelization is a very attractive feature due to the current trends in the development of computer hardware - the introduction of affordable multi-core computers, capable of handling 4, 8 or 16 paralell processes, and the introduction of processing using Graphical Processing Units, which are in fact very large-scale parallel processing architectures. As mentioned before, this was a very important goal for us to reach with the WMD model and the experiments have proven that it has been indeed successful.

The shapes of interest present in the input images are represented with a volumetric mesh, composed of nodes interconnected with edges. This mesh can be defined with different levels of density (more nodes per width or height of the input image) and the higher is the density, the more accurate will be the obtained result. Usually in similar solutions the increase of the density of the mesh would mean a significant increase in the segmentation time. However, experiments have proven that with the WMD model the segmentation time is dependent in a very small factor from the density of the mesh. This is a very desirable and also unique feature of our method, as it allows to obtain high quality results without the drawback of increased segmentation time. As described before, it was possible to achieve because the higher number of mesh nodes in the WMD model translates to a larger amount of resources that can be used for object segmentation.

The segmentation time depends also very little from the contents of the input image. This refers to the fact, that in typical scenarios of application for the modern image segmentation algorithms the contents of the analyzed images can be unpredictable and the objects of interest can be distributed in an uneven manner. Using the traditional approach of the DMs the segmentation algorithm would need to search the area of the input images and expand or retract accordingly, to incorporate the entire object of interest. This can also mean relocating the Deformable Model far from its original initialization area. What this means is that for several images of the same resolution and size the segmentation times could be completely different. This is not the case for the WMD model - our approach to the process of deformation and searching only in the nearest neighborhood of each node has resulted in almost complete independence of the execution time from the contents of the input images.

With all the performed experiments it was possible to note that the only factor that defines the execution time of the WMD model segmentation algorithm in a noteworthy manner is the resolution of the input image. The higher the resolution, the larger the neighborhoods that each node needs to examine and the longer the execution time of the whole procedure. However, it

is still important to observe that this dependency is still not as strong as in some other similar solutions, like for example the TAV model.

The segmentation results delivered by the WMD model show exactly the same level of quality as with other popular solutions. The segmented shapes are represented with high precision and several objects can be detected in the scenes of interest thanks to the Dynamic Topology Changes mechanism. This has been assessed by comparing the segmentation results obtained with the WMD and TAV solutions using medical segmentation software.
The dependency on user interaction and on initialization of segmentation is very low. There is no need to manually select values of the input parameters, as they can be chosen automatically using a set of rules, which have been defined experimentally, and a simple analysis of the input data, which the WMD model can perform. Also, there is no need to manually initialize the shape of the model at the beginning of the segmentation procedure, because the WMD model covers by default the entire scene of interest. These characteristics make the dependency from the user significantly lower than in other approaches using the same concept of volumetric mesh-based segmentation.
The tests that we have performed using real-world medical images have proven that those features allow our solution to perform very well in medical applications. The WMD model can be adopted in any medical lab, either large-scale or small ones, and bring the possibility to perform very efficient segmentation of large medical images, with high precision and in very competitive execution times.

8.2 Future Work

The WMD model in its current shape is ready to serve as the basis of segmentation algorithms that can perform analysis of images in research settings and in medical facilities. However, it is still possible to extend its capabilities or improve the current ones. A straightforward continuation of work on the WMD model would be to improve the features that define the possibilities of the model. The optimization of the topological changes or the 3D movement of the nodes could increase the capacity of the WMD model to deliver precise results in short times.
Another possibility is to increase the capacity of the WMD model by implementing new features into it. The segmentation process of the WMD model depends in large part on the formulation of the Energy Function. The behavior of the model can be controlled by changing the values of the weights of different function components, as well as by extending the function with new modules and therefore introducing new types of behavior. This can be seen as a modular composition of the model, which allows to extend the model with new capabilities. A great set of new possibilities of image segmentation methods lies in the capacity to incorporate prior knowledge into the process using statistical models [SvZ09]. This refers to using solutions like Active Shape Models [CTCG95], [LU09], [SS12] or Active Appearance Models [CET01], [BC10], [TM12] to represent the typical features of objects present in the scene of interest. This allows to highly increase the robustness of the segmentation procedure to flaws like noise or incomplete data and to increase the overall quality of segmentation process. Therefore, incorporation of prior knowledge is a very interesting topic to research in the future developments of the WMD model.

Bibliography

[AB94] R. Adams and L. Bischof. Seeded region growing. *Pattern Analysis and Machine Intelligence, IEEE Transactions on*, 16(6):641–647, 1994. 9

[AC06] Roberto Ardon and Laurent Cohen. Fast constrained surface extraction by minimal paths. *International Journal of Computer Vision*, 69(1):127–136, 2006. 10.1007/s11263-006-6850-z. 17

[ACY05] R Ardon, L D Cohen, and A Yezzi. A new implicit method for surface segmentation by minimal paths: Applications in 3d medical images. *EMMCVPR05*, pages 520–535, 2005. Available from: `http://ieeexplore.ieee.org/lpdocs/epic03/wrapper.htm?arnumber=1529749`. 17, 27

[ACY07] Roberto Ardon, Laurent D. Cohen, and Anthony Yezzi. A new implicit method for surface segmentation by minimal paths in 3d images. *Applied Mathematics and Optimization*, 55(2):127–144, 2007. 10.1007/s00245-006-0885-y. 17

[AGzN94] Andr, Gu, ziec, and Ayache Nicholas. Smoothing and matching of 3-d space curves. *Int. J. Comput. Vision*, 12(1):79–104, 1994. 181453. 7

[Alb76] Martelli Alberto. An application of heuristic search methods to edge and contour detection. *Commun. ACM*, 19(2):73–83, 1976. 360004. 7

[ALPM00] F. M. Ansia, J. Lopez, M. G. Penedo, and A. Mosquera. Automatic 3d shape reconstruction of bones using active nets based segmentation. In *Pattern Recognition, 2000. Proceedings. 15th International Conference on*, volume 1, pages 486–489 vol.1, 2000. 21

[AR99] P. Mangan Alan and T. Whitaker Ross. Partitioning 3d surface meshes using watershed segmentation. *IEEE Transactions on Visualization and Computer Graphics*, 05(4):308–321, 1999. 10

[ATW88a] A. A. Amini, S. Tehrani, and T. E. Weymouth. Using dynamic programming for minimizing the energy of active contours in the presence of hard constraints. In *Computer Vision., Second International Conference on*, pages 95–99, 1988. 12, 27

[ATW88b] A.A. Amini, S. Tehrani, and T.E. Weymouth. Using dynamic programming for minimizing the energy of active contours in the presence of hard constraints. In *International Conference on Computer Vision*, pages 95–99, 1988. xii

[Bak70] D. W. Baker. Pulsed ultrasonic doppler blood-flow sensing. *IEEE Transactions on Sonics and Ultrasonics*, 17(3):170–184, 1970. 2

[BC10] K. Babalola and T. Cootes. Using parts and geometry models to initialise active appearance models for automated segmentation of 3d medical images. In *Biomedical Imaging: From Nano to Macro, 2010 IEEE International Symposium on*, pages 1069–1072, 2010. xxv, 81

[Bea06] Richard Beare. A locally constrained watershed transform. *IEEE Trans. Pattern Anal. Mach. Intell.*, 28(7):1063–1074, 2006. 1137546 Member - Richard Beare. 17

[BG02] V. Boskovitz and H. Guterman. An adaptive neuro-fuzzy system for automatic image segmentation and edge detection. *Fuzzy Systems, IEEE Transactions on*, 10(2):247–262, 2002. 12

[BIC13] N. Bova, O. Ibanez, and O. Cordon. Image segmentation using extended topological active nets optimized by scatter search. *Computational Intelligence Magazine, IEEE*, 8(1):16–32, 2013. 21

[BL79] S. Buecher and C. Lantuéjoul. Use of watershed in contour detection. In *Int. Workshop Image Processing, Real-Time Edge and Motion Detection/Estimation*, pages 17–21, 1979. 10

[BP05] N. Barreira and M. G. Penedo. Topological active volumes. *EURASIP J. Appl. Signal Process.*, 2005:1939–1947, 2005. xiii, xix, xxi, 3

[BPAR08] N. Barreira, M. G. Penedo, C. Alonso, and J. Rouco. Handling topological changes in the topological active volumes model. In *Proceedings of the 5th International Conference on Image Analysis and Recognition*, volume 5112, pages 121–131, 2008. xiii, xix, xxi, 3, 23

[BPMA03] N. Barreira, M. G. Penedo, C. Mariño, and F. M. Ansia. *Topological Active Volumes*, volume Volume 2756/2003, pages 337–344. Springer Berlin / Heidelberg, 2003. 21, 22, 27

[BS94] C. A. Bouman and M. Shapiro. A multiscale random field model for bayesian image segmentation. *Image Processing, IEEE Transactions on*, 3(2):162–177, 1994. 11

[CA79] G. B. Coleman and H. C. Andrews. Image segmentation by clustering. *Proceedings of the IEEE*, 67(5):773–785, 1979. 11

[Can86] J. Canny. A computational approach to edge detection. *IEEE Transaction on Pattern Analysis and Machine Intelligence*, 8(6):679–698, November 1986. Available from: `http://portal.acm.org/citation.cfm?id=11275`. xvi, 33

[Cas95] V. Caselles. Geometric models for active contours. In *International Conference on Image Processing*, pages III: 9–12, 1995. xii

[CBET99] Timothy F. Cootes, C. Beeston, Gareth J. Edwards, and Christopher J. Taylor. A unified framework for atlas matching using active appearance models, 1999. 658360 322-333. 15

[CET01] T.F. Cootes, G.J. Edwards, and C.J. Taylor. Active appearance models. *Pattern Analysis and Machine Intelligence, IEEE Transactions on*, 23(6):681–685, 2001. xxv, 81

[CJ97] Xu Chenyang and L. Prince Jerry. Gradient vector flow: A new external force for snakes, 1997. 794344 66. 14

[CJPM+96] O. Cuisenaire, Thiran J.-P., B.M. Macq, C. Michel, A. de Volder, and F. Marques. Automatic registration of 3d mr images with a computerized brain atlas. *Medical Imaging 1996: Image Processing*, 2710:438–448, 1996. 14

[CK96] Laurent D. Cohen and Ron Kimmel. Global minimum for active contour models: A minimal path approach, 1996. 794528 666. 20

[CK97] V. Chalana and Y. Kim. A methodology for evaluation of boundary detection algorithms on medical images. *Medical Imaging, IEEE Transactions on*, 16(5):642–652, 1997. 7

[CKS95a] V. Caselles, R. Kimmel, and G. Sapiro. Geodesic active contours. In *Fifth International Conference on Computer Vision*, Massachusetts, June 1995. 2, 53

[CKS95b] V. Caselles, R. Kimmel, and G. Sapiro. Geodesic active contours, 1995. 840137 694. 12, 20, 27

[CM00] Ting Chen and Dimitris Metaxas. *Image Segmentation Based on the Integration of Markov Random Fields and Deformable Models*, pages 256–265. 2000. 19

[CM03] Ting Chen and Dimitris Metaxas. *Gibbs Prior Models, Marching Cubes, and Deformable Models: A Hybrid Framework for 3D Medical Image Segmentation*, pages 703–710. 2003. 19

[CO07] J Carlson and D Ortendahl. Segmentation of magnetic resonance images using fuzzy clustering. In *Proc. Information Processing in Medical Imaging*, pages 91–106. C. de Graaf and M. Viergever eds., 2007. 7

[CP11] M.C.J. Christ and R.M.S. Parvathi. Fuzzy c-means algorithm for medical image segmentation. In *Electronics Computer Technology (ICECT), 2011 3rd International Conference on*, volume 4, pages 33–36, 2011. 11

[CSD96] A. Chakraborty, L. H. Staib, and J. S. Duncan. Deformable boundary finding in medical images by integrating gradient and region information. *Medical Imaging, IEEE Transactions on*, 15(6):859–870, 1996. 7

[CTCG95] T.F. Cootes, C.J. Taylor, D.H. Cooper, and J. Graham. Active shape models-their training and application. *Computer Vision and Image Understanding*, 61(1):38 - 59, 1995. Available from: `http://www.sciencedirect.com/science/article/pii/S1077314285710041`. xxv, 81

[CTWA92] D. Louis Collins, M. Peters Terence, Dai Weiqian, and C. Evans Alan. Model-based segmentation of individual brain structures from mri data. volume 1808, pages 10–23. SPIE, 1992. Visualization in Biomedical Computing '92 1. 7

[CV01a] T. F. Chan and L. A. Vese. Active contours without edges. *IEEE Transaction on Image Processing*, 10(2):266–277, 2001. xii

[CV01b] T. F. Chan and L. A. Vese. Active contours without edges. *Image Processing, IEEE Transactions on*, 10(2):266–277, 2001. 12

[CZK+98] D. L. Collins, A. P. Zijdenbos, V. Kollokian, J. G. A. Sled J. G. Sled, N. J. A. Kabani N. J. Kabani, C. J. A. Holmes C. J. Holmes, and A. C. A. Evans A. C. Evans. Design and construction of a realistic digital brain phantom. *Medical Imaging, IEEE Transactions on*, 17(3):463–468, 1998. 19

[Del94] H. Delingette. Simplex meshes: a general representation for 3d shape reconstruction. In *Computer Vision and Pattern Recognition, 1994. Proceedings CVPR '94., 1994 IEEE Computer Society Conference on*, pages 856–859, 1994. 22

[Dem99] Terzopoulos Demetri. Artificial life for computer graphics. *Commun. ACM*, 42(8):32–42, 1999. 310966. 23

[DET07] I. Dagher and K. El Tom. Waterballoons: A hybrid watershed balloon snake segmentation. In *Neural Networks, 2007. IJCNN 2007. International Joint Conference on*, pages 1–6, 2007. 17

[DHI92] H. Delingette, M. Hebert, and K. Ikeuchi. Shape representation and image segmentation using deformable surfaces. *Image Vision Comput.*, 10(3):132–144, 1992. 2

[DHT+99] B. M. Dawant, S. L. Hartmann, J. P. Thirion, F. Maes, D. Vandermeulen, and P. Demaerel. Automatic 3-d segmentation of internal structures of the head in mr images using a combination of similarity and free-form transformations. i. methodology and validation on normal subjects. *Medical Imaging, IEEE Transactions on*, 18(10):909–916, 1999. 14

[DLW05] Feng Ding, Wee Kheng Leow, and Shih-Chang Wang. Segmentation of 3d ct volume images using a single 2d atlas. In *Proceedings of the First international conference on Computer Vision for Biomedical Image Applications*, CVBIA'05, pages 459–468, Berlin, Heidelberg, 2005. Springer-Verlag. Available from: `http://dx.doi.org/10.1007/11569541_46`. 14

[DM00] H. Delingette and J. Montagnat. Shape and topology constraints on parametric active contours. *Computer Vision and Image Understanding*, 83(2):140–171, 2000. xii

[Dun73] J.C. Dunn. A fuzzy relative of the isodata process and its use in detecting compact well-sparated clusters. *Journal of Cybernetics*, 3:32–57, 1973. 11

[EAUC13] E. Erdil, A.O. Argunsah, D. Unay, and M. Cetin. A watershed and active contours based method for dendritic spine segmentation in 2-photon microscopy images. In *Signal Processing and Communications Applications Conference (SIU), 2013 21st*, pages 1–4, 2013. 10

[EBG08] Ayman El-Baz and G. Gimel'farb. Image segmentation with a parametric deformable model using shape and appearance priors. In *Computer Vision and Pattern Recognition, 2008. CVPR 2008. IEEE Conference on*, pages 1–8, 2008. 16

[EJ75] R. C. Eggleton and K. W. Johnston. Real time mechanical scanning system compared with array techniques. *IEEE Transactions on Sonics and Ultrasonics*, 896(74):16–18, 1975. 2

[FJD02] Yong Fan, Tianzi Jiang, and Evans David. Volumetric segmentation of brain images using parallel genetic algorithms. *IEEE transactions on medical imaging*, 21(8):904–909, 2002. 18, 27

[FS06a] K. Fritscher and R. Schubert. 3d image segmentation by using statistical deformation models and level sets. *International Journal of Computer Assisted Radiology and Surgery*, 1(3):123–135, 2006. xii

[FS06b] Karl Fritscher and Rainer Schubert. 3d image segmentation by using statistical deformation models and level sets. *International Journal of Computer Assisted Radiology and Surgery*, 1(3):123–135, 2006. 10.1007/s11548-006-0048-2. 23

[FVB81] J Frank, A Verschoor, and M Boublik. Computer averaging of electron micrographs of 40s ribosomal subunits. *Science*, 214:1353–1355, 1981. 7

[GFL04] Leo Grady and Gareth Funka-Lea. *Multi-label Image Segmentation for Medical Applications Based on Graph-Theoretic Electrical Potentials*, pages 230–245. 2004. 16

[GLBr99] Aubert Gilles, F. Laure Blanc, and raud. Some remarks on the equivalence between 2d and 3d classical snakes and geodesic active contours. *Int. J. Comput. Vision*, 34(1):19–28, 1999. 334385. 20

[GMA+04] V. Grau, A. U. J. Mewes, M. Alcaniz, R. Kikinis, and S. K. Warfield. Improved watershed transform for medical image segmentation using prior information. *Medical Imaging, IEEE Transactions on*, 23(4):447–458, 2004. 10

[Gol89] David Goldberg. *Genetic Algorithms in Search, Optimization, and Machine Learning*. Addison-Wesley Professional, 1989. 21

[HBM03] Park Hyunjin, P. H. Bland, and C. R. Meyer. Construction of an abdominal probabilistic atlas and its application in segmentation. *Medical Imaging, IEEE Transactions on*, 22(4):483–492, 2003. 14

[HK98] S. A. Hojjatoleslami and J. Kittler. Region growing: a new approach. *Image Processing, IEEE Transactions on*, 7(7):1079–1084, 1998. 9

[HMT01] Ghassan Hamarneh, Tim McInerney, and Demetri Terzopoulos. Deformable organisms for automatic medical image analysis, 2001. 711020 66-76. 23

[HPCH56] D. Howry, G. Posakony, R. Cushman, and J. Holmes. Three-dimensional and stereoscopic observation of body structures by ultrasound. *Journsl of Applied Physiology*, 9(2):304–306, 1956. 2

[HS88] L. Hertz and R. W. Schafer. Multilevel thresholding using edge matching. *Comput. Vis. Graph. Image Process.*, 44:279–295, 1988. 9

[HS97] William E. Higgins and Roderick D. Swift. Distributed system for processing 3d medical images. *Computers in Biology and Medicine*, 27(2):97 – 115, 1997. Available from: `http://www.sciencedirect.com/science/article/pii/S001048259600042X`. 39

[HY05] Li Hua and A. Yezzi. A hybrid medical image segmentation approach based on dual-front evolution model. In *Image Processing, 2005. ICIP 2005. IEEE International Conference on*, volume 2, pages II–810–13, 2005. 20

[InBSP06] O. Ibáñez, N. Barreira, J. Santos, and M. G. Penedo. Topological active nets optimization using genetic algorithms. In *Proceedings of the Third international conference on Image Analysis and Recognition - Volume Part I*, ICIAR'06, pages 272–282, Berlin, Heidelberg, 2006. Springer-Verlag. Available from: `http://dx.doi.org/10.1007/11867586_26`. 18, 21, 22, 26, 27

[JDJ00] A. K. Jain, R. P. W. Duin, and Mao Jianchang. Statistical pattern recognition: a review. *Pattern Analysis and Machine Intelligence, IEEE Transactions on*, 22(1):4–37, 2000. 12

[JF90] A. K. Jain and F. Farrokhnia. Unsupervised texture segmentation using gabor filters. In F. Farrokhnia, editor, *Systems, Man and Cybernetics, 1990. Conference Proceedings., IEEE International Conference on*, pages 14–19, 1990. 7

[JFSD92] Rivest Jean-Francois, Beucher Serge, and J. Delhomme. Marker-controlled segmentation: an application to electrical borehole imaging. *Journal of Electronic Imaging*, 1(2):136–142, 1992. 17

[JN00] S. Duncan James and Ayache Nicholas. Medical image analysis: Progress over two decades and the challenges ahead. *IEEE Transactions on Pattern Analysis and Machine Intelligence*, 22(1):85–106, 2000. 7

[KBP+92] J. Shane Kippenhan, Warren W. Barker, Shlomo Pascal, Joachim Nagel, and Ranjan Duara. Evaluation of a neural-network classifier for pet scans of normal and alzheimer's disease subjects. *The Journal of Nuclear Medicine*, 33(8):1459–1467, 1992. 7

[KMCP94] A.E. Klietz, A.V. Malevsky, and K. Chin-Purcell. Mix-and-match high performance computing. *Potentials, IEEE*, 13(3):6–10, 1994. 39

[KNG10] P. Kanungo, P.K. Nanda, and A. Ghosh. Parallel genetic algorithm based adaptive thresholding for image segmentation under uneven lighting conditions. In *Systems Man and Cybernetics (SMC), 2010 IEEE International Conference on*, pages 1904–1911, 2010. 19

[KR79] R. L. Kirby and A. Rosenfeld. A note on the use of gray level, local average gray level! space as an aid in threshold selection. *IEEE Trans. Syst. Man Cybern.*, SMC-9:860–864, 1979. 9

[KSW85] J. N. Kapur, P. K. Sahoo, and A. K. C. Wong. A new method for gray-level picture thresholding using the entropy of the histogram. *Graph. Models Image Process.*, 29:273–285, 1985. 9

[KWT88a] M. Kass, A. Witkin, and D. Terzopoulos. Snakes: Active contour models. *International Journal of Computer Vision*, 1(4):321–331, January 1988. xii, xv, 1, 32, 33

[KWT88b] Michael Kass, Andrew Witkin, and Demetri Terzopoulos. Snakes: Active contour models. *International Journal of Computer Vision*, 1(4):321–331, 1988. 10.1007/BF00133570. 7, 12, 14, 20, 27

[LE12] C.-S. Lee and A. Elgammal. Non-linear factorised dynamic shape and appearance models for facial expression analysis and tracking. *Computer Vision, IET*, 6(6):567–580, 2012. 16

[Lef07] Sébastien Lefèvre. Knowledge from markers in watershed segmentation. In *Proceedings of the 12th international conference on Computer analysis of images and patterns*, CAIP'07, pages 579–586, Berlin, Heidelberg, 2007. Springer-Verlag. Available from: `http://dl.acm.org/citation.cfm?id=1770904.1770984`. 17

[LEGF00] M. Leventon, W. Eric, L. Grimson, and O. Faugeras. Statistical shape influence in geodesic active contours. In *Proceeding of the IEEE Computer Society Conference on Computer Vision and Pattern Recognition*, volume 1, pages 316–323, 2000. xii

[LGF00] M. E. Leventon, W. E. L. Grimson, and O. Faugeras. Statistical shape influence in geodesic active contours. In *Computer Vision and Pattern Recognition, 2000. Proceedings. IEEE Conference on*, volume 1, pages 316–323 vol.1, 2000. 15

[LL93] C. H. Li and C. K. Lee. Minimum cross-entropy thresholding. *Pattern Recogn.*, 26:617–625, 1993. 9

[LLL+11] Hongying Liu, Yi Liu, Qian Li, Hongyan Liu, and Yongan Tong. Medical image segmentation based on contourlet transform and watershed algorithm. In *IT in Medicine and Education (ITME), 2011 International Symposium on*, volume 2, pages 224–227, 2011. 10

[LM05] Diane Lingrand and Johan Montagnat. Levelset and b-spline deformable model techniques for image segmentation: a pragmatic comparative study. In *Proceedings of the 14th Scandinavian conference on Image Analysis*, SCIA'05, pages 25–34, Berlin, Heidelberg, 2005. Springer-Verlag. Available from: `http://dx.doi.org/10.1007/11499145_4`. 20

[LPFF08] Przemyslaw Lenkiewicz, Manuela Pereira, Mario Freire, and Jose Fernandes. Accelerating 3d medical image segmentation with high performance computing. In *First Workshops on Image Processing Theory, Tools and Applications*, pages 1–8, 2008. xiv, 6, 43

[LPFF09a] P. Lenkiewicz, M. Pereira, M. Freire, and J. Fernandes. The whole mesh deformation model for 2d and 3d image segmentation. In *Image Processing (ICIP), 2009 16th IEEE International Conference on*, pages 4045 –4048, nov. 2009. xiv, 5, 38

[LPFF09b] P. Lenkiewicz, M. Pereira, M.M. Freire, and J. Fernandes. The dynamic topology changes model for unsupervised image segmentation. In *Multimedia Signal Processing, 2009. MMSP '09. IEEE International Workshop on*, pages 1 –5, oct. 2009. 6, 56

[LPFF09c] P. Lenkiewicz, M. Pereira, M.M. Freire, and J. Fernandes. A new 3d image segmentation method for parallel architectures. In *Multimedia and Expo, 2009. ICME 2009. IEEE International Conference on*, pages 1813 –1816, 28 2009-july 3 2009. 6, 43, 74

[LPFF09d] Przemyslaw Lenkiewicz, Manuela Pereira, Mario Freire, and Jose Fernandes. The dynamic topology changes model for unsupervised image segmentation. In *IEEE International Workshop on Multimedia Signal Processing - MMSP'09*, 2009. xiv

[LPFF09e] Przemyslaw Lenkiewicz, Manuela Pereira, Mario Freire, and Jose Fernandes. A new 3d image segmentation method for parallel architectures. In *IEEE International Conference on Multimedia and Expo*, 2009. xiv

[LPFF11a] P. Lenkiewicz, M. Pereira, M.M. Freire, and J. Fernandes. Extended whole mesh deformation model: Full 3d processing. In *Image Processing (ICIP), 2011 18th IEEE International Conference on*, pages 1601–1604, 2011. xiv, 6, 60

[LPFF11b] Przemyslaw Lenkiewicz, Manuela Pereira, Mário M. Freire, and José Fernandes. *Techniques for Medical Image Segmentation: Review of the Most Popular Approaches*, pages 1–33. IGI Global, Hershey, PA, USA, 2011. Avail-

able from: http://services.igi-global.com/resolvedoi/resolve.aspx?doi=10.4018/978-1-60566-280-0.ch001. 5

[LPFF13] Przemyslaw Lenkiewicz, Manuela Pereira, Mario Freire, and Jose Fernandes. The whole mesh deformation model: a fast image segmentation method suitable for effective parallelization. *EURASIP Journal on Advances in Signal Processing*, 2013(1):55, 2013. Available from: http://asp.eurasipjournals.com/content/2013/1/55. xiv, 6, 38

[LPP91] R Lutz, T Pun, and C Pellegrini. Colour displays and look-up tables: real time modification of digital images. *Computerized Medical Imaging and Graphics*, 15(2):73–84, 1991. 7

[LPW12] Boren Li, Mao Pan, and Zixing Wu. An improved segmentation of high spatial resolution remote sensing image using marker-based watershed algorithm. In *Geoinformatics (GEOINFORMATICS), 2012 20th International Conference on*, pages 1–5, 2012. 17

[LU09] Jiamin Liu and J.K. Udupa. Oriented active shape models. *Medical Imaging, IEEE Transactions on*, 28(4):571–584, 2009. xxv, 81

[Mal89] S. G. Mallat. A theory for multiresolution signal decomposition: The wavelet representation. *IEEE Transactions on Pattern Analysis and Machine Intelligence*, 11(7):674–693, 1989. 7

[Mar92] M. Fleck Margaret. Some defects in finite-difference edge finders. *IEEE Trans. Pattern Anal. Mach. Intell.*, 14(3):337–345, 1992. 132062. 7

[MB04] Sezgin Mehmet and Sankur Bulent. Survey over image thresholding techniques and quantitative performance evaluation. *Journal of Electronic Imaging*, 13(1):146–168, 2004. 8

[MBMC01] Droske Marc, Meyer Bernhard, Rumpf Martin, and Schaller Carlo. An adaptive level set method for medical image segmentation, 2001. 658517 416-422. 20

[MD00] Johan Montagnat and Herve Delingette. Space and time shape constrained deformable surfaces for 4d medical image segmentation, 2000. 759797 196-205. 20, 23

[MH06a] C. McIntosh and G. Hamarneh. Vessel crawlers: 3d physically-based deformable organisms for vasculature segmentation and analysis. In G. Hamarneh, editor, *Computer Vision and Pattern Recognition, 2006 IEEE Computer Society Conference on*, volume 1, pages 1084–1091, 2006. 24, 27

[MH06b] Chris McIntosh and Ghassan Hamarneh. Spinal crawlers: Deformable organisms for spinal cord segmentation and analysis. In Rasmus Larsen, Mads Nielsen, and Jon Sporring, editors, *Lecture Notes in Computer Science*, volume 4190 of *Lecture Notes in Computer Science*, pages 808–815. Springer, 2006. inproceedings conf/miccai/2006-1. 24

[MKA+96] Medical Images Malladi, R. Kimmel, D. Adalsteinsson, G. Sapiro, and J. A. Sethian. A geometric approach to segmentation and analysis of. In *In IEEE Workshop on Mathematical Methods in Biomedical Image Analysis*, pages 244–252. IEEE Computer Society Press, 1996. 2

[MLM+05] U. Meier, O. Lopez, C. Monserrat, M. C. Juan, and M. Alcaniz. Real-time deformable models for surgery simulation: a survey. *Computer Methods and Programs in Biomedicine*, 77(3):183–197, 2005. 23

[mLS08] Xiao mei Lin and Wei Song. Research on segmentation algorithm for 3d medical image based on neural network. In *Natural Computation, 2008. ICNC '08. Fourth International Conference on*, volume 2, pages 517–521, 2008. 12

[MM99] Achim Mayer and Hans-Peter Meinzer. High performance medical image processing in client/server-environments. *Computer Methods and Programs in Biomedicine*, 58(3):207 – 217, 1999. Available from: `http://www.sciencedirect.com/science/article/pii/S0169260798000856`. 39

[MPP12] G. Mirajkar, S. Patil, and M. Pawar. Skull stripping using geodesic active contours in magnetic resonance images. In *Computational Intelligence, Communication Systems and Networks (CICSyN), 2012 Fourth International Conference on*, pages 301–306, 2012. 20

[MSB91] H. Muhlenbein, M. Schomisch, and J. Born. The parallel genetic alghorithm as function optimizer. *Parallel computing*, 17(6-7):619–632, 1991. 18

[MSV95a] R. Malladi, J. Sethian, and B. Vemuri. Shape modeling with front propagation: A level set approach. *IEEE Transactions on Pattern Analysis and Machine Intelligence*, 17(2):158–175, 1995. xii

[MSV95b] R. Malladi, J. A. Sethian, and B. C. Vemuri. Shape modeling with front propagation: a level set approach. *Pattern Analysis and Machine Intelligence, IEEE Transactions on*, 17(2):158–175, 1995. 7

[MT95] T. Mcinerney and D. Terzopoulos. Topologically adaptable snakes. In *Medical Image Analysis*, pages 840–845, 1995. xii

[MT96a] T. Mcinerney and D. Terzopoulos. Deformable models in medical image analysis: A survey. *Medical Image Analysis*, 1:91–108, 1996. xii

[MT96b] Tim McInerney and Demetri Terzopoulos. Deformable models in medical image analysis: a survey. *Medical Image Analysis*, 1(2):91–108, 1996. 23

[MT99a] T. Mcinerney and D. Terzopoulos. Topology adaptive deformable surfaces for medical image volume segmentation. *IEEE Transactions on Medical Imaging*, 18(10):840–850, 1999. xii, 2, 53

[MT99b] Tim Mcinerney and Demetri Terzopoulos. Topology adaptive deformable surfaces for medical image volume segmentation. *IEEE Transactions on Medical Imaging*, 18:840–850, 1999. 2

[MT04] D. Metaxas and Chen Ting. A hybrid 3d segmentation framework. In Chen Ting, editor, *Biomedical Imaging: Nano to Macro, 2004. IEEE International Symposium on*, pages 13–16 Vol. 1, 2004. 19, 27

[NBPS12] Jorge Novo, Noelia Barreira, ManuelGonzalez Penedo, and Jose Santos. Topological active volume 3d segmentation model optimized with genetic approaches. *Natural Computing*, 11:161–174, 2012. Available from: `http://dx.doi.org/10.1007/s11047-011-9275-8`. 22

[NJ02] C. Nicolescu and P. Jonker. A data and task parallel image processing environment. *Parallel Computing*, 28(7-8):945–965, 2002. xiii

[NK95] R. Natarajan and D. Krishnaswamy. A case study in parallel scientific computing: The boundary element method on a distributed-memory multicomputer. In *Proceedings of the IEEE/ACM Supercomputing Conference*, pages 33–33, San Diego, California, USA, December 1995. xiii

[NR79] Y. Nakagawa and A. Rosenfeld. Some experiments on variable thresholding. *Pattern Recogn.*, 11(11):191–204, 1979. 9

[NSP13] J. Novo, J. Santos, and M.G. Penedo. Multiobjective differential evolution in the optimization of topological active models. *Applied Soft Computing*, 13(6):3167 – 3177, 2013. <ce:title>Swarm intelligence in image and video processing.</ce:title>. Available from: `http://www.sciencedirect.com/science/article/pii/S1568494612005546`. 23

[OD92] P.P. Ohanian and R.C. Dubes. Performance evaluation for four classes of tectural features. *Pattern Recognition*, 25:819–833, 1992. 7

[ODJG98] T. O'Donnell, M. P. Dubuisson-Jolly, and A. Gupta. A cooperative framework for segmentation using 2d active contours and 3d hybrid models as applied to branching cylindrical structures. In M. P. Dubuisson-Jolly, editor, *Computer Vision, 1998. Sixth International Conference on*, pages 454–459, 1998. 19

[OS88] S. Osher and J. Sethian. Fronts propagating with curvature dependent speed: Algorithms based on hamilton-jacobi formulations. *Journal of Computational Physics*, 79(1):12–49, 1988. xii

[OS01] S. D. Olabarriaga and A. W. M. Smeulders. Interaction in the segmentation of medical images: A survey. *Medical Image Analysis*, 5(2):127–142, 2001. 7

[Ots79] N. Otsu. A threshold selection method from gray-level histograms. *Systems, Man and Cybernetics, IEEE Transactions on*, 9(1):62–66, 1979. 8

[PA02] F. Payan and M. Antonini. Multiresolution 3d mesh compression. In *Image Processing. 2002. Proceedings. 2002 International Conference on*, volume 2, pages II–245–II–248 vol.2, 2002. 22

[PB02] Frederic Precioso and Michel Barlaud. B-spline active contour with handling of topology changes for fast video segmentation. *EURASIP J. Appl. Signal Process.*, 2002(1):555–560, 2002. 1283158. 20

[PGR94] T. Pun, G. Gerig, and O. Ratib. Image analysis and computer vision in medicine, 1994. 7

[PGX08] Lei Pan, Lixu Gu, and Jianrong Xu. Implementation of medical image segmentation in cuda. In *Information Technology and Applications in Biomedicine, 2008. ITAB 2008. International Conference on*, pages 82–85, 2008. 39

[PHA+88] T. Pun, D.F. Hochstrasser, R.D. Appel, M. Funk, and V. Villars-Augsburger. Computerized classification of two-dimensional gel electrophoretograms by correspondence analysis and ascendant hierarchical clustering. *Appl Theor Electrophor*, 1(1):3–9, 1988. 7

[PJT+11] G. Prasad, A.A. Joshi, P.M. Thompson, A.W. Toga, D.W. Shattuck, and D. Terzopoulos. Skull-stripping with deformable organisms. In *Biomedical Imaging: From Nano to Macro, 2011 IEEE International Symposium on*, pages 1662 –1665, 30 2011-april 2 2011. 24

[PL90] T. Pavlidis and Y.-T. Liow. Integrating region growing and edge detection. *Pattern Analysis and Machine Intelligence, IEEE Transactions on*, 12(3):225–233, 1990. 9

[RLVC+02] D. Rueckert, M. Lorenzo-Valdes, R. Chandrashekara, G. L. Sanchez-Ortiz, and R. Mohiaddin. Non-rigid registration of cardiac mr: application to motion modelling and atlas-based segmentation. In *Biomedical Imaging, 2002. Proceedings. 2002 IEEE International Symposium on*, pages 481–484, 2002. 14

[RPM06] Huang Rui, Vladimir Pavlovic, and Dimitris Metaxas. A tightly coupled region-shape framework for 3d medical image segmentation. In V. Pavlovic, editor, *Biomedical Imaging: Nano to Macro, 2006. 3rd IEEE International Symposium on*, pages 426–429, 2006. 19

[SD92] L. H. Staib and J. S. Duncan. Boundary finding with parametrically deformable models. *Pattern Analysis and Machine Intelligence, IEEE Transactions on*, 14(11):1061–1075, 1992. 15

[SD96] L. H. Staib and J. S. Duncan. Model-based deformable surface finding for medical images. *Medical Imaging, IEEE Transactions on*, 15(5):720–731, 1996. 7

[SD13] D. Selvathi and R. Dhivya. Segmentation of tissues in mr images using modified spatial fuzzy c means algorithm. In *Signal Processing Image Processing Pattern Recognition (ICSIPR), 2013 International Conference on*, pages 136–140, 2013. 11

[Sez85] M. I. Sezan. A peak detection algorithm and its application to histogram-based image data reduction. *Graph. Models Image Process.*, 29:47–59, 1985. 8

[SHPA05] M. Salomon, F. Heitz, G. R. Perrin, and J. P. Armspach. A massively parallel approach to deformable matching of 3d medical images via stochastic differential equations. *Parallel Comput.*, 31(1):45–71, January 2005. Available from: `http://dx.doi.org/10.1016/j.parco.2004.12.003`. 39

[SKBG95] G. Székely, A. Kelemen, Ch Brechbühler, and G. Gerig. *Segmentation of 3D objects from MRI volume data using constrained elastic deformations of flexible Fourier surface models*, pages 493–505. 1995. 10.1007/BFb0034992. 7

[SPF05] F. Segonne, J. Pacheco, and B. Fischl. Active contours under topology control genus preserving level sets. In *Computer Vision for Biomedical Image Applications*, volume 3765, pages 135–145, 2005. xii

[SR09] S. Shah and A. Ross. Iris segmentation using geodesic active contours. *Information Forensics and Security, IEEE Transactions on*, 4(4):824–836, 2009. 20

[SS12] K. Seshadri and M. Savvides. An analysis of the sensitivity of active shape models to initialization when applied to automatic facial landmarking. *Information Forensics and Security, IEEE Transactions on*, 7(4):1255–1269, 2012. xxv, 81

[SSP05] Hong Shen, Yonggang Shi, and Zhigang Peng. Applying prior knowledge in the segmentation of 3d complex anatomic structures. In *Proceedings of the First international conference on Computer Vision for Biomedical Image Applications*, CVBIA'05, pages 189–199, Berlin, Heidelberg, 2005. Springer-Verlag. Available from: http://dx.doi.org/10.1007/11569541_20. 16

[SvZ09] Herman Stehouwer and Menno van Zaanen. Language models for contextual error detection and correction. In *Proceedings of the EACL 2009 Workshop on Computational Linguistic Aspects of Grammatical Inference*, CLAGI '09, pages 41–48, Stroudsburg, PA, USA, 2009. Association for Computational Linguistics. Available from: http://dl.acm.org/citation.cfm?id=1705475.1705482. 81

[TB97] Alain Tremeau and Nathalie Borel. A region growing and merging algorithm to color segmentation. *Pattern Recognition*, 30(7):1191 – 1203, 1997. Available from: http://www.sciencedirect.com/science/article/pii/S0031320396001471. 9

[TGC01] F. Cootes Timothy, J. Edwards Gareth, and J. Taylor Christopher. Active appearance models. *IEEE Trans. Pattern Anal. Mach. Intell.*, 23(6):681–685, 2001. 378090. 15

[THCH93] F. Cootes Timothy, A. Hill, J. Taylor Christopher, and J. Haslam. The use of active shape models for locating structures in medical images, 1993. 660403 33-47. 15

[The83] C. Thenien. An estimation-theoretic approach to terrain image segmentation. *Comput. Vision Graphics Image Processing*, vol. 22(313-326), 1983. 11

[Tho96] K. E. Thomenius. Evolution of ultrasound beamformers. In *IEEE Ultrasonics Symposium*, pages 1615–1622, Texas, November 1996. 2

[tHRFKV91] Bart ter Haar Romeny, Luc Florack, Jan Koenderink, and Max Viergever. *Scale space: Its natural operators and differential invariants*, pages 239–255. 1991. 10.1007/BFb0033757. 7

[TM12] R. Toth and A. Madabhushi. Multifeature landmark-free active appearance models: Application to prostate mri segmentation. *Medical Imaging, IEEE Transactions on*, 31(8):1638–1650, 2012. xxv, 81

[TMT+01] R.-I. Taniguchi, Y. Makiyama, N. Tsuruta, S. Yonemoto, and D. Arita. Software platform for parallel image processing and computer vision. In *SPIE Proceedings Parallel and Distributed Methods for Image Processing, Hongchi Shi; Patrick C. Coffield; Eds.*, volume 3166, pages 2–10, 2001. xiii

[TWK88] Demetri Terzopoulos, Andrew Witkin, and Michael Kass. Constraints on deformable models: Recovering 3d shape and nonrigid motion. *Artificial Intelligence*, 35, 1988. 20

[TWMM07] Gabriel Tsechpenakis, Jianhua Wang, Brandon Mayer, and Dimitris A. Metaxas Dimitris Metaxas. Coupling crfs and deformable models for 3d medical image segmentation. In Jianhua Wang, editor, *Computer Vision, 2007. ICCV 2007. IEEE 11th International Conference on*, pages 1–8, 2007. 19

[TY89] K. Tsumiyama and K Yamamoto. Active net: Active net model for region extraction. *IPSJ SIG notes*, 89(96):1–8, 1989. 21, 27

[US96] Jayaram K. Udupa and Supun Samarasekera. Fuzzy connectedness and object definition: Theory, algorithms, and applications in image segmentation. *Graphical Models and Image Processing*, 58(3):246 – 261, 1996. Available from: `http://www.sciencedirect.com/science/article/pii/S1077316996900210`. 10

[US03] J. K. Udupa and P. K. Saha. Fuzzy connectedness and image segmentation. *Proceedings of the IEEE*, 91(10):1649–1669, 2003. 10

[VS91] L. Vincent and P. Soille. Watersheds in digital spaces: an efficient algorithm based on immersion simulations. *Pattern Analysis and Machine Intelligence, IEEE Transactions on*, 13(6):583–598, 1991. 10, 17

[WBKC09] J.P. Walters, V. Balu, S. Kompalli, and V. Chaudhary. Evaluating the use of gpus in liver image segmentation and hmmer database searches. In *Parallel Distributed Processing, 2009. IPDPS 2009. IEEE International Symposium on*, pages 1–12, 2009. 39

[WK07] D.J. Withey and Z.J. Koles. Medical image segmentation: Methods and software. In *Noninvasive Functional Source Imaging of the Brain and Heart and the International Conference on Functional Biomedical Imaging, 2007. NFSI-ICFBI 2007. Joint Meeting of the 6th International Symposium on*, pages 140 –143, oct. 2007. 7, 8

[WR78] J. S. Weszka and A. Rosenfeld. Threshold evaluation techniques. *IEEE Trans. Syst. Man Cybern.*, SMC-8:627–629, 1978. 8

[WS92a] D.J. Williams and M. Shah. A fast algorithm for active contours and curvature estimation. *CVGIP: Image Understanding*, 55(1):14–26, January 1992. xvi

[WS92b] Donna Williams and Mubarak Shah. A fast algorithm for active contours and curvature estimation. *CVGIP: Image Understanding*, 55(1):14–26, 1992. 13, 27

[WY02] Kuo-Lung Wu and Miin-Shen Yang. Alternative c-means clustering algorithms. *Pattern Recognition*, 35(10):2267–2278, 2002. 11

[WZW+06] Zhifeng Wang, Wei Zheng, Yuhang Wang, James Ford, Fillia Makedon, and Justin D. Pearlman. *Neighboring Feature Clustering*, volume 3955/2006, pages 605–608. Springer Berlin / Heidelberg, 2006. 11

[XP98] C. Xu and J. Prince. Snakes, shapes, and gradient vector flow. *EEE Transactions on Image Processing*, 7(3):359–369, 1998. xvi, 33

[XXP03] X., , C. Xu, and J. Prince. A topology preserving level set method for geometric deformable models. *IEEE Transactions on Pattern Analysis and Machine Intelligence*, 25(6):755–768, 2003. xii

[YD03] Jing Yang and James Duncan. *3D Image Segmentation of Deformable Objects with Shape-Appearance Joint Prior Models*, pages 573–580. 2003. 15

[Yin95] Liu Ying. *Document image binarization based on texture analysis*. PhD thesis, 1995. 240204. 9

[YIT80] M Yachida, M Ikeda, and S Tsuji. Plan-guided analysis of cineangiograms for measurement of dynamic behavior of heart wall. *Ieee Trans. Pattern Analy. And Mach. Intellig*, 2(6):537–542, 1980. 7

[YPH+06] Paul A. Yushkevich, Joseph Piven, Heather Cody Hazlett, Rachel Gimpel Smith, Sean Ho, James C. Gee, and Guido Gerig. User-guided 3d active contour segmentation of anatomical structures: Significantly improved efficiency and reliability. *NeuroImage*, 31(3):1116 – 1128, 2006. Available from: http://www.sciencedirect.com/science/article/pii/S1053811906000632. 2, 53

[YSGD07] Zhang Yifei, Wu Shuang, Yu Ge, and Wang Daling. A hybrid image segmentation approach using watershed transform and fcm. In *Fuzzy Systems and Knowledge Discovery, 2007. FSKD 2007. Fourth International Conference on*, volume 4, pages 2–6, 2007. 19

[ZC10] Yan Zhang and Xiaoping Cheng. Medical image segmentation based on watershed and graph theory. In *Image and Signal Processing (CISP), 2010 3rd International Congress on*, volume 3, pages 1419–1422, 2010. 10

[ZZ10] Wei Zhou and J.M. Zurada. Discrete-time recurrent neural networks for medical image segmentation based on competitive layer model with lt neurons. In *Biomedical Engineering and Computer Science (ICBECS), 2010 International Conference on*, pages 1–4, 2010. 12